

POLITECNICO DI MILANO
School of Civil, Environmental and Land Management
Engineering
Polo Territoriale di Como



Master of Science in Environmental and Geomatic Engineering

**COMPARISONS BETWEEN GLOBAL AND HELIDEM
TRANSALPINE MODELS – PROBLEM IDENTIFICATION**

Supervisor: Prof. Ludovico Giorgio Aldo BIAGI

Master Graduation Thesis by:
Nadya STAMBOLIYSKA
Student Id. 796960

Academic Year 2014 / 2015

Table of Contents

ABSTRACT	4
1 Introduction to DEM.....	7
1.1 Definition	7
1.2 DSM vs. DTM	7
1.3 Sampling and measurement	8
1.4 Techniques for DEM source data acquisition.....	9
1.4.1 Cartographic digitalization.....	9
1.4.2 Ground surveying.....	10
1.4.3 Photogrammetry	13
1.4.4 Synthetic Aperture Radar (SAR) Imaging	14
1.4.5 Airborne Laser Scanning (ALS) or LiDAR (Light Detection and Ranging)	15
1.4.6 Comparison between DEM data acquired through different techniques	17
1.5 Surface Modeling and DEM Networks: GRID vs. TIN.....	18
1.6 Storing formats	19
1.7 Grid interpolation methods	19
1.8 Quality of DEMs	20
1.9 Different spatial scales of DEMs	20
1.10 Open Data.....	21
2 Global (low resolution) Digital Elevation Models (DEMs).....	23
2.1 Advanced Spaceborne Thermal Emission and Reflection Radiometer (ASTER).....	23
2.2 Shuttle Radar Topography Mission (SRTM)	27
2.3 Global Multi-resolution Terrain Elevation Data 2010 (GMTED2010)	30
3 Local (high resolution) HELvetia-Italy Digital Elevation Model (HELI-DEM)	34
3.1 Overview and Mission.....	34

3.2	Preprocessing of HELI-DEM data	36
3.3	Generation technique	45
3.4	Conclusions.....	51
4	Geographic Resources Analysis Support System (GRASS GIS)	52
4.1	Definition	52
4.1.1	Free and Open Source meaning	52
4.1.2	Main capabilities	53
4.2	GRASS structure	54
4.2.1	Vector data.....	55
4.2.2	Raster data	56
5	Download of GDEMs, Start of a new project in GRASS, Import of GDEMs and Re-projection of HELI-DEM.....	57
5.1	Download of global DEMs	57
5.1.1	Download of ASTER and SRTM data	57
5.1.2	Download of GMTED2010 data.....	61
5.2	Start of a new project	62
5.2.1	Creating a Location for the Global DEMs	62
5.2.2	Creating a Location for the Local DEM	67
5.3	Import of global DEMs	69
5.3.1	Import of ASTER and SRTM data.....	69
5.3.2	Import of GMTED2010 data.....	71
5.4	Import of HELI-DEM.....	77
5.5	Statistics of Data	80
5.6	Re-projection of HELI-DEM.....	81
6	Comparison between ASTER Global DEM and HELI-DEM Local DEM.....	88
6.1	Analysis of the differences between ASTER and HELIDEM.....	88
6.2	Histogram of the differences between ASTER and HELIDEM and classification of the outliers	90
6.3	Spatial identification of severe outliers	92

6.4	Identification of correlation between the heights of HELIDEM and their differences with ASTER	94
6.5	Identification of correlation between the slopes of HELIDEM and the differences between ASTER and HELIDEM	96
7	Comparison between SRTM Global DEM and HELI-DEM Local DEM	104
7.1	Analysis of the differences between SRTM and HELIDEM.....	104
7.2	Histogram of the differences between SRTM and HELIDEM and classification of the outliers	106
7.3	Spatial identification of severe outliers	107
7.4	Identification of correlation between the heights of HELIDEM and their differences with SRTM	108
7.5	Identification of correlation between the slopes of HELIDEM and the differences between SRTM and HELIDEM	110
8	Comparison between GMTED2010 Global DEM and HELI-DEM Local DEM	117
8.1	Analysis of the differences between GMTED and HELIDEM ...	117
8.2	Histogram of the differences between GMTED and HELIDEM and classification of the outliers.....	119
8.3	Spatial identification of severe outliers	120
8.4	Identification of correlation between the heights of HELIDEM and their differences with GMTED.....	121
8.5	Identification of correlation between the slopes of HELIDEM and the differences between GMTED and HELIDEM.....	123
	CONCLUSION.....	129
	List of figures	131
	List of tables	135
	Bibliography.....	136
	Web sources	138
	<i>Acknowledgments</i>	140

ABSTRACT

Digital Elevation Models (DEMs) provide a mathematical description of the terrain surface and have the trait to represent it in a visual way as well. Various tools using computer technologies have been developed since the middle of the 20th century and one of the most important and powerful technique to represent terrain data is the digital modeling. It calculates the elevation of a point of the surface through different interpolation methods and the obtained altitudes of the terrain are set down to a certain reference frame.

Depending on the data set that DEMs represent they could be distinguished in Digital Surface Models (DSMs) and Digital Terrain Models (DTMs). The first one refers to the Earth's surface including all the objects that belong to or are built on it (buildings, vegetation and other features elevated above the land). DTMs represent for the elevations of the bare ground without any objects.

Other differentiation could be done regarding the specific need, the size of the area that the user has to describe and the level of accuracy that he wants to obtain. If a big portion of the Earth surface has to be studied, like an entire region or an entire country, but with low details, a global DEM can be used; on the contrary local DEM can be adopted when there is the need to be analyzed a small portion of the surface but with high details. Another important feature that has to be taken into account is that the accuracy depends on the equipment performing the acquisition. There are a lot of acquisition techniques for generating data with the aim to create DEMs but for sure one of the most advantageous is using satellite sensors for obtaining remotely-sensed elevation data.

The topic of this study is based on all these facts. The present work aims to compare the different most well-known global Digital Elevation models namely Advanced Spaceborne Thermal Emission and Reflection Radiometer (ASTER), Shuttle Radar Topography Mission (SRTM) and Global Multi-resolution Terrain Elevation Data 2010 (GMTED2010) with the local transalpine Helvetia-Italy Digital Elevation Model (HELI-DEM), and then to identify the existing problems.

The ASTER GDEM was developed in cooperation of the U.S. National Aeronautics and Space Administration (NASA) and Japan's Ministry of Economy, Trade, and Industry (METI) and covers land surfaces between 83°N and 83°S which is 99% of Earth's landmass. ASTER data are posted on a 1 arc-second (approximately 30 m) grid.

The SRTM is an international joint project developed by The National Aeronautics and Space Administration (NASA) and the National Geospatial-Intelligence Agency (NGA). The collected data covers about 80% of the Earth's

land surface between 60°N and 56°S latitude. The derived products are two DTMs at resolution level of 1 arc-second (approximately 30 m) at the present available only for USA area and 3 arc-second (approximately 90 m) for worldwide coverage.

The GMTED2010 is a global elevation model developed by the U.S. Geological Survey (USGS) in collaboration with the National Geospatial-Intelligence Agency (NGA) with the aim to replace the Global Topographic Data GTOPO30. The previous model has horizontal resolution of 30 arc-seconds for the entire Earth and provided elevation data that widely vary in quality. The new model has been generated at three separate resolutions of 30 arc-second (approximately 1 km), 15 arc-second (approximately 500 m) and 7.5 arc-second (approximately 250 m). GMTED2010 data covers all land areas from 84°N to 56°S latitude for most products, and coverage from 84°N to 90°S latitude for several products.

Each of the three GDEMs is posted on a Lat/Lon grid and referenced to the 1984 World Geodetic System (WGS84) horizontal datum and 1996 Earth Gravitational Model (EGM96) vertical datum. All the data are available in GeoTIFF format as SRTM could be downloaded in Arc-Info ASCII format as well. The models are considered as Open data so they are available online and could be obtained free of charge from users worldwide.

The local HELI-DEM has been developed with the aim to create a unified DEM for the area of Italian and Swiss Alps. HELI-DEM covers two regions in Italy – Lombardy and Piedmont and two cantons in Switzerland – Ticino and Grisons. The model covers the ETRF2000 rectangle comprised by the following boundaries: from 45.10° N to 46.70° N latitude and from 7.80° E to 10.70° E longitude. It is gridded in geographical coordinates (as the global ones) and has a spatial resolution of 2×10^{-4} degrees.

The present thesis is built in 8 chapters that are briefly explained below:

Chapter 1: This chapter contains a brief overview of the Digital Elevation Models, and it describes the different techniques used for obtaining elevation data. Here are explained modeling and interpolation methods, and storing formats. The main features regarding the quality of DEMs are described, as well as the standards for DEMs classification regarding the different levels of their representation adopted nowadays.

Chapter 2: This chapter explains three of the most important and well-known Digital Elevation Models regarding to a global scale. They are categorized as low resolution ones when are compared with the local model. Nevertheless, taking into account that the acquisition is done for almost the entire Earth's surface could be said that these models (especially ASTER and SRTM) generate a high resolution database. Moreover, the purchase of the products is for free since they are considered as Open data.

Chapter 3: This chapter presents the HELI-DEM project, the collected data and all the pre-processing steps that have been done on it in order to be used for the producing of the unified DTM, as well as the main operations of creating the local HELI-DEM. This model is considered as a high resolution DEM when is compared with the global ones. HELI-DEM has been developed as a research project and it covers the whole alpine area between Italy and Switzerland.

Chapter 4: In this chapter the GRASS GIS software used to process the available elevation data and its main functionalities are explained. It is Free and Open Source software which allows reading, visualizing, editing and analyzing the information in a unique geographic platform.

Chapter 5: This chapter explains step by step the process of downloading ASTER, SRTM and GMTED2010. Then are presented in details the first steps in defining a new project, creating locations and setting region extents in the GRASS platform so that further data management, analysis, processing, etc. could be initiated. Later, the way of importing the global and the local models into the GRASS platform is described. Here is indicated as well the sampling procedure for the HELI-DEM by decreasing its resolution until it reaches the ones of the global models. This action allows computations, comparisons and further analyses to be initiated. Three cases are going to be presented.

Chapter 6, 7 and 8: In each of these chapters a final map of the difference between the local and the global model is produced and analyzed. Histogram with the empirical and the normal distribution with the same mean and standard deviation as the data are presented. Furthermore, a correlation index between the height (h) and the difference of heights between the two models (Δh) is calculated as well as the correlation index between the slope and again the difference of heights between the two models (Δh). The general analysis is completed by computing the same correlation indices but this time using the absolute values of the differences.

Conclusions: In this part are given the results of the comparisons from the present work and their analyses are briefly stated.

Keywords: Digital Elevation Model, HELI-DEM, Global Model, Local Model

Chapter 1

1 Introduction to DEM

This chapter contains a brief overview of the Digital Elevation Models, and it describes the different techniques used for obtaining elevation data. Here are explained modeling and interpolation methods, and storing formats. The main features regarding the quality of DEMs are described, as well as the standards for DEMs classification regarding the different levels of their representation adopted nowadays.

1.1 Definition

Digital Elevation Models (DEMs) provide a mathematical description of the terrain surface and have the trait to represent it in a visual way as well. Various tools using computer technologies have been developed since the middle of the 20th century and one of the most important and powerful technique to represent terrain data is the digital modeling. It calculates the elevation of a point of the surface through different interpolation methods and the obtained altitudes of the terrain are set down to a certain reference frame.

1.2 DSM vs. DTM

Depending on the data set that DEMs represent they could be distinguished in Digital Surface Models (DSMs) and Digital Terrain Models (DTMs). The first one refers to the Earth's surface including all the objects that belong to or are built on it (buildings, vegetation and other features elevated above the land). Concerning DTM, it stands for the elevations of the bare ground without any objects (Maune, 2001).

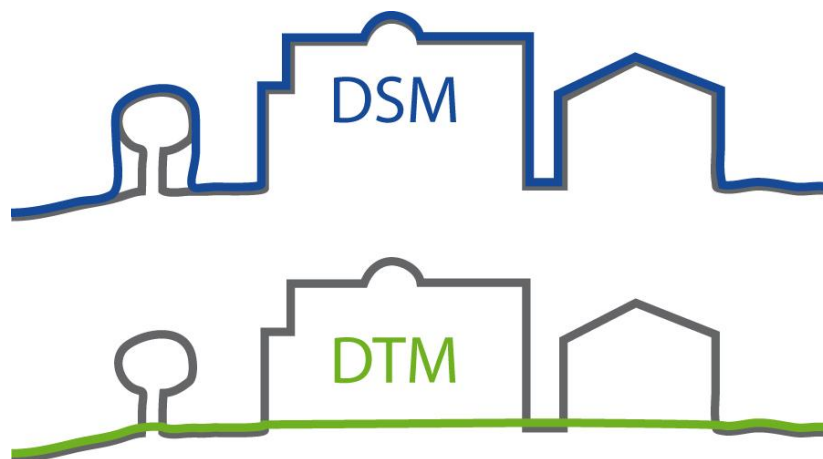


Figure 1 DSM vs. DTM

DSMs are very useful for landscape modeling, city modeling and visualization applications, while DTMs are used for flood or drainage modeling, land-use and geological studies.

1.3 Sampling and measurement

The first step that has to be done in the process of digital terrain modeling is the acquisition of data which is carried out in two stages: sampling and measurement. **Sampling** is the process of selecting the points that have to be measured and it is characterized by two parameters, namely *distribution* and *density* (Gao, 1995). During the measurement 2-D planimetric (x, y) coordinates are determined and concerned with another attribute, *accuracy*. The sampling process can take place before or after the measurement. If it is done after, a set of measured points with great density are selected.

The **distribution** of sampled data is usually specified by the terms of *location* and *pattern*. The *location* is defined by two positional coordinates (Lat/Lon or North/East). There is a variety of different available *patterns* and an example of one their classification is shown on the figure bellow.

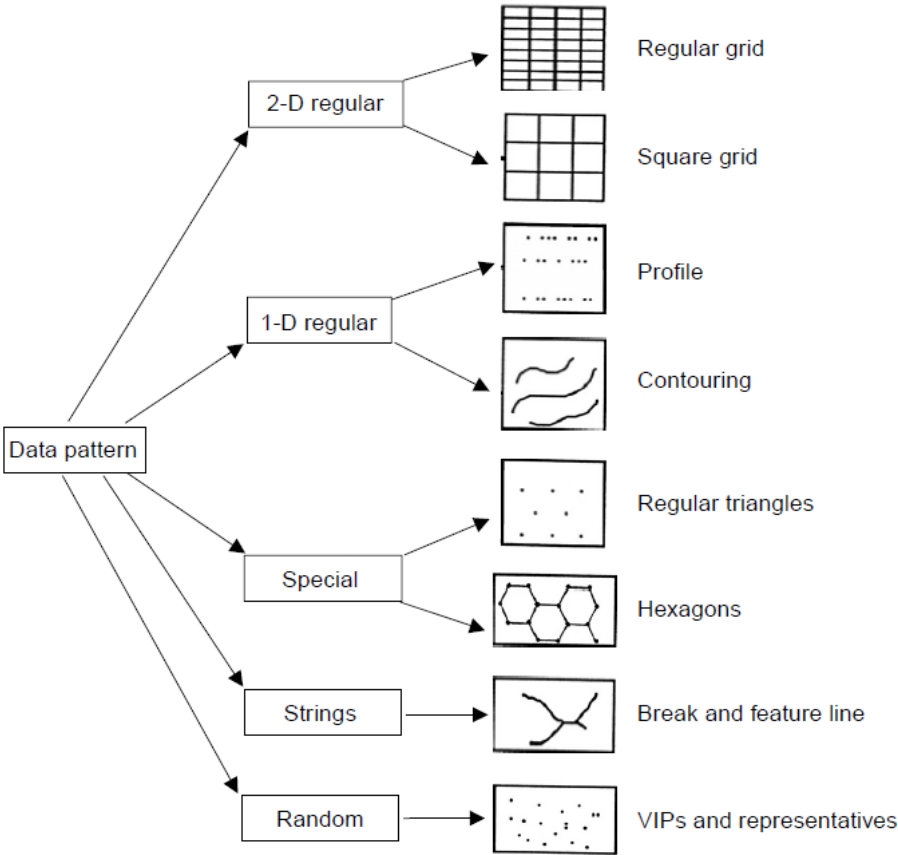


Figure 2 Patterns of sampled data points

As another attribute, the **density** can be specified by measures like the distance between two points, the number of points per unit area and so on.

The **accuracy** of sampled data largely depends on the methods used for measurement, such as the mode of measurement, instruments used, and technique adopted (Li, Zhu, & Gold, 2005).

1.4 Techniques for DEM source data acquisition

DEM source data means data collected from data sources of digital elevation modeling and it can be obtained by different acquisition techniques (Karel, Pfeifer, & Briese, 2006):

- Cartographic digitalization using as a source existing topographic maps
- Ground surveying obtaining data coming by traditional (topographic) or spatial (GNSS) survey techniques
- Photogrammetry using stereo pairs of aerial and satellite images as a source
- Interferometric Synthetic Aperture Radar (InSAR or IfSAR): using two or more Synthetic Aperture Radar (SAR) images as a source.
- Airborne Laser Scanning (ALS) and LiDAR (Light Detection and Ranging): using ultraviolet, visible and infra-red regions of the electromagnetic spectrum

1.4.1 Cartographic digitalization

Using topographic maps as a source of elevation data, generally there are two cartographic digitalization techniques that can be applied: the vector-based line following and the raster-based scanning. In both cases digitalization can be done either manually or by automated devices.

In **manual line-following digitalization** is used a digitizer table on which the map is put and an operator traces the contour lines using a cursor. Coordinates are recorded in two ways, in point mode or in stream mode. In point mode digitalization, the operator has to decide which points to be measured and each time he presses a button, the x and y coordinates of the cursor position are recorded. Stream mode means that the tracing process is carried out dynamically through recording the coordinates of points, while the cursor is moving along the contour lines.

In **manual raster scanning** a regular grid is superimposed onto the map and then in a matrix is recorded 1 or 0 depending whether contours pass through these grid cells or not.

Automated vectorization is done with algorithms while in **automated raster scanning** each line scan is divided into resolution units and for each unit the scan provides different returns (binary code) whether or not a contour line is present.

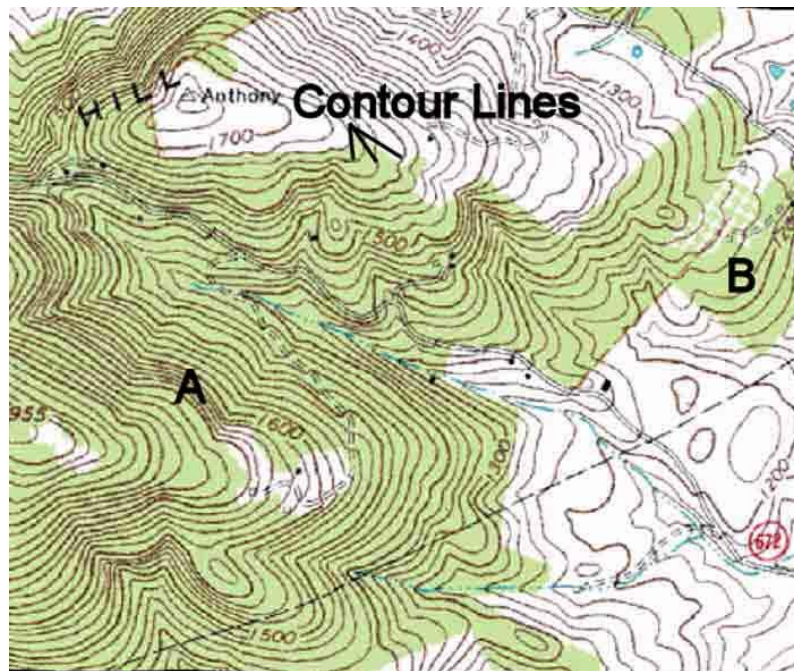


Figure 3 Example of a topographic map

1.4.2 Ground surveying

Land surveying has been used for decades for collection of high resolution elevation data. A modern **Total Station** is an electronic device that has the ability to measure a position horizontally and vertically at the same time. It is composed by two parts, a machine mounted on a static tripod, set up at a base station, and a prism (the target) on a metal support, which is moved around the site. The machine, whose coordinates are calculated in advance, sends out a light signal, which bounces back from the prism giving a time interval that is used to calculate the distance between the station and the target. The Total Station has a microprocessor which automatically collects these measurements, calculates the trigonometrical equations and converts them into grid coordinates. Its disadvantage is that it is very slow and requires intensive work by at least two operators and visibility between stations.

Global Positioning System (GPS) initially developed for military use, is used today for positioning purposes and measurements of the Earth surface. For that kind surveying is required less operator work and no inter visibility between stations so that terrain information can be obtained directly without the need for measuring angles and distances between intermediate points. Still the equipment and calculations are quite complex but for the user the process is very simple.

The GPS system is composed by three parts: the space segment, the ground control system and the user segment.

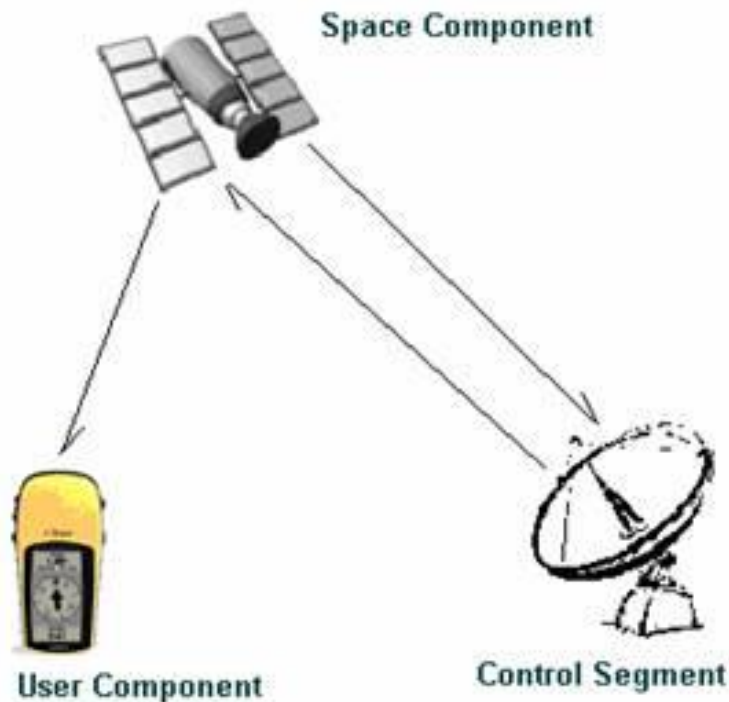


Figure 4 GPS segments

Space segment refers to the GPS constellation of 32 satellites, that orbit at about 20'000 km above the Earth surface and continuously broadcast measurement signals and navigation messages to the GPS users (Biagi, 2012). Each satellite continuously transmits a message by two different electromagnetic waves or carries (L_1 and L_2), modulated with pseudo-random signals. The message includes information about:

- the time the message was transmitted
- broadcast orbital information (the ephemeris) of all the GPS satellites
- the general system health

The control segment consists of ground stations that manage the satellite constellation. It is composed by one master control station located in Colorado, a couple monitor stations spread all over the world and three ground antennas. The master control station collects the signal coming from the satellites, tracked by the monitor stations, than computes and predicts the satellite orbit and later sends it to the satellites that distribute the information.

The user segment consists of receivers utilized by the final users: they can be applied in mobile phones, transport navigation, search and rescue equipments, field surveying, etc. A GPS receiver is constituted of hardware and software for receiving, decoding, storing and processing the signal from the satellites. The GPS receiver computes its position by timing the signal sent by GPS satellites.

In general, to determine an unknown position in a 3-D space through GPS-based measurement, three distances from three known points are needed, e.g. three satellites must be available. These distances, between satellites and the unknown receiver, can be obtained by measuring the time needed by the signal to travel from the satellite to the receiver. The time can be easily computed by knowing the propagation velocity of the signal through the path. However, GPS constellation is designed to guarantee at least four visible satellites from every place of the Earth in order to compute the clock offset since the receiver's clock is not aligned to a common reference time scale.

GPS data are affected by a big number of different errors, related to a variety of causes. As mentioned before, the calculation is very complex but the GPS data serves to the final user in a very simple way.

Through GPS measurements is possible also to carry out measurements in different modalities, to which different accuracies correspond. The most used are:

- Absolute positioning or point positioning is performed with a single receiver using the code and/or phase of the GNSS signal. The position of the point can be obtained in real time using a single epoch or occupying the same point for many epochs with a long measurement (static measurement that lasts for some hours). In the first case the position accuracy is of the order of 5-10 meters, in the second case the accuracy can reach ten centimeters.
- Relative positioning which can be distinguished three types according to the different processing techniques:
 - Differential positioning (DGPS) with accuracy of the order of 0.5 meters
 - Relative RTK positioning in which two receivers are used. The former is fixed on a points with known position (called “base” or “reference”), while the latter (called “rover”) is in motion and occupies points at unknown positions. The accuracy of the coordinates has a magnitude of few centimeters.
 - Relative static positioning is performed using at least two receivers, one of which is located in a known position. The accuracy of the baselines components depends on the baseline length and on the length of the session so it can reach few millimeters.

1.4.3 Photogrammetry

The word photogrammetry comes from the Greek words *photos* (meaning *light*), *gramma* (meaning that which is drawn or written) and *metron* (meaning *to measure*). It originally signified “measuring graphically by means of light” (Whitmore and Thompson 1966).

Photogrammetry has undergone four stages of development, that is, analog, numerical, analytical, and digital photogrammetry.

In aerial photogrammetry the camera is mounted on an aircraft and is usually pointed vertically towards the ground and multiple overlapping photos of the ground are taken while the aircraft flies along its flight path. The collected photos are then processed in a stereo plotter which allows the operator to view at the same time two photos in a stereo view.

The fundamental principle of photogrammetry is to make use of a pair of stereo images (or simply stereo pair) to reconstruct the original shape of 3-D objects, then to form the stereo model, and later to measure the 3-D coordinates of the objects on the stereo model. *Stereo pair* refers to two images of the same scene photographed at two slightly different places so that they have a certain degree of overlap, the only area in which the 3-D models can be reconstructed.

In aerial photography, in general there is 60% overlap in the flight direction and 30% between the flight strips. Each photograph is characterized by six orientation elements, three angular elements (one for each of x, y and z axes) and three translations (x, y and z coordinates in a coordinate system).

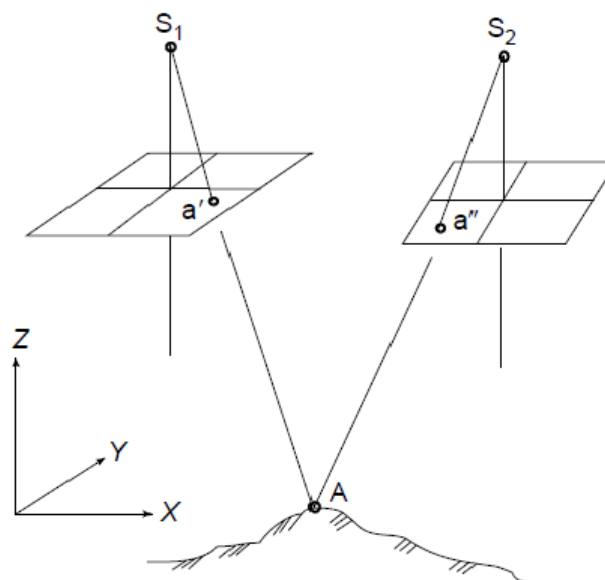


Figure 5 A stereo model is formed by projecting image points from a stereo pair

In this figure, S_1 and S_2 are the projection centers, a' and a'' are the two image points on the left and right images, respectively. The light rays from S_1a' and

S_2a ” intersect at point A which is on the stereo model. The relationship between an image point, the corresponding ground point, and the projection center (camera) is described by an analytical function, called the colinearity condition.

The six orientation elements can be determined by mounting GPS receivers on the airplane or by measuring a few control points (both on the ground and on images) and using the colinearity condition.

In analytical photogrammetry, the measurement of image coordinates has been carried out by the operator. Nowadays, in digital photogrammetry, the images are in digital form so they go through an internal orientation and thus the coordinates of a point are determined by pixel coordinates (rows and columns) which are transformed into image coordinates referenced to a coordinate system, originated in the center of the projection. When given an image point on the left image, the system will search the corresponding point on the right image (called conjugate point) automatically by a procedure called *image matching*.

1.4.4 Synthetic Aperture Radar (SAR) Imaging

Synthetic Aperture Radar is a microwave imaging radar developed in the 1960s. It is composed by a radar mounted onboard a flying platform such as an airplane or a satellite (Freeman, 1992). The antenna, pointed down to the direction of motion of the platform, is an active sensor providing its own illumination to a portion of the terrain, by emitting short a cone-shaped microwave beam (pulses), characterized by frequencies between 500 MHz and 30 GHz. During the movement along the predetermined path, the pulses are sent continuously at regular intervals to the ground, with a certain side-looking angle in the direction perpendicular to the flying track (azimuth direction).

Each time, the energy sent by the imaging radar forms a radar footprint on the ground. This area may be regarded as consisting of many small cells. The echo backscattered from each ground cell within the footprint is received and its intensity is recorded as a pixel in the grey scale image plane according to the slant range between the antenna and the ground cell. During the flying mission, the area swept by the radar footprint forms a swath of the ground, thus a radar image of the swath is obtained.

The resulted reflectivity map contains information about the phase and amplitude of the registered signal. The amplitude information is very useful because it indicates the soil coverage (Graham, 1974). Unlike optical and infrared imaging sensors, imaging radar is able to take clear pictures day and night under all weather conditions.

By combining two or more SAR images of the same area, it is also possible to generate elevation maps and surface change maps with high precision and resolution. This technique is called SAR interferometry, also abbreviated InSAR

or IfSAR. InSAR is an active technique with sensors that transmit pulses of electromagnetic energy and record the backscattered signal to derive the spatial position of the survey target. InSAR sensors are usually installed on a fast moving aircraft which can also fly at high altitudes. Usually two-side looking antennas (separated by a known baseline) are mounted on it. In this “single pass” configuration, the first antenna transmits radio waves and both antennas receive the backscattered signal. This configuration enables the system to scan the same target simultaneously from two different antenna positions. Advanced SAR data processing enables the system to generate a pair of high resolution images of the same scene. Each pixel preserves amplitude and phase of the backscattered signal. That information is exploited in the interferometry process where both images are differentiated. The resulting phase differences are then unwrapped and converted to heights and finally a DEM is generated.

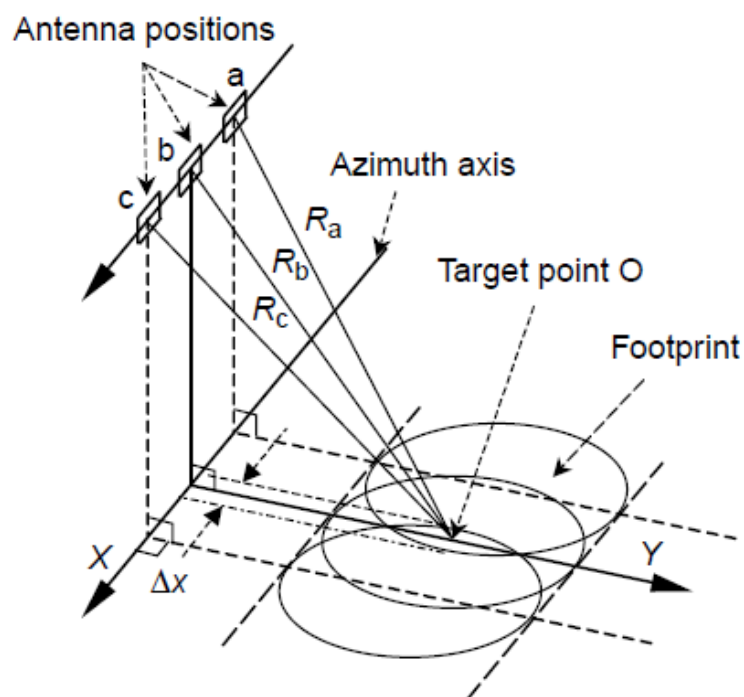


Figure 6 Imaging geometry of SAR

1.4.5 Airborne Laser Scanning (ALS) or LiDAR (Light Detection and Ranging)

ALS is a complex integrated system, consisting of a laser range finder (LRF), a computer system to control the on-line data acquisition, a storage medium, a scanner, and a GPS/INS system for determining the position and orientation of the system. It is an active remote sensing technique where a short laser pulse is sent out, and then the deflection angle and the round trip time of echoes are recorded (Lemmens, 2007). Multiplying this round trip time by the group velocity of the laser, the estimation of the 3-D coordinates of the scanned targets is allowed. LiDAR is composed by three components:

- the aircraft position, determined by kinematic dual frequencies GPS, typically at 1 second
- the aircraft orientation or attitude, continually monitored by a sensitive Inertial Reference System (IRS), typically at 50 times per second
- the terrain measurement device, that emits a number of discrete laser beams (typically 50000 to 25000 per second), measuring the time taken by the beam to reflect from the ground back to the aircraft

The laser scanner consists of a pulse generator of laser and a receiver to get the signal of scattered and reflected pulses from targets (Pfeifer & Briese, 2007). The laser pulses have a wavelength in the range of 0.8μ to $1.6 \mu\text{m}$, they have duration from 4 to 5 ns and a peak energy of several millijoules. Laser pulses are emitted at a rate up to 250 kHz to the Earth surface. The distance between the LiDAR sensor and the object can be calculated by multiplying the speed of light by the time the signal takes to reach the target and return to the sensor (Wehr & Lohr, 1999).

Since all the three coordinates are observed at the same time, one single scan is sufficient to compute a three-dimensional point cloud of the whole object if it is visible from one viewpoint.

Today LiDAR is one of the most used methods for terrain data collection and DEMs generation because data with high energy and high accuracy can be generated. In addition, it doesn't dependent on sunlight or on clear sky. LiDAR is also useful in DTM generation in urban areas because LiDAR data are free of shadow.

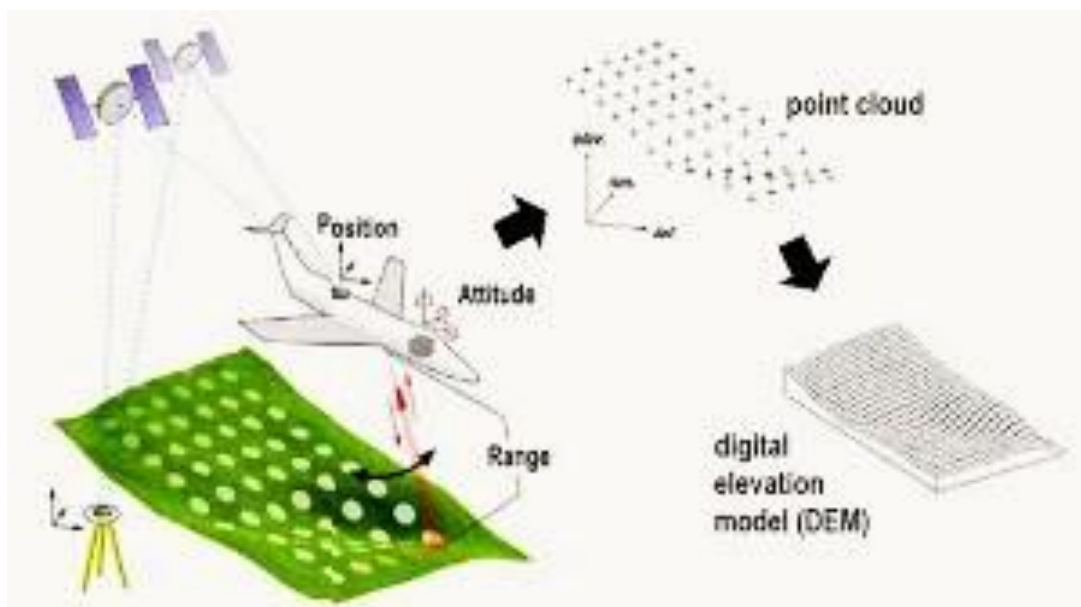


Figure 7 Principle of LiDAR

1.4.6 Comparison between DEM data acquired through different techniques

Each of the acquisition techniques described in the present chapter has its advantages and disadvantages. Therefore the choice of a method will be based on the purpose, for which the data will be used, accuracy and time requirements, price etc. A comparison between these methods is shown in the following table (Li et al., 2005).

In terms of measurement accuracy, can be seen that the most accurate are the ground surveying and LiDAR techniques which corresponds to the cost. At the same time, other disadvantage of the ground surveying is the small coverage domain for more time and its labor intensiveness, while the LiDAR can measure large areas very fast. Even if in cartographic digitalization human work is needed during the raster and vector conversion, as well as when the scanning process is automated, contour maps are the major source for digital elevation modeling in countries where they are available. Concerning the area of interest, medium or large, photogrammetry is preferable because most of the processes today are automated and data acquisition is more efficient. Regarding data for production of global DEMs, LiDAR and space photogrammetry are the ones able to obtain it.

Acquisition method	Accuracy of data	Speed	Cost	Application domain
Traditional surveying	High (cm-m)	Very slow	Very high	Small areas
GPS survey	Relatively high (cm-m)	Slow	Relatively high	Small areas
Photogrammetry	Medium: from some meters to tenth of m High: from cm to dm	Fast	Relatively low	Medium to large areas
InSAR	Low (m)	Very fast	Low	Large areas
LiDAR	High (cm)	Fast	High	Medium to large areas
Map digitalization	Relatively low (m)	Slow	High	Any area size
Map scanning	Relatively low (m)	Fast	Low	Any area size
Space photogrammetry	Low to medium (m)	Very fast	Low	Large areas

Table 1 Comparison of various DEM acquisition methods

1.5 Surface Modeling and DEM Networks: GRID vs. TIN

Surface modeling of elevation data can be represented through different methods but the most used ones are Triangulated Irregular Network (TIN) and regular-grid (or elevation matrices).

A TIN is a vector based representation of the physical land surface, made up of irregularly distributed nodes and lines with three dimensional coordinates (x, y, z). They are arranged in a network of non-overlapping triangles that have different shapes and dimensions depending on the morphology of the terrain. The advantage of using TIN method for smooth areas is that it is faster for computation and needs fewer points to achieve the same accuracy.

Grids are georeferenced regular matrices of $(x_i; y_i)$ nodes, in which the elevations are stored. The horizontal coordinates of the nodes can be either in a cartographic (x: East, y: North) or geographic (x: λ , y: ϕ) projection. The horizontal spacing between nodes (the grid **resolution** Δx and Δy) is equal in both directions. When geographic coordinates are used, an equal resolution in latitude and longitude implies that the cells are no metrically squared. The storage size of a grid is inversely proportional to the squared resolution. The use of grid has the advantage of simple data storage.

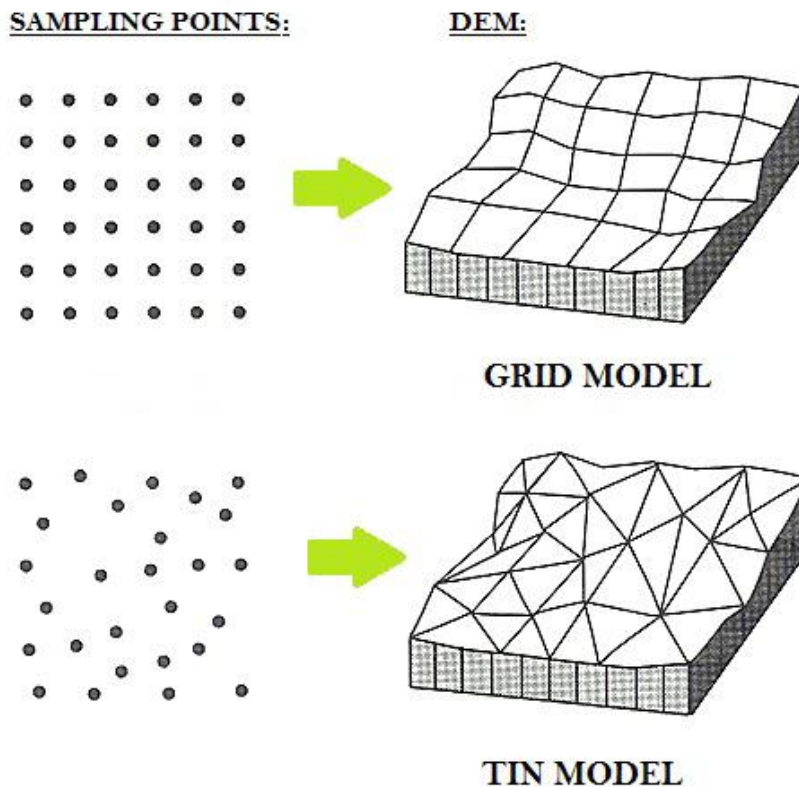


Figure 8 Different DEM representation methods: GRID and TIN

1.6 Storing formats

Since grid is a model that can be easily accessed, visualized and spatially analyzed, it is the most popular DEM representation method. The main way of storing a DEM grid is an **ASCII file** composed by two parts:

- the header containing the number of rows and columns of the matrix, the horizontal coordinates of the lower left corner of the grid, the horizontal spacing between cells (only one parameter if the cells are squared, two parameters in case Δx and Δy are different), and finally the value associated to pixels that do not have an available elevation value
- the matrix containing the elevations of all the cells composing the grid

Another very used format of storing data is **GeoTIFF** referring to TIFF files which have georeferenced data embedded as tags within the TIFF file. The geographic data can then be used to position the image in the correct location and geometry on the screen of a geographic information display. GeoTIFF is a metadata format, which provides geographic information to associate with the image data. But the TIFF file structure allows both the metadata and the image data to be encoded into the same file. The potential additional information includes map projection, coordinate systems, ellipsoids, datums, and everything else necessary to establish the exact spatial reference for the file.

1.7 Grid interpolation methods

In digital elevation modeling, interpolation is used to obtain the elevation of a point that doesn't coincide with the stored nodes.

In the **nearest neighbor** resampling method the approach assigns the value of the closest input pixel (in terms of coordinate location) to the corresponding output pixel. The advantages of nearest neighbor include simplicity and the ability to preserve original values in the unaltered scene. The disadvantages include noticeable position errors, especially along linear features where the realignment of pixels is obvious.

Bilinear interpolation is done by assigning the average value of the four pixels closest to the input pixel (in a 2x2 window) to the corresponding output pixel.

In **bicubic interpolation** the average value of the sixteen pixels closest to the input pixel (in a 4x4 window) is assigned to the corresponding output pixel. Cubic convolution is considered as the most accurate of the three methods but it requires more computation time.

1.8 Quality of DEMs

Once a DEM has been created, it is important to estimate its quality, which is related to the resolution, and consists of the components accuracy and reliability.

The **accuracy** of a DEM is the degree of closeness of measurement of the attribute value (for instance, the height value) to its actual true value.

The **reliability** is the consistency of a set of measurements, often used to describe a test, and it is inversely related to random error.

The accuracy is one of the most important features regarding a DEM and it depends on a variety of factors (Karel et al., 2006):

- the source of the elevation data, which includes the techniques used for measuring the elevation, the locations and the density of samples
- the methods used to construct the DEM from elevation data
- the data model, which can be a grid, contour lines, or a triangulated irregular network
- the topographic complexity of the landscape being represented
- the algorithms used to calculate different terrain attributes

1.9 Different spatial scales of DEMs

Depending on the specific need, the size of the area that the user has to describe and the level of accuracy that he wants to obtain, different kinds of DEMs can be used. If a big portion of the Earth surface has to be studied, like an entire region or an entire country, but with low details, a global DEM can be used; on the contrary local DEM can be adopted when there is the need to analyze a small portion of the surface but with high details. In general grid DEMs can be divided into three main categories:

- global DEMs which cover the whole Earth surface and are usually characterized by low resolution and accuracy
- national/regional DEMs which cover an entire nation or region and are characterized by low/medium resolution and accuracy
- local DEMs which cover small portions of the Earth surface (a river bank, a landslide area, etc.) and are characterized by high accuracy and resolution

It is very difficult or almost impossible to be satisfied together both requirements of large coverage and high accuracy. Usually a global DEM are obtained by SAR data and in some cases by photogrammetry.

1.10 Open Data

DEMs can be produced with different purposes and used for private or released for public services. The global models used in the present work are considered as Open data which is described in the following lines.

Open Source Geospatial Foundation (OSGeo) is the main organization that deals with OpenData. It provides financial, organizational and legal support to the open source geospatial community in which the members can contribute code, funding and other resources and their contributions will be maintained for public benefit. OSGeo also provides a common forum and shared infrastructure for improving cross-project collaboration. The foundation's projects are all freely available and useable under an OSI-certified open source license.

OSGeo Mission Statement is to support the collaborative development of open source geospatial software, and promote its widespread use. The following more detailed goals support the overall mission (“About the Open Source Geospatial Foundation | OSGeo.org,” n.d.):

- To provide resources for foundation projects - eg. infrastructure, funding, legal.
- To promote freely available geodata - free software is useless without data.
- To promote the use of open source software in the geospatial industry (not just foundation software) - eg. PR, training, outreach.
- To encourage the implementation of open standards and standards-based interoperability in foundation projects.
- To ensure a high degree of quality in foundation projects in order to build and preserve the foundation "brand".
- To make foundation and related software more accessible to end users - eg. binary "stack" builds, cross package documentation.
- To provide support for the use of OSGeo software in education via curriculum development, outreach, and support.
- To encourage communication and cooperation between OSGeo communities on different language (eg. Java/C/Python) and operating system (eg. Win32, Unix, MacOS) platforms.
- To support use and contribution to foundation projects from the worldwide community through internationalization of software and community outreach.
- To operate an annual OSGeo Conference, possibly in cooperation with related efforts (eg. EOGEO).

- To award the Sol Katz award for service to the OSGeo community.

Since the previous technologies have been implemented and improved to measure the Earth Surface and, in some way, to facilitate these data in regions where maps do not exist, the possibility to share them for free is considered by the following definition of Open Data that says:

“Open data and content can be freely used, modified, and shared by anyone for any purpose.” (“The Open Definition, Open Content and Open Knowledge,” n.d.)

Chapter 2

2 Global (low resolution) Digital Elevation Models (DEMs)

This chapter explains three of the most important and well-known Digital Elevation Models regarding to a global scale. They are categorized as low resolution ones when are compared with the local model. Nevertheless, taking into account that the acquisition is done for almost the entire Earth's surface could be said that these models (especially ASTER and SRTM) generate a high resolution database. Moreover, the purchase of the products is for free since they are considered as Open data.

2.1 Advanced Spaceborne Thermal Emission and Reflection Radiometer (ASTER)

Terra (previously AM-1) is the first Earth Observing System (EOS) satellite launched into Earth orbit by NASA on December 18, 1999. The satellite, crossing the equator at about 10:30 AM local time each day (and night), flies in a Sun-synchronous orbit which means that the angle between the Sun and the Earth's surface remains relatively constant in order to allow consistent scientific observations (Thome, n.d.). On February 24, 2000, Terra began collecting data that will become a new, 15-year global data set about the state of the atmosphere, land, oceans, and their interactions with one another and with solar radiation. Also, the instruments on Terra examined the changing composition of the atmosphere, including aerosol pollution and concentration of carbon dioxide, that has increased by about 20% as result of industrialization, in order to meet the increasing interest in global warming and declining levels of ozone (both globally and in the ozone "hole" in the Antarctic).

The Advanced Spaceborne Thermal Emission and Reflection Radiometer (ASTER) is one of a number of state-of-the-art instrument sensor systems on-board Terra along with CERES, MISR, MODIS and MOPITT, all designed to collect surface data in order to monitor the state of Earth's and climate changes.

ASTER provides data with wide spectral coverage and relatively high spatial resolution that enable to improve understanding of the local and regional scale processes occurring on or near the earth's surface and lower atmosphere, including surface-atmosphere interactions. The data are collected in 14 spectral bands with resolution ranging between 15 to 90 meters, depending on the telescope (Abrams & Hook, 2002):

- VNIR (visible and near-infrared) sensor provides 3 bands at 15 meter resolution.

- SWIR (shortwave infrared) sensor provides 6 bands at 30 meter resolution.
- TIR (thermal infrared) sensor provides 5 bands at 90 meter resolution.

The swath width for all sensors is 60 kilometers.

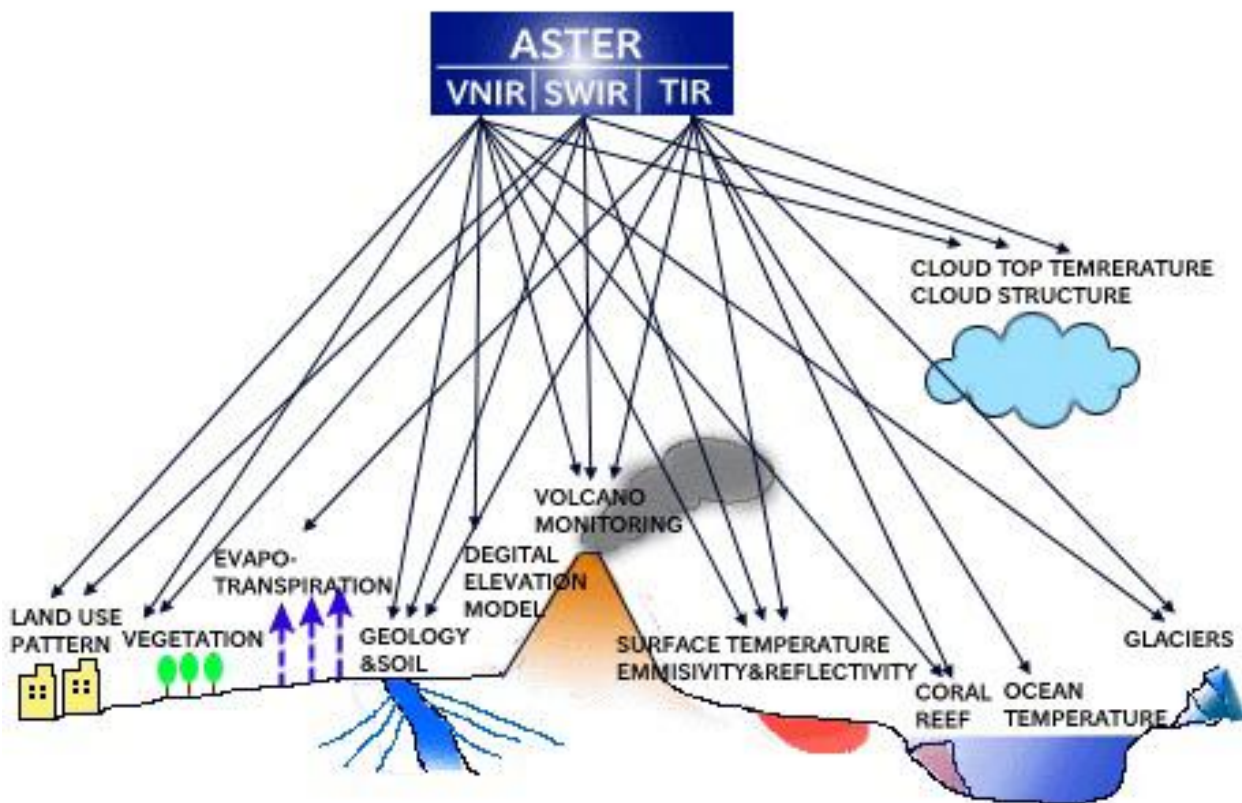


Figure 9 ASTER subsystems and their applications

ASTER data are distributed from the Land Processes Distributed Active Archive Center. They are available in the Universal Transverse Mercator (UTM) projection, with a resampling method of cubic convolution for daytime scenes and nearest neighbor for nighttime scenes.

Files are in the HDF-EOS or GeoTIFF format with the exception of ASTER Level-3 products, which are available in GeoTIFF format only. The available products and services are the following (“Advanced Spaceborne Thermal Emission and Reflection Radiometer (ASTER) | The Long Term Archive,” n.d.):

- Level-1 Reconstructed Unprocessed Instrument Data
- Level-2 Registered Radiance at the Sensor
- Level-2 On-Demand Decorrelation Stretch (VNIR, SWIR & TIR)
- Level-2 Brightness Temperature (TIR)
- Level-2 Surface Emissivity (TIR)

- Level-2 Surface Reflectance (VNIR & SWIR)
- Level-2 Surface Reflectance Crosstalk-Corrected (VNIR & SWIR)
- Level-2 Surface Kinetic Temperature (TIR)
- Level-2 Surface Radiance (VNIR, SWIR & TIR)
- Level-2 Surface Radiance Crosstalk-Corrected (VNIR & SWIR)
- Level-2 Polar Surface and Cloud Classification (VNIR)
- Level-3 ASTER DEM; created from Level 1A data (VNIR)
- Level-3 ASTER Orthorectified; created from Level 1A data (VNIR)
- Level-3 ASTER DEM and Orthorectified; created from Level 1A data (VNIR)
- Level-4 ASTER Global Digital Elevation Model (DEM) – WIST: Log-in as Registered User

ASTER data contributes to a wide array of global change-related application areas including vegetation and ecosystem dynamics, hazard monitoring, geology and soils, hydrology, and land cover change.

ASTER Global Digital Elevation Model

The 4th Level product of ASTER is the GDEM which was developed in cooperation of the U.S. National Aeronautics and Space Administration (NASA) and Japan's Ministry of Economy, Trade, and Industry (METI).

ASTER is capable of collecting in-track stereo using nadir- and aft-looking near infrared cameras. Since 2001, these stereo pairs have been used to produce single-scene (60 x 60 km) digital elevation models (DEM) having vertical accuracies in term of root mean squared error (RMSE) generally between 10 and 25 m (“ASTGTM | LP DAAC :: NASA Land Data Products and Services,” n.d.).

Stereo-correlation is used to produce over one million individual scene-based ASTER DEMs, to which cloud masking is applied to remove cloudy pixels. All cloud-screened DEMs are stacked and residual bad values and outliers are removed. Selected data are averaged to create final pixel values, and residual anomalies are corrected before partitioning the data into 1 x 1 degree tiles.

Stereo-pair images collected by the ASTER instrument onboard Terra were used for the generation of the first version of the ASTER GDEM, released in June 2009. The ASTER GDEM covers land surfaces between 83°N and 83°S which is 99 percent of Earth's landmass. It is consisted of 22'702 tiles and these of them that contain at least 0.01% land area are included as well (Tachikawa, Kaku, Iwasaki, & Gesch, 2011). ASTER data are available in geographic

coordinates, referenced to the 1984 World Geodetic System (WGS84)/ 1996 Earth Gravitational Model (EGM96) geoid and posted on a 1 arc-second (approximately 30 m) grid.

The improved ASTER GDEM V2, released on October 17, 2011, adds 260'000 additional stereo-pairs, improving coverage and reducing the occurrence of artifacts, e.g. step, pit-in-bump, mole-run, etc. which mostly disappear.

Voids are decreased in northern area and lakes are perfectly flat thanks to new water body detection algorithm. The ASTER GDEM V2 maintains the same gridding and tile structure as V1, with 30 m postings and 1 x 1 degree tiles (Tachikawa, Hato, Kaku, & Iwasaki, 2011).

Version 2 is significantly improved over the previous release, e.g. improved spatial resolution, increased horizontal and vertical accuracies. The data still may contain anomalies which can introduce large elevation errors on local scales.

As a contribution from METI and NASA to the Global Earth Observation System of Systems (GEOSS), ASTER GDEM V2 data are available free of charge to users worldwide from the Land Processes Distributed Active Archive Center (LP DAAC) and J-spacesystems (“ASTER Global Digital Elevation Map,” n.d.). The data are available in GeoTIFF format and could be obtained through these URL:

<http://gdex.cr.usgs.gov/gdex/>

<http://earthexplorer.usgs.gov/>

(“Global Data Explorer (Powered by GeoBrain),” n.d.)

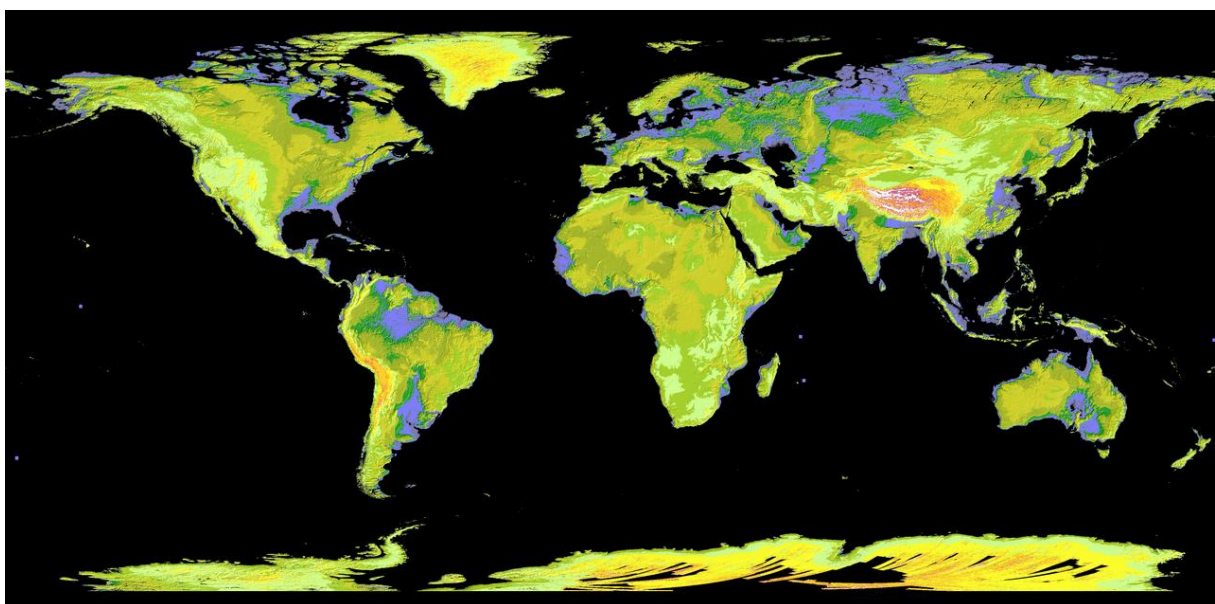


Figure 10 ASTER global DEM

2.2 Shuttle Radar Topography Mission (SRTM)

The Shuttle Radar Topography Mission (SRTM) is an international joint project developed by The National Aeronautics and Space Administration (NASA) and the National Geospatial-Intelligence Agency (NGA), aimed to acquire radar data and to create the first near-global set of land elevations. SRTM was flown aboard the STS-99 mission of the space shuttle Endeavour which launched February 11, 2000. It orbited Earth 16 times each day during the 11-day mission, completing 176 orbits (“SRTMGL1 | LP DAAC :: NASA Land Data Products and Services,” n.d.).

At first on board the Endeavour were flown the C-band Spaceborne Imaging Radar and the X-Band Synthetic Aperture Radar (X-SAR), respectively in April and October 1994. For the purpose of the SRTM the technology, based on the one created for the previous two missions, was developed to use a single-pass interferometry, which compared two radar images or signals at the same time, taken at slightly different angles by two different radar antennas. An antenna located on board the space shuttle collected one data set and the other data set was acquired by an antenna located at the end of a 60-meter mast that was extended from the shuttle, as shown on the next figure (“Shuttle Radar Topography Mission (SRTM) Void Filled | The Long Term Archive,” n.d.).

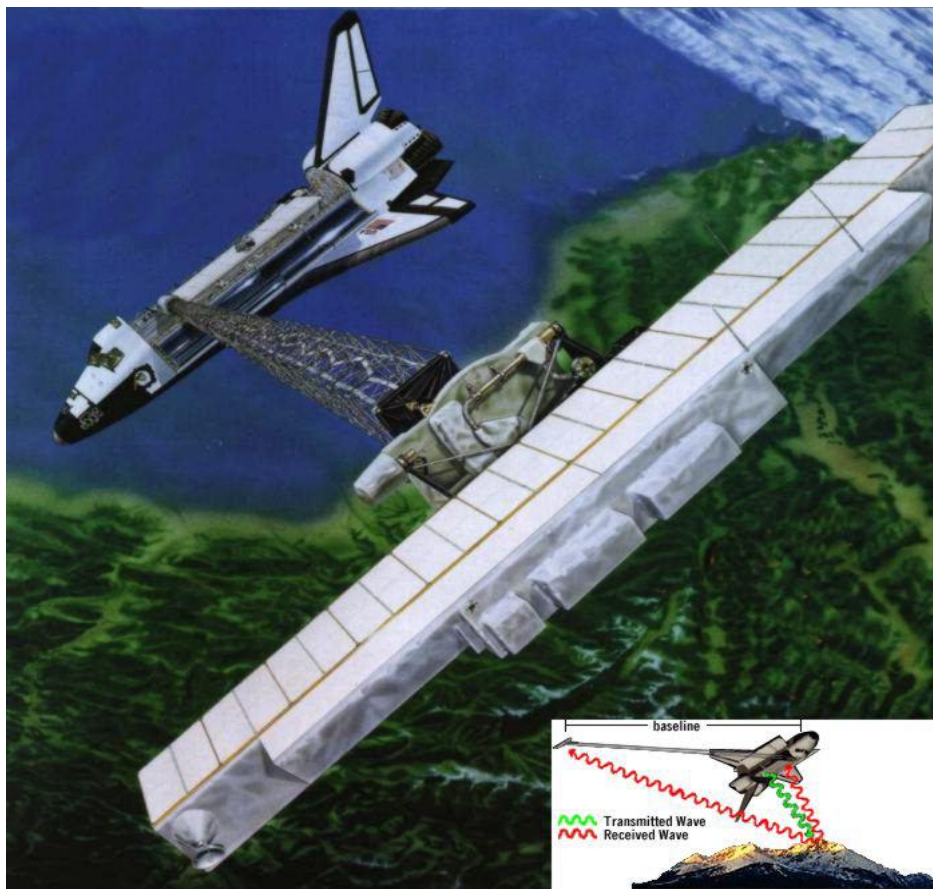


Figure 11 SRTM configuration: the main antenna sends the signal, both main and outboard antenna receive the backscattered signal.

The antenna pairs operating in C-band and X-band were simultaneously illuminated and recording radar signals. The first transmitted and received microwave pulses. The second antenna acted as a receiver. With this configuration, in which two antennas received and reflected radar pulses at the same time, single pass interferometry was allowed and respectively a calculation of surface elevation through differences between the two signals.

The instrument operated almost flawlessly and imaged 99.96% of the targeted landmass at least one time, 94.59% at least twice and about 50% at least three or more times within a 222.4-hour period. The goal was to image each terrain segment at least twice from different angles (on ascending, or north-going, and descending, or south-going, orbit passes) and the areas shadowed from the radar beam by terrain to be filled in.

In result, data about 80% of the Earth's land surface between 60° north and 56° south latitude were collected successfully (“Shuttle Radar Topography Mission,” n.d.-a). The data are posted on a Lat/Lon grid and are referenced to the WGS84 horizontal and EGM96 vertical datum with accuracy in elevation of about 16 m and in planimetry of about 20 m.

The derived products are two DTMs at resolution level of 1 arc-second (approximately 30 m) at the present available only for USA area and 3 arc-second (approximately 90 m) for worldwide coverage.

Even if the data coverage is theoretically global, some regions are missing data, because of some problems during the data collection, such as a lack of contrast in the radar image, presence of water or excessive atmospheric interference. These data holes are present along rivers, in lakes and in steep regions, for example on hillsides with a similar aspect due to shadowing. There are a total of 3'436'585 voids and its non-random distribution impeded the potential use of the SRTM data. In order to solve this problem some “filling in” algorithms have been implemented (“SRTM 90m Digital Elevation Database v4.1 | CGIAR-CSI,” n.d.).

Version 1: SRTM data were processed using the Ground Data Processing System (GDPS) supercomputer system at the NASA Jet Propulsion Laboratory. It transformed the radar echoes into a strip for each of the 1'000 swaths. These strips were eventually mosaicked into 14'549 tales 1 x 1 degree. The data were processed on a continent-by-continent basis beginning with North America and proceeding through South America, Eurasia, Africa, Australia and Islands, with the aim to reduce residual errors.

Version 2: Next, NGA applied several post-processing procedures to the NASA SRTM data. Spikes and pits were detected and voided out if they exceeded 100 m compared to surrounding elevation data. Water bodies were depicted, e.g. the ocean elevation was set to 0 and lakes of 600 m or more in length were flattened and set to a constant height (Farr & Others, 2007). Following these "finishing"

steps data were returned to NASA for distribution to the scientific and civil user communities as well as the public.

Version 3: Elimination of the voids in the NASA SRTM DEM was the primary goal of a project under the NASA MEaSUREs (Making Earth System Data Records for Use in Research Environments) Program. Ultimately this was achieved by filling the small voids by interpolation of elevation data primarily from the ASTER GDEM2 (Global Digital Elevation Model Version 2) and secondarily from the USGS GMTED2010 elevation model or the USGS National Elevation Dataset (NED), while large voids were left in the data (“Shuttle Radar Topography Mission,” n.d.-b).

The SRTM 90m DEM’s are available for download in both Arc-Info ASCII format, and as GeoTIFF, for easy use in most GIS and Remote Sensing software applications. In addition, a binary Data Mask file is available for download, allowing users to identify the areas within each DEM which has been interpolated. The data are available online from U.S. Geological Survey (USGS) and could be obtained through this URL:

<http://gdex.cr.usgs.gov/gdex/>

(“Global Data Explorer (Powered by GeoBrain),” n.d.)

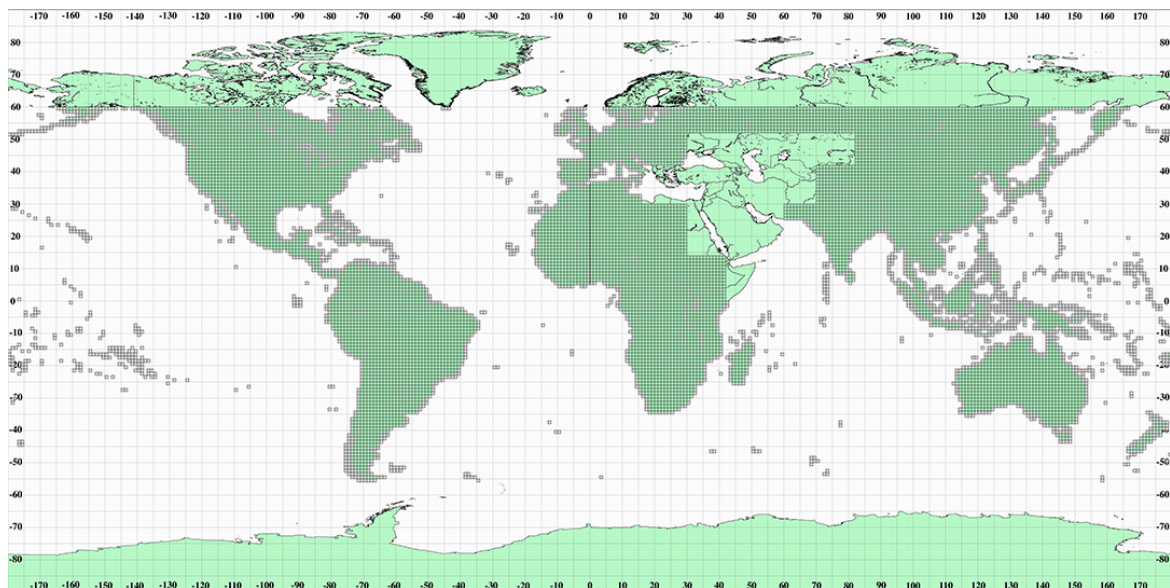


Figure 12 SRTM global DEM

2.3 Global Multi-resolution Terrain Elevation Data 2010 (GMTED2010)

The Global Multi-resolution Terrain Elevation Data 2010 (GMTED2010) is a global elevation model developed by the U.S. Geological Survey (USGS) in collaboration with the National Geospatial-Intelligence Agency (NGA) with the aim to replace the Global Topographic Data GTOPO30. The previous model has horizontal resolution of 30 arc-seconds for the entire Earth and provided elevation data that widely vary in quality (Danielson & Gesch, 2011).

For its enhancement the following data sources were included: global Digital Terrain Elevation Data (DTED) from the Shuttle Radar Topography Mission (SRTM), Canadian elevation data, Spot 5 Reference3D data, and data from the Ice, Cloud, and land Elevation Satellite (ICESat).

The new model has been generated at three separate resolutions (lately called products) of 30 arc-second (about 1 km), 15 arc-second (about 500 m) and 7.5 arc-second (about 250 m). This new product suite provides global coverage of all land areas from 84°N to 56°S latitude for most products, and coverage from 84°N to 90°S latitude for several products (“Global Multi-resolution Terrain Elevation Data 2010 (GMTED2010) | The Long Term Archive,” n.d.). Some areas, namely Greenland and Antarctica, do not have data available at the 15- and 7.5-arc-second resolutions because the input source data do not support that level of detail.

The data are in a geographic coordinate system referenced to the WGS84 horizontal datum, with the horizontal coordinates expressed in decimal degrees. The vertical units for the elevation values are integer meters, referenced in most cases to the EGM96 geoid as vertical datum.

The estimated global vertical accuracy of GTOPO30 provided by NGA in term of RMSE is 66 m while the one of GMTED2010 is essentially improved to the value of 6 m. For each product the values of the RMSE are presented in the following table:

Resolution of the product	RMSE range
GMTED2010, 30 arc-second resolution	varies between 25 and 42 m
GMTED2010, 15 arc-second resolution	varies between 29 and 32 m
GMTED2010, 7.5 arc-second resolution	varies between 26 and 30 m

Table 2 Vertical accuracies of the GMTED2010 products

In areas where new sources of higher resolution data were available, the GMTED2010 products are substantially improved. On the contrary, in areas above 60° N latitude the lack of good elevation data still exists.

An additional advantage of the new multi-resolution global model over GTOPO30 is that seven new raster elevation products are available at each resolution, in total 21. They have been produced using the following aggregation methods (Danielson & Gesch, 2011):

1. Minimum elevation map
2. Maximum elevation map
3. Mean elevation
4. Median elevation

The first 4 maps have been produced using the corresponding (to the name of the map) elevation as an aggregation method, i.g. subtracts respectively the minimum/maximum/mean/median value from the processing window.

On the figure down is shown an example, which presents the principle applied for the minimum, maximum, mean and median aggregation methods.

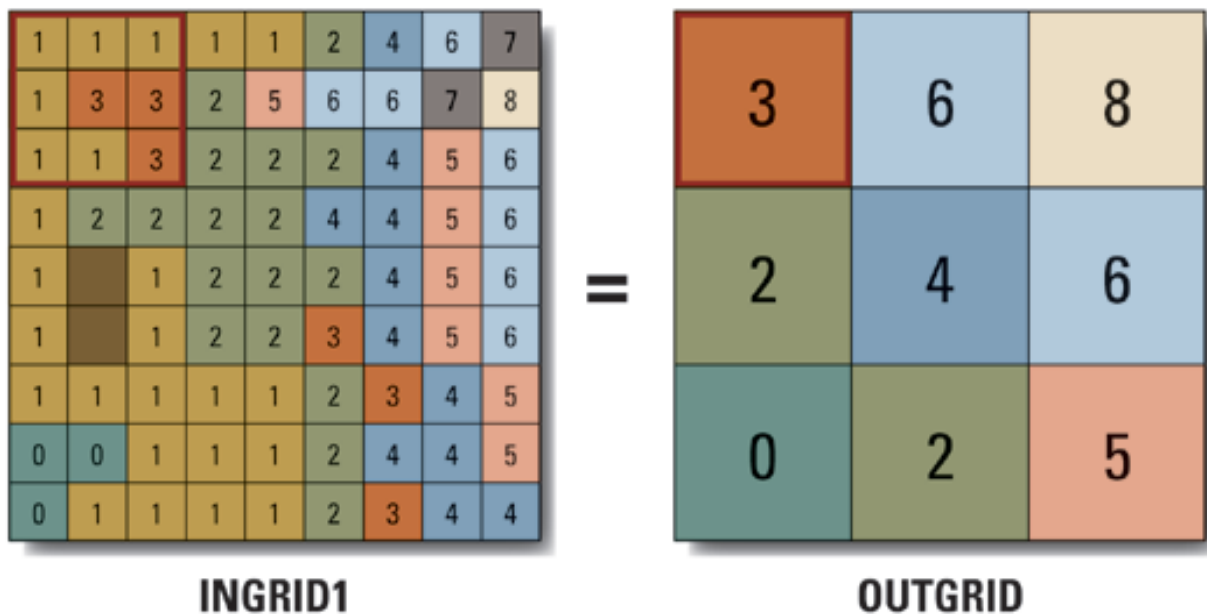


Figure 13 Example of implementing maximum aggregation method; applicable as well for minimum, mean and median methods.

5. Standard deviation map: It has been produced using a combination of two functions in ArcGIS. A Blockstd function finds the standard deviation for the specified posts defined by the neighborhood blocks and sends the computed standard deviation to the post location in the corresponding

blocks on the output raster grid. An example is shown on the next figure. The Blockstd output was then generalized to the desired output resolution of 30, 15 or 7.5 arc-second using neighbor resampling.

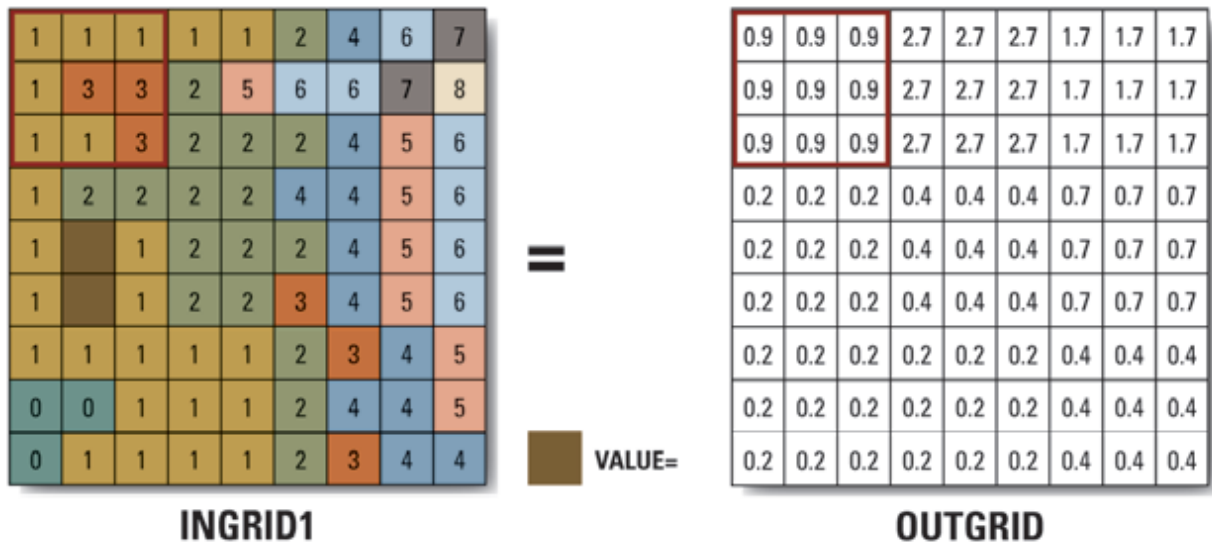


Figure 14 Example of implementing a Blockstd function applied for the creation of Standard deviation map

6. Systematic subsample map: It was defined using a nearest neighbor resampling function, whereby an actual elevation value is extracted from the input source at the center of a processing window.
7. Break-line emphasis map: It was used to produce reduced resolution products that maintain stream (channel) and ridge (divide) characteristics as delineated in the full resolution source data. Break-line emphasis maintains the critical topographic features within the landscape by maintaining any minimum elevation or maximum elevation value on a break-line that passes within the specified analysis window. Remaining elevation values are generalized using the median statistic. The break-line emphasis methodology can be summarized into three steps:
 - a) Topographic break-lines (ridges and streams) are extracted from the full resolution DEM and then used to guide selection of generalized values.
 - b) Full resolution streams are automatically thresholded, which enables easy extraction of the level one through five Strahler stream orders.
 - c) Full resolution ridges are extracted by selecting the flow accumulation values that are equal to zero. Using focal and block image processing functions, ridges are thinned so that only critical divides are maintained.

The new products will be used in a variety of application situations. For example, the maximum elevation product could be used for the global calculation of airport runway surface heights or to determine the height of vertical obstructions. The minimum elevation product is useful for determining stream channel areas and the water surface. Comparison of the minimum and maximum products will provide a measure of the local relief in a given area. The standard deviation product provides a measure of the texture, or local variation in elevation, of the landscape surface. The break-line emphasis products will be useful for most hydrologic modeling that involves watershed extraction and surface streamlines routing. The remaining products, specifically the mean and systematic subsample products, will be useful for general visualization exercises and all-purpose morphological processing.

The data are available online in GeoTIFF format from U.S. Geological Survey (USGS) and could be obtained through this URL:

<http://earthexplorer.usgs.gov/>

(“EarthExplorer,” n.d.)

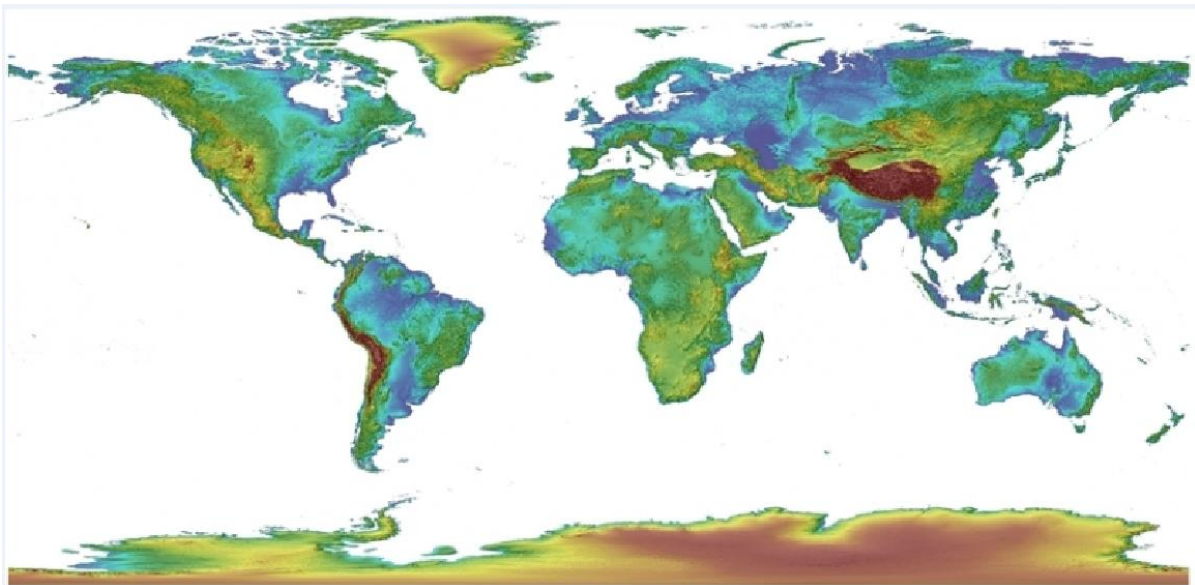


Figure 15 GMTED2010 global DSM

The three DEMs required for this study are considered as Open data (described in Chapter 1) so they have been downloaded for free from the subsequent links (“Global datasets - GRASS-Wiki,” n.d.):

ASTER: <http://gdex.cr.usgs.gov/gdex/>

SRTM: <http://gdex.cr.usgs.gov/gdex/>

GMTED: <http://earthexplorer.usgs.gov/>

In Chapter 5 the download process (for each Digital Elevation Model) is explained step by step.

Chapter 3

3 Local (high resolution) HELvetia-Italy Digital Elevation Model (HELI-DEM)

This chapter presents the HELI-DEM project, the collected data and all the pre-processing steps that have been done on it in order to be used for the producing of the unified DTM, as well as the main operations of creating the local HELI-DEM. This model is considered as a high resolution DEM when is compared with the global ones. HELI-DEM has been developed as a research project and it covers the whole alpine area between Italy and Switzerland.

3.1 Overview and Mission

Because of the management problems of geographic data between two cross border regions, many countries produce their own DEMs. In that way both Italy and Switzerland did so but there are a lot of differences between the elevation data, reference frames technologies, accuracies, resolutions, etc. HELI-DEM (HELvetia-Italy Digital Elevation Model) has been developed with the aim to create a unified DEM for the area of Italian and Swiss Alps. It is a project that has been funded by the European Regional Development Fund (ERDF) and the following institutions has been involved: Fondazione Politecnico di Milano, Politecnico di Milano, Politecnico di Torino, Regione Lombardia, Regione Piemonte, Scuola Universitaria della Svizzera Italiana and as external partners: SwissTopo and the IGMI (Istituto Geografico Militare Italiano).

HELI-DEM covers two regions in Italy – Lombardy and Piedmont and two cantons in Switzerland – Ticino and Grisons. The area of interest involves mainly the Alps but also some subalpine parts are considered so that the height difference varies till more than 4500 m.

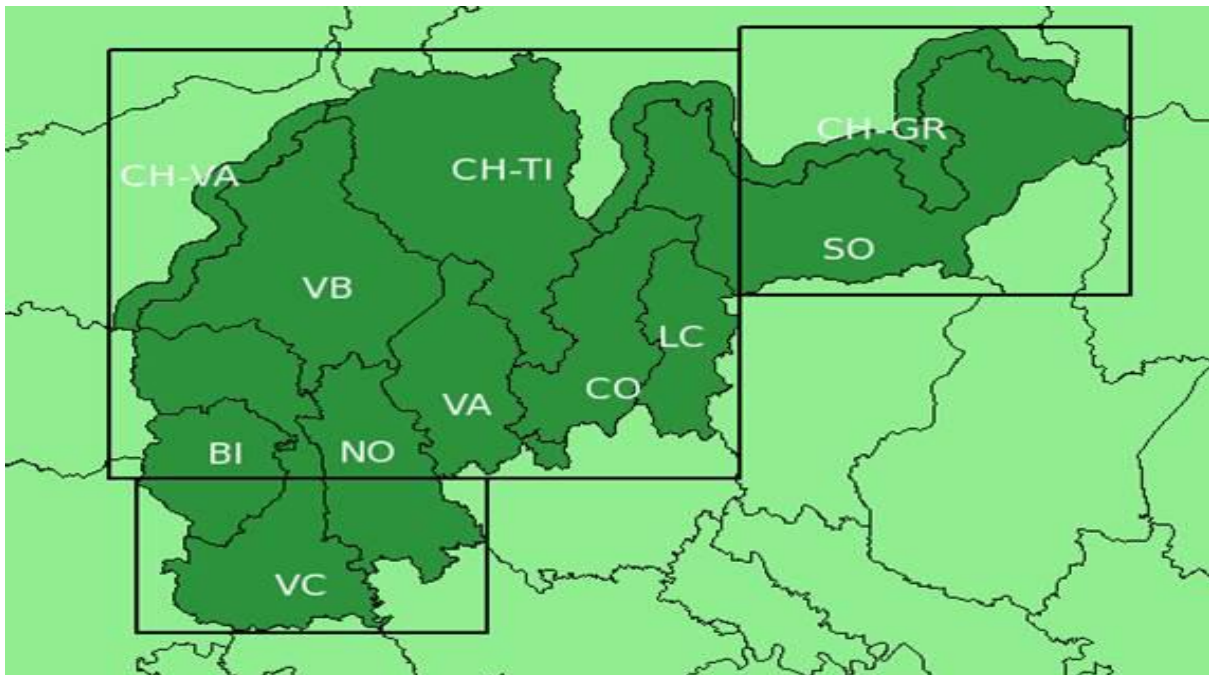


Figure 16 Area of interest of HELI-DEM project: Lombardy and Piedmont Italian Regions and Ticino and Grisons Swiss Cantons

The following operations have been realized in order to produce the HELI-DEM product (Biagi et al., 2014). They are explained more detailed in the next pages.

- Collection and analysis of all the elevation data available (DTMs, GPS data, geoid data, etc.)
- Cross-check of the existing geoids and recomputation of a unified geoid that covers the area of the project
- Creation of a cross-border GNSS permanent network aimed to collect punctual high accuracy data for the validation and georeferencing of the data
- Cross-check of the DTMs including internal cross-validation and external validation with higher accuracy elevation data
- Integration of all the available and already validated DTMs to create the final unified DTM
- Implementation of algorithms to correct the unified low resolution DTM with the higher resolution data.

3.2 Preprocessing of HELI-DEM data

Collection of the available elevation data

First of all the available data have been collected:

- some medium/low resolution local DTMs as the **regional DTMs of Lombardy and Piedmont** (from at least 50 m till 5 m planimetric resolution), released by the regional Italian authorities and the **national Swiss DTM** released by SwissTopo (25 m)
- two high resolution DTMs (1 m) realized through LiDAR techniques: the first one produced by the Piedmont Region that covers the whole Piedmont area and the other is named PST-A DTM, released by the Italian Ministry of Environment under the Piano Straordinario di Telerilevamento Ambientale (Extraordinary Plan of Environmental Remote Sensing) that covers the hydrographic basins of Lombardy and Piedmont

The coverage of the local DTMs collected for the HELI-DEM project are shown on the figure:

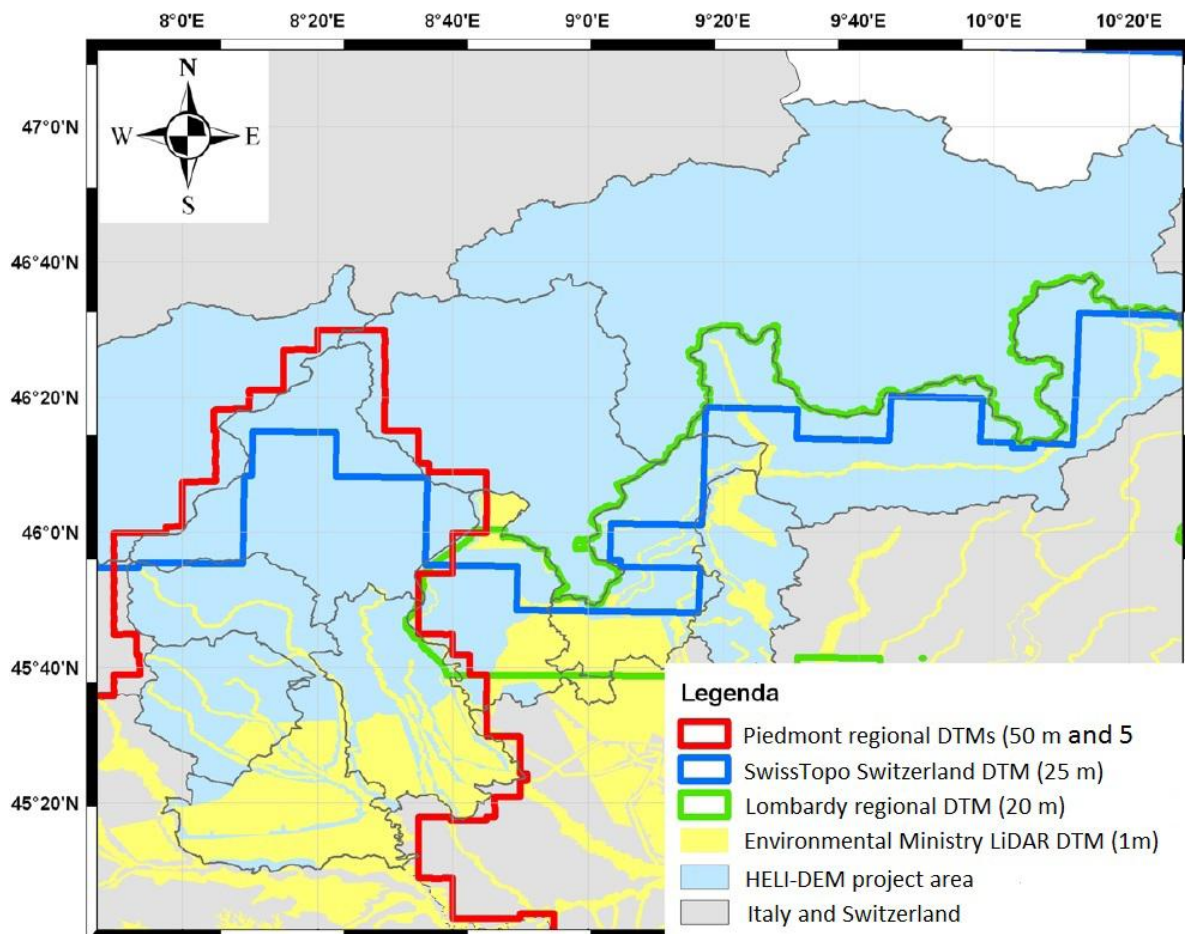


Figure 17 Coverage of the local DTMs collected for the HELI-DEM project

In addition also geoid data are collected and some other elevation data as previously surveyed GNSS markers.

The data collected for the project can be divided in two categories: DTMs derived from cartography and DTMs acquired by LiDAR techniques. The first ones are usually characterized by low vertical accuracies (meters or tens of meters) and low resolution (tens of meters) but they cover big portion of the territory while the second group models have higher vertical accuracies (some decimeters) and high spatial resolution (1 m) but they cover small portions as rivers, lakes, etc.

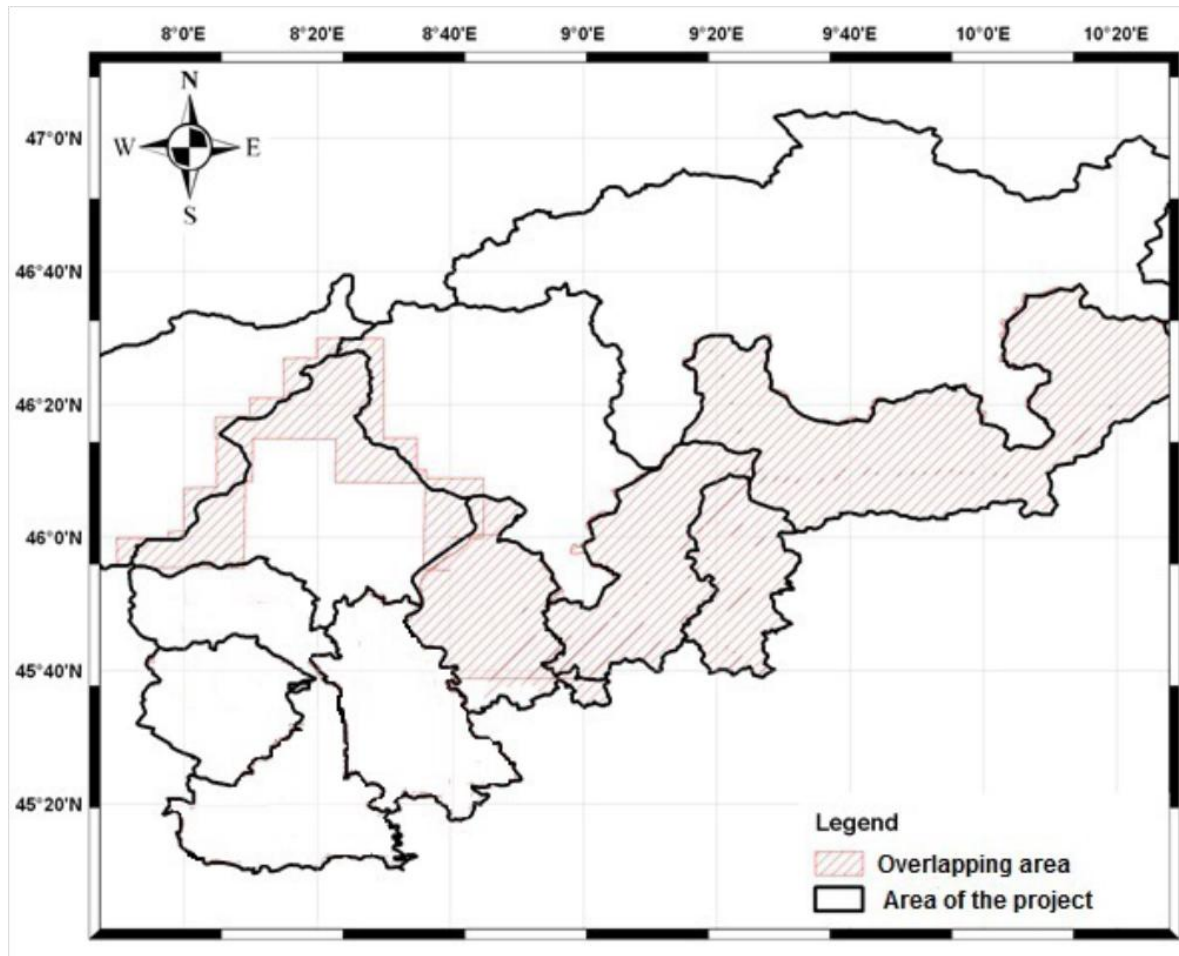


Figure 18 Overlapping areas of the DTMs collected for the HELI-DEM project

The figure above shows where at least two or more DTMs exist and that area is 24% of the whole project territory.

All the collected DTMs are stored in ASCII grids with an assigned cell size. The regional DTMs of Piedmont and Lombardy are in cartographic coordinates ($\Delta E; \Delta N$) and DTM of Swiss and LiDAR are in geographic coordinates ($\Delta \phi; \Delta \lambda$).

The various models are available in different reference frames as following:

- Low resolution
 - Lombardy regional DTM, 20m – Roma40
 - Piedmont regional DTM, 50m – WGS84 - IGM95 (ETRF89)
 - SwissTopo DTM, 25m – ETRF89
- Medium and high resolution
 - High Resolution Piedmont regional DTM, 5m – WGS84 - IGM95 (ETRF89)
 - High resolution Ministry of Environment PST-A LiDAR DTM, 1m – WGS84 - IGM95 (ETRF89)

Also the main available models of the geoid have been collected in the full accurate version. They are recently realized and have different reference frames and resolution. The data cover the same area (45°N - 47°N in latitude and 7°E - 11°E in longitude) and they are stored in ESRI grid format.

- The official Italian geoid **Italgeo2005** that covers the territory of Italy and some small neighbor areas. It is consistent with the altimetric national model of IGMI, with the zero reference height on the Genoa marigraph. The vertical accuracy of the model is about 10 cm and the resolution is 3' (5 km).
- The official Swiss geoid **CHGeo2004** that has been regularized using local models of the neighboring countries. It has a precision of the order of 2-3 cm and a resolution of 30'' (less than 1 km).
- The global model of the Earth gravitational field **EGM2008** that has a resolution of 5' (10 km) and a vertical accuracy of the order of 5-7 cm inside the HELI-DEM area.
- The global geoid model derived by satellite observations **GOCEPWR2** that has a vertical accuracy is of about 4 cm and low spatial resolution (80 km) but since the observations have been acquired by the same instrument all over the world it does not contain biases.

Cross-check of the geoid models

The two local models Italgeo2005 and CHGeo2004 have been cross-validated. The results of the comparison have presented that at the border between Italy and Switzerland exist some inconsistencies and discontinuities. They are mainly due to the different height datum implemented in the estimation of the local geoid models that have been used during the project to convert ellipsoidal to orthometric heights (and vice-versa). Therefore, for the whole HELI-DEM area

has to be created a unique accurate (of the magnitude of few centimeters) “unbiased” geoid model. It has been done through estimation of the biases of the two local geoids by a least square adjustment and their combination collocation procedure (Carcano, 2013).

Creation of a cross-border GNSS permanent network

The next step is the implementation of the GNSS transnational reference network in order to validate the collected DTMs. An analysis of the status of already operating permanent stations able to provide data for real time positioning is needed so the ones mostly located inside the HELI-DEM area and some other of the neighbor areas have been selected. They belong to the already existing GNSS permanent networks: **GPSLombardia** (“Gps Lombardia,” n.d.) for Lombardy, **GNSSPiemonte** (“Rete GNSS Regione Piemonte,” n.d.) and **GeoTop** (only two stations) for Piedmont and **AGNES** (“AGNES,” n.d.) for Switzerland. The height where the stations are situated varies from 300 to more than 3500 m. The permanent stations of the HELI-DEM network have been adjusted in the IGS08 reference frame, with 2011.8 as reference epoch.

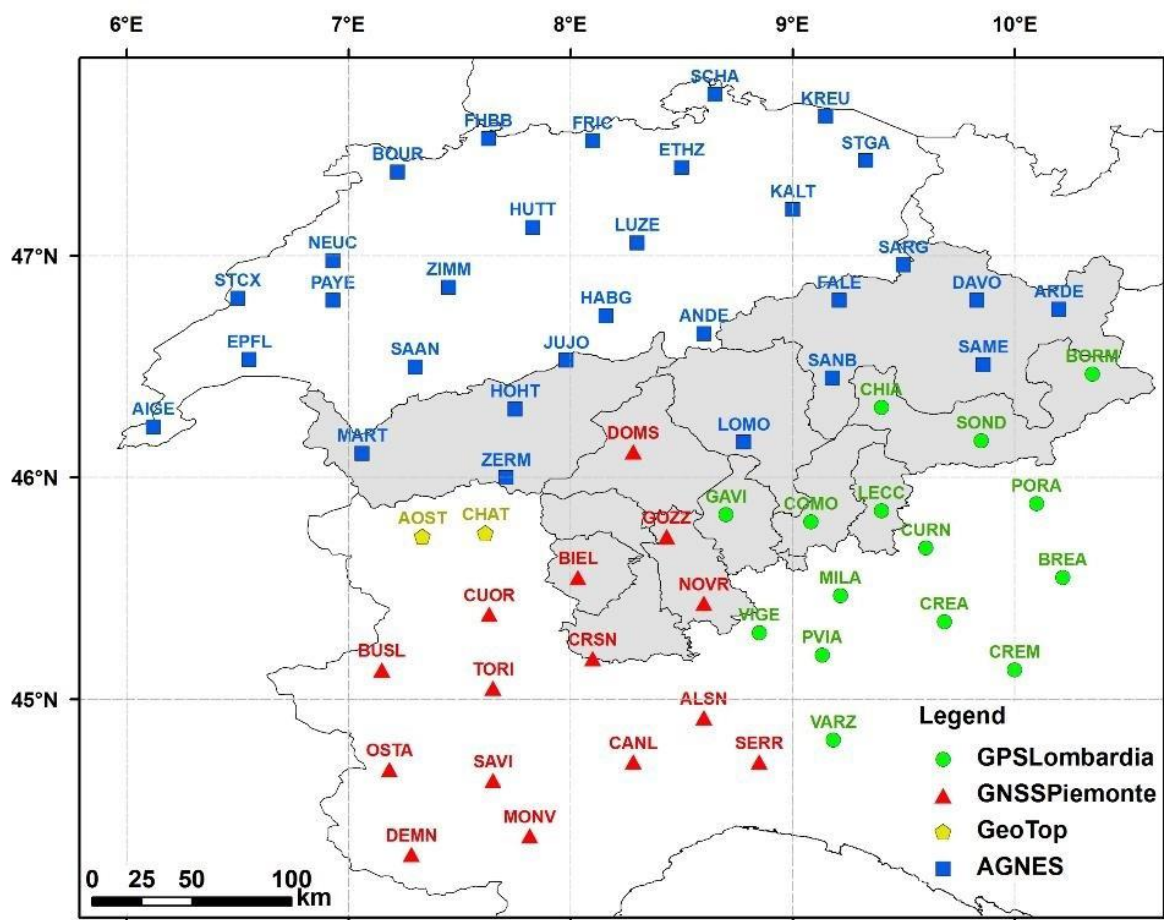


Figure 19 GNSS permanent stations inside the HELI-DEM project area (area in grey)

Transformation of DTMs into a common reference frame

As before mentioned, the DTMs are in different reference frames and before doing any cross-validation and merging, they have to be transformed into a common one. HELI-DEM project is founded by the European Community and according to the EUREF (IAG Reference Frame Sub-Commission for Europe) guidelines since the final unified DTM has a transnational extension, ETRF2000 has been chosen. In principle the transformation between ETRF89 and ETRF2000 could be avoided because the differences between different realizations of ETRFyy have a magnitude of few centimeters (very small with respect to the spatial resolution of the original DTMs and the final unified DTM). On the contrary, the transformation is not negligible in case of Roma40, because the differences between Roma40 and ETRFyy have a magnitude of hundred meters.

The program that has been used is GK2CNV developed in FORTRAN language under the GNU General Public License. GK2CNV implements the standard transformation between reference frames as written by EUREF at the European scale and IGM for Italian scale.

After a unique reference frame has been adjusted for all the available DTMs thus a check of the accuracies can be initiated through a cross-validation in order to be decided which of them can be used for the creation of the final unified DTM.

Cross-validation between DTMs with similar low resolutions

To do that two different analyses have been carried out. The first one is the cross-validation between cross-border DTMs with similar planimetric resolution and height accuracies, where they overlap, i.e. at the border between their domains. It is done for all the three possible couples between the regional DTMs (Lombardy, 20 m; Piedmont, 50m; Switzerland, 25m).

Since all of them have similar but different resolutions and accuracies no one of them can be considered as truth so the comparison has been done between randomly extracted points with a uniform spatial distribution within the area of overlapping so that the inter-distance between two nearest points in both x and y directions is of about 100 meters. Elevations have been obtained through bicubic interpolation and the elevation differences have been calculated as well. The analysis on the differences includes statistical analysis, subdivision into classes and computation of the percentage of points belonging to each class, spatial analysis of the distribution. Results and statistics of the comparison between the DTMs are similar as following:

- The statistical analysis presents that the samples are not biased or the values are not significant. The standard deviations exceed the vertical nominal accuracies of the DTMs but are comparable with them.

- In one of the comparisons the results from the classification by absolute values show that more than 80% of the points present differences smaller than 20 meters which means that the results are satisfactory, whereas, several (964) outliers ($|\Delta h| > 100\text{m}$) are present. In other case the differences smaller than 20 meters are less than 70 % and more outliers are present (4'637).
- As concerns the distribution of the samples it is analyzed that do not exist a good correspondence between the frequency curves of the height differences and the Gaussian ones computed with the same mean and standard deviation of the samples within the interval $-3\sigma \div +3\sigma$. The same statement is confirmed by the classical chi square adapting test.
- Moreover, the correlations between the differences and both elevations and slopes have been computed and none of them is significant (the both values are smaller than 0.05).

In general, the elevation differences are homogeneously distributed in the area and the anomalies are probably due to some problem during the realization of one of the DTMs (i.e. errors in the digitization of the original cartography). Moreover, Lombardy DTM contains other anomalous values in an area that has experienced severe landslides in the last years (Lat 46.40°; Lon 10.35°) (Biagi et al., 2014).

External validation of low resolution with high resolution DTMs

The second comparison, which can be considered as an external validation, has been performed between low and high resolution DTMs in the areas where the latter ones exist.

Here is analyzed in short only the comparison between the Lombardy regional DTM and PST-A LiDAR Ministry of Environment DTM. Analogous procedures have been adapted by Politecnico di Torino to the comparisons between the Piedmont regional DTM with PST-A LiDAR Ministry of Environment DTM and the Piedmont regional DTM 5 meters resolution but they are not described here in details.

Both two DTMs fall partly in the coverage of HELI-DEM project respectively: Lombardy DTM - 12'068 km² and the PST-A LiDAR DTM - 2'342 km², which doesn't allow a complete correction of the low resolution DTM through the high resolution data. The two DTMs have different reference frames, coordinate systems, resolutions and vertical accuracies but since the PST-A DTM is characterized by higher resolution and accuracy, therefore in the comparison it has been considered as truth and the regional Lombardy DTM has been transformed into ETRF89.

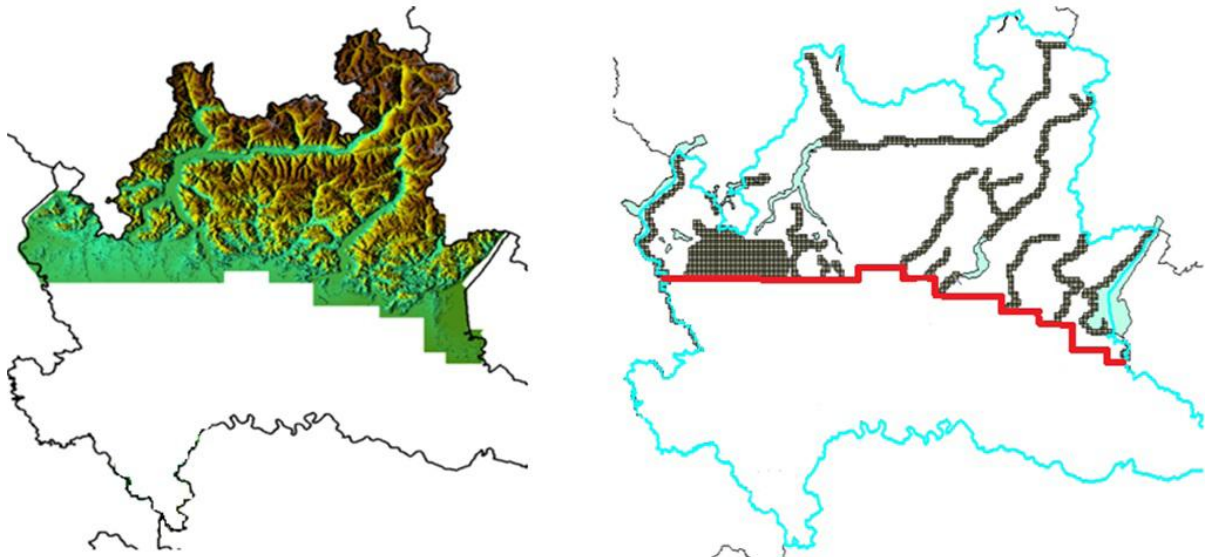


Figure 20 Area covered by the regional Lombardy DTM (on the left) and the Lombardy part of the PST-A DTM (on the right)

The result is a list of 3-D coordinates that are almost regularly spaced but no more on a regular grid. To perform the comparison, for each point from the low resolution DTM has been checked the difference between its elevation and mean of the portion ($20 \times 20 \text{ m}^2$) around the same point of the high resolution DTM.

Considering the nominal accuracies of the Lombardy DTM, the statistics of the differences are distributed as expected, with a mean smaller than one meter and a standard deviation smaller than ten meters. To verify the existence of global biases, the differences have been clustered in eight classes, according to their absolute values. The 79% of the points have a difference lower than 5 meters and only the 7% of the differences are greater than 10 meters.

Then some detailed analyses on the differences have been done as subdividing the Lombardy regional DTM on grids, other statistics, histograms and classes. Finally the existence of translations and biases of the regional DTM with respect to the local PST-A LiDAR DTM has been verified through an algorithm in MATLAB environment that has been implemented for the height of a certain point as a function of the heights of the two DTMs and the observation noises.

External validation of the DTMs through GPS data

From the comparison between the Lombardy regional DTM and the PST-A LiDAR DTM, some local biases seem to exist. In order to check if these biases are really present, the two DTMs have been externally validated, using GPS data. Two different approaches have been used.

- DTMs comparison with IGM95 benchmarks

For the comparison have been used GPS data of geodetic network IGM95 which are downloaded from the official website of IGMI (“Vertici e Capiisaldi IGM,” n.d.). Firstly the IGM95 benchmarks located in the HELI-DEM study area have been selected. In total 64 IGM95 points are available inside the area covered by the Lombardy regional DTM and 45 of them are located also inside the area of the PST-A LiDAR DTM.

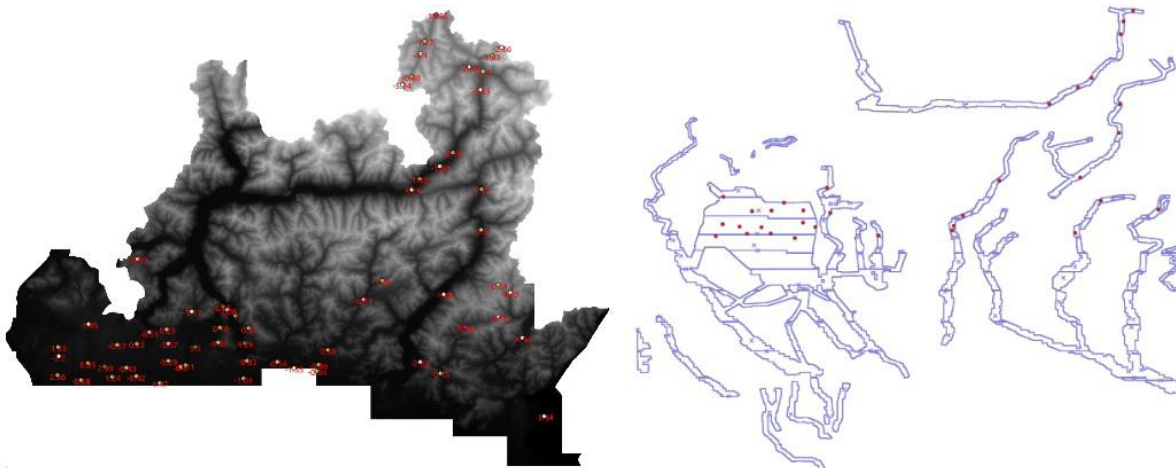


Figure 21 IGM95 points that fall inside the area of the Lombardy LR DTM (left) and inside the area of the PST-A DTM (right)

The comparison has been executed interpolating the orthometric elevation of the considered DTM on each of the selected IGM95 points. The ROMA40 cartographic planimetric coordinates in case of the Lombardy DTM have been considered to perform the comparison. In case of PST-A LiDAR DTM, the coordinates have been previously transformed to ETRF89, using the tools available on the GPS Lombardia website (“Gps Lombardia,” n.d.). In this way for each point the difference between the estimated DTM elevation and the elevation of the IGM95 point has been computed.

Making a deep analysis of these benchmarks, not all of them are located on the ground, for example on walls or road embankments that clearly are not in the DTM. Therefore these points have been excluded from the whole set before computing the statistics of the differences so at the end the number of the selected points is 28.

In the comparison between the Lombardy regional DTM and the IGM95 points, the mean difference is about 1 meter and the standard deviation is 3 meters. These results are consistent with the nominal accuracy of the DTM. Despite the small number of check points, the results of the comparison between the PST-A LiDAR DTM and IGM95 are completely satisfactory, compared to the nominal accuracy of the PST-A DTM (less than 50 cm in elevation). The mean is about 6 cm, with a standard deviation of 13 cm and a maximum value of 32 cm. The results from the both comparisons are reported in the following table.

	Lombardy regional DTM - IGM95	PST-A LiDAR DTM - IGM95
Number of points	64	28
Mean (m)	-1.38	0.06
Std (m)	3.45	0.13
Min (m)	-13.36	-0.16
Max (m)	-6.35	0.32

Table 3 Statistics of the differences between the two DTMs (Lombardy regional and PST-A LiDAR) and the IGM95 points

- PST-A LiDAR DTM comparison with RTK surveys

Even if in the comparison between the Lombardy regional DTM and the PST-A LiDAR DTM the results are acceptable and also the comparisons of the two DTMs with the IGM95 benchmarks are satisfactory, in some areas differences greater than 10 meters between the two DTMs are present. Probably these high differences are due to some incorrect data in the Lombardy regional DTM but in order to verify the correctness of the PST-A DTM, it has to be validated with some more accurate data.

Since no IGM95 benchmarks are available in these areas, GNSS Real Time Kinematic (RTK) survey has been planned because it provides accuracies typically better than one decimeter. Surveys campaigns have been repeated two times. To collect GNSS RTK data twelve areas have been chosen where differences greater than 10 m are present. For each area at least 50 points have been surveyed in each campaign so in total 1300 RTK points have been collected successfully, considering the alpine nature of the case study.

Data collected during surveys, have been analyzed using Leica Geo Office software which to visualize, import, manage and process GNSS data and RTK results. Then, the RTK results have been converted to text files for further analyses with other GIS and statistic softwares.

Since the RTK results are in ITRF2008 while PST-A DTM is in ETRF89, before the comparison, RTK results have been converted to ETRF89 by the standard transformations. In order to compare the estimated elevation to the RTK height, the PST-A DTM has to be transformed from geodetic to orthometric by applying the undulation of the official Italian geoid Italgeo08 (Barzaghi et al., 1987). After the conversion, the comparison between PST-A DTM and RTK has been possible.

Each RTK result consists of the 3-D coordinates of a point measured on the ground. A simple routine has been implemented in MATLAB: its inputs are the DTM grids and a list of the RTK estimated coordinates. For each RTK point, the

sixteen nearest nodes of the DTM are searched; the elevation assumed by the DTM in the RTK point is estimated by exact bicubic interpolation from the sixteen nodes. The elevation difference between the elevation obtained by DTM interpolation and the RTK orthometric height is computed. Clearly, in this way, horizontal RTK errors are neglected, but for the purpose of this comparison they can be considered as not significant.

The results in general are satisfactory since all the differences are lower than 45 cm. The ones that are greater than 50 cm have been considered as outliers and have been removed from the datasets but still their percentage is acceptable.

Analyses on different DTM interpolation methods

In the moment of unifying the different partly overlapping DTMs on a common grid, an interpolation problem arises. This is a particular case of the HELI-DEM project and several analyses have been carried out in order to be chosen the best interpolation procedure; comparison between bilinear and bicubic polynomial surfaces to re-grid DTMs has been done.

When interpolating an input DTM on an output grid, the input nodes used to estimate the elevation of an output node can be geometrically distributed in a way that might cause numerical instability of the interpolation system (Carcano, 2013). In these cases a simple interpolation could not produce good results; some approaches useful to stabilize the system exist and have been studied and implemented.

Analyses have been carried out and confirmed that the bicubic polynomial surface gives better results with respect to the bilinear approach also on this case study.

3.3 Generation technique

Finally, various procedures can be adopted to produce a unified output DTM from different original elevation data. At the end the product called HD-1 has been obtained through merging the interpolated elevations between two or more DTMs, where they overlap. Correction of possible anomalies has been performed through high resolution DTMs when possible and HD-2 was realized.

The model is georeferenced in ETRF2000, gridded in geographic coordinates with a spatial resolution of 2×10^{-4} sexagesimal degrees which means about 15 m in longitude and 22 m in latitude. Its coverage has the following boundaries: $\lambda=7.80^\circ$ East and $\lambda=10.70^\circ$ East, $\phi=45.10^\circ$ North and $\phi=46.70^\circ$ North. The output matrix is composed by 8'000 rows and 14'500 columns for a total of 116 million nodes.

Integration of DTMs to create a unified model

In order to find the best procedure to create the final model a preprocessing has been performed on the original data. The elaboration can be synthetically schematized as the sequence of three main operations:

- a) pre-elaboration of the data consisted of transforming the following low and medium resolution available data in ETRF2000 reference frame:
 - SwissTopo DTM (res. 25 m), available in ETRF89, geographic coordinates (λ, ϕ) with a grid spacing of about 30 meters
 - Lombardy regional DTM (res. 20 m), available in Roma40, in Gauss-Boaga coordinates (E,N) with a grid spacing of 20 meters
 - Piedmont regional DTM (res. 5 m), available in ETRF89, UTM coordinates; reasonably used since it is the one with highest resolution for this region.

After the transformation each DTM is a list of three-dimensional points that have to be interpolated on the output grid. No data values have been deleted from the datasets and a validation has been performed as well. After these operations the numbers of useful data are 29'287'577, 607'997'593 and 19'400'361 respectively for Lombardy, Piedmont and Switzerland. The total number of useful data is about 650 millions.

- b) elaboration, or interpolation of the DTMs to create HD-1

The three DTMs, converted to the output reference frame, have been independently interpolated on the output final grid. A bicubic method has been chosen to perform the interpolation and estimate the elevations of the nodes of the final grid.

At this point a unique final unified DTM has to be obtained. To do that the three interpolated and eroded DTMs have been averaged. Therefore each node of the output unified HD-1 grid assumes a value equal to:

- the average of three elevations if all the three interpolated DTMs have useful values in this node
- the average of two elevations if only two of the three interpolated DTMs have useful values in this node,
- the value of the elevation assumed by one of the three DTMs, if only this DTM exists in this node,
- no data value if none of the three DTMs exists in this node

In total about 72 million nodes are actually interpolated, the other nodes of the rectangular output grid (8000 x 14500 nodes) are outside the project area and assume no data value.

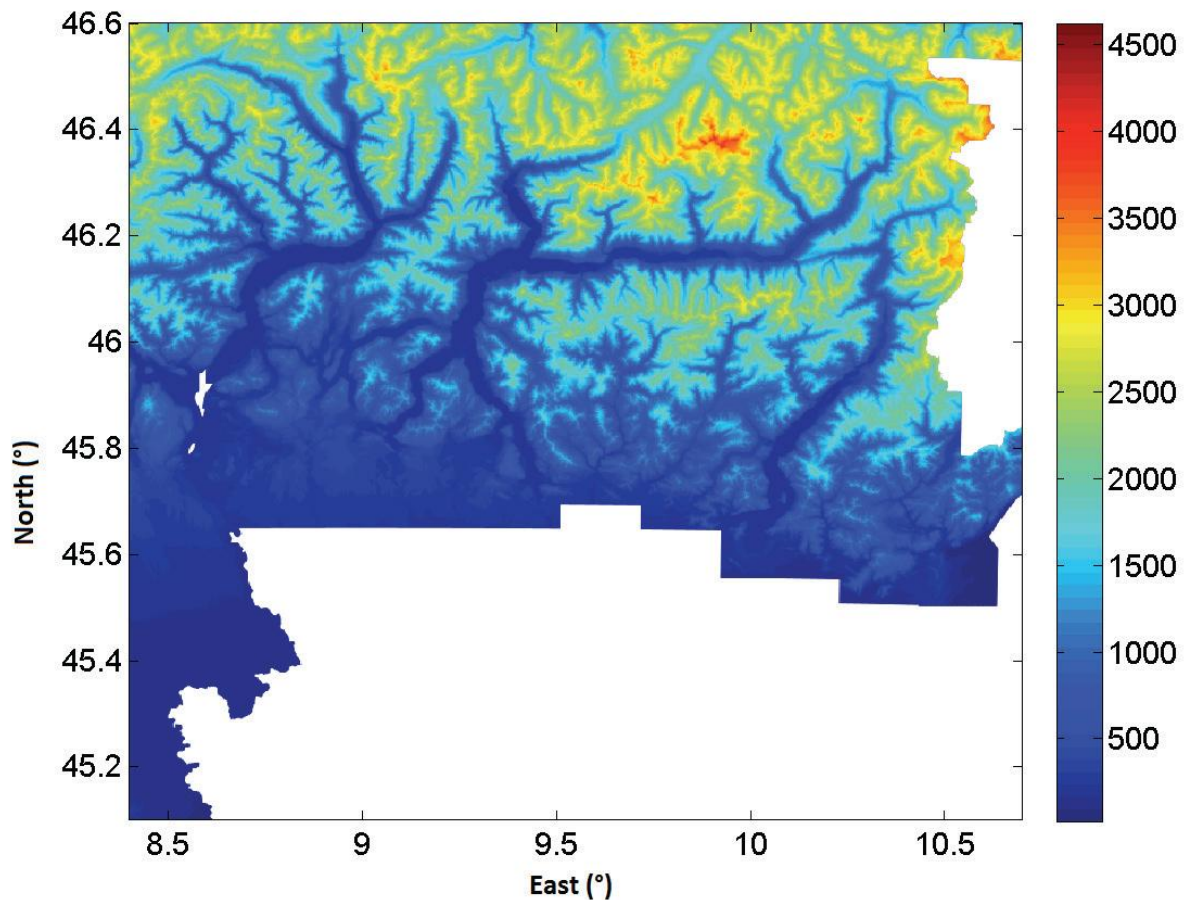


Figure 22 Unified HELI-DEM DTM (HD-1) obtained through merging of Lombardy, Piedmont and Swiss low/medium resolution models

c) post-elaboration, or correction of HD-1 for lake areas

In some DTMs lakes points are stored as a constant reference value, while in others they are variable in space (of the magnitude of few centimeters). Moreover the lakes elevation can be different in the different DTMs therefore a post-elaboration for these areas is required. During the creation of HD-1 a reference constant value has been computed as the minimum elevation among all the already interpolated coastline points and it has been set for the nodes belonging to the surface of each lake.

In addition the applied correction has proved to be less reliable and for this reason for each of the major lakes (Como Lake, Maggiore Lake, Lugano Lake, Iseo Lake, Orta Lake) a buffer 100 meters wide, which extends from the border of the lake to the inland, has been created and for its interpolation only the input points that fall inside it have been used.

- d) correction of possible anomalies and outliers in HD-1 by more accurate data where they are available: production of HD-2.

Clearly, the low resolution final DTM still contains all the possible anomalies and outliers that were present in the input data used to interpolate it. Once HD-1 has been produced and the lake areas have been corrected, some analyses have to be done to enhance the model with more accurate data where they exist. After the realization of all these procedures the final corrected model HD-2 is present.

The available high resolution DTM is LiDAR and it is gridded in ETRF2000 geographic coordinates; it has a resolution of 10^{-5} degrees and a vertical accuracy better than 0.5 meters; it covers the valleys of the main river basins of Lombardy and Piedmont. It is produced by the Italian Department for Environment within the national remote sensing project for the Environment (Piano Straordinario di Telerilevamento Ambientale) and is named PST-A.

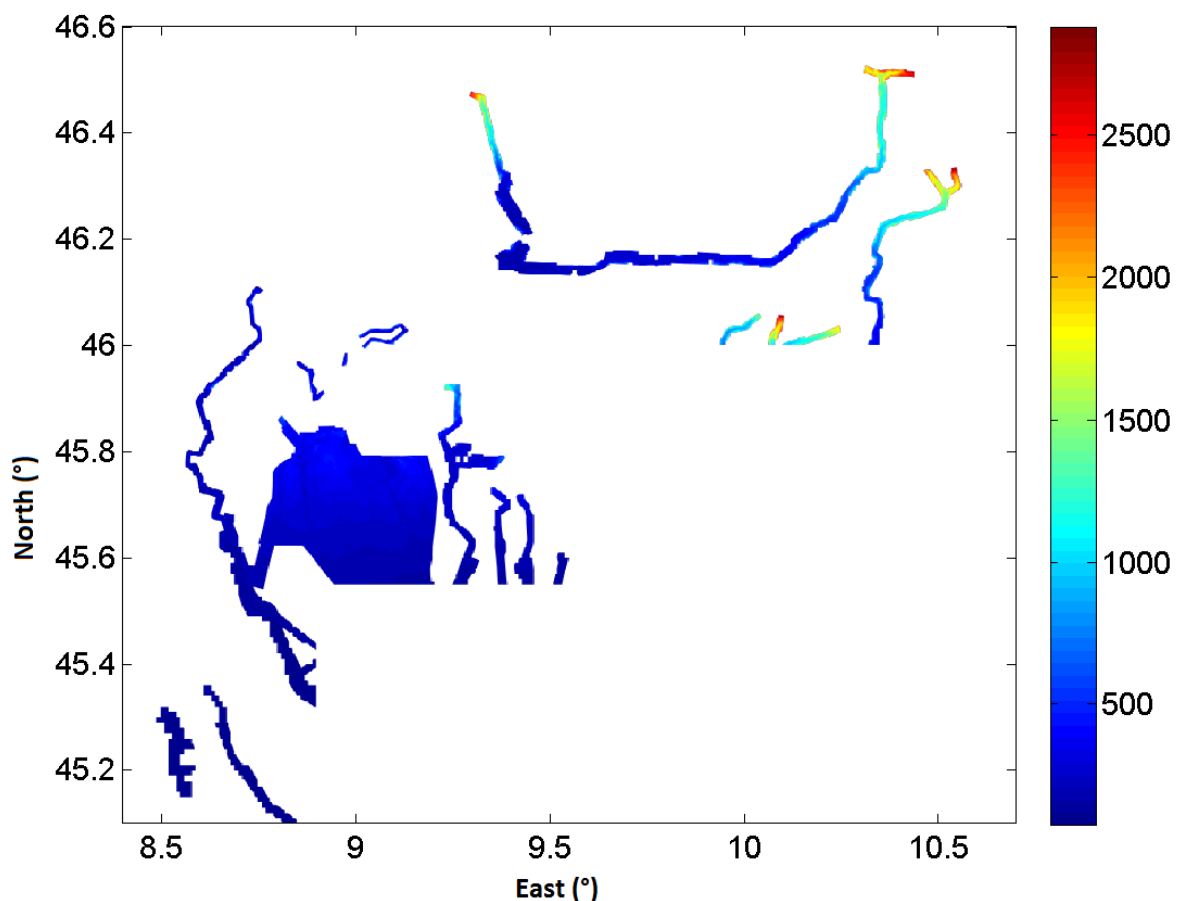


Figure 23 Portion of PST-A LiDAR DTM overlapped with HD-1

Correcting a DTM with a local model that has better horizontal resolution and accuracy but is not present in all the area creates jumps at the border between the zones. In order to produce a reasonably smooth model, which at the same time preserves as much as possible the accuracy of the correction is needed a proper filtering of the corrections before their application.

The general methodology that has been applied can be shown schematically in the following way (Carcano, 2013):

1. Computation of the corrections. The high resolution PST-A has been subsampled on the low resolution HD-1 on whose nodes corrections have to be computed. Then, their differences have been computed and in the nodes where subsampled PST-A does not exist, differences have been set to zero. The model of the differences is called “corrections model”.

2. Appropriate filtering of the corrections. A low pass filter allows smoothing the discontinuities in the corrections, particularly where they pass from null value to a value different from zero. The Butterworth filter has been used: it is given by the following formula:

$$f(i, j) = \frac{1}{1 + \left[\frac{i^2 + j^2}{D_0^2} \right]^n} = \frac{1}{1 + \left[\frac{d}{D_0} \right]^{2n}}$$

n and D_0 parameters are set by the user.

Actually, an iterative version has been implemented by FFT, according to the following schema:

1. Computation of the model of the corrections,
2. Construction of the Butterworth Filter,
3. Computation of the FFTs of both corrections and filter,
4. Iterated product of the two FFTs,
5. Inverse FFT (IFFT) of the product for the reconstruction of the filtered corrections.

3. Application of the filtered corrections. The filtered corrections have been applied to HD-1 and the corrected DTM is called HD-2.

	Bias (m)	Std (m)	Max (m)	Min (m)
PST-A - HD-1 (original)	0.3	6.0	186.8	-174.6
PST-A - HD-2 (corrected)	0.0	0.4	108.4	-97.4

Table 4 Statistics of the differences between PST-A LiDAR DTM and HD-1 DTM / HD-2

Bias: mean difference; Std: standard deviation of the differences

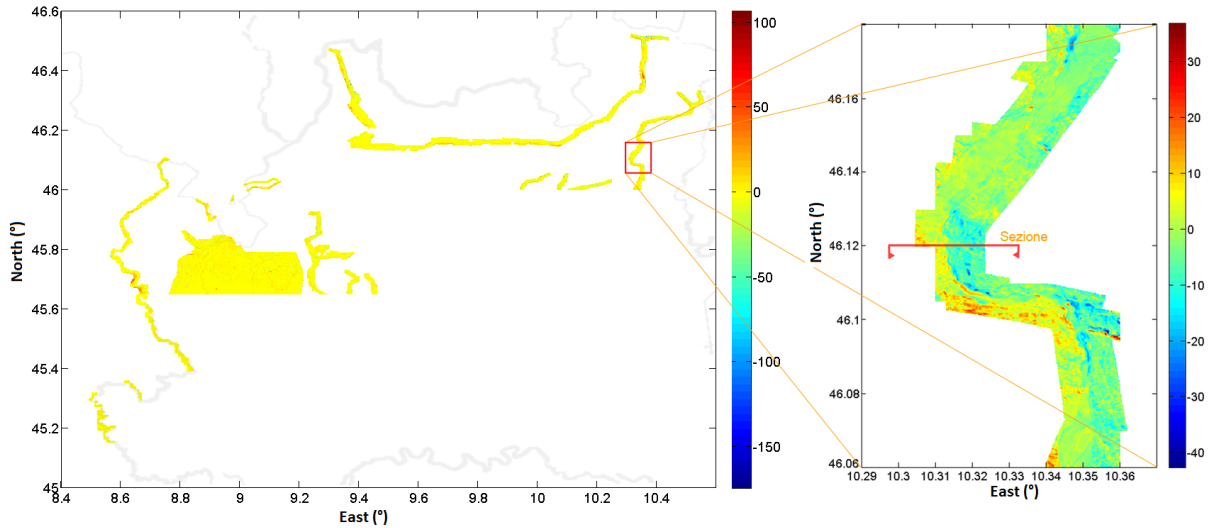


Figure 24 On the left: coverage of PST-A DTM and its differences with HD-1. At the right: Differences values in meters, zoom

This internal validation of HD-2 DTM gives very satisfactory results but also an external validation will be realized. For this purpose a set of 1000 measures has been collected in Valtellina area by GNSS RTK technique (Hofmann Wellenhof, 2008) with accuracy better than 10 cm.

The elevations of the GPS points (943 points in total) have been collected into a unique dataset. Then HD-1, the subsampled PST-A and HD-2 have been interpolated by bicubic interpolation on the GPS points. Finally, the differences between the three models and the GPS elevations have been computed.

	Bias (m)	Std (m)	Max (m)	Min (m)
HD-1 - RTK	3.4	5.5	24.2	0.0
PST-A - RTK	-0.3	1.0	7.2	0.0
HD-2 - RTK	-0.4	1.7	8.8	0.0

Table 5 Statistics of the modulus of the differences between HD-1, PST-A and HD-2 DTMs and RTK

Bias: mean difference; Std: standard deviation of the differences

The statistics prove the reliability of the applied correction: the differences between HD-2 and RTK are significantly better than those of HD-1 and are comparable with those of PST-A.

3.4 Conclusions

The HELI-DEM (Helvetia-Italy Digital Elevation Model) project was produced as a research with the aim of creating a unified DTM of the Italian and Swiss Alpine region through merging the available low resolution elevation data for Lombardy, Piedmont and Switzerland. At first, all the DTMs have been transformed in ETRF2000. Then the low resolution ones have been independently interpolated on the output final grid using a bicubic method. They have been compared and averaged in their overlapping boundaries. The final product HD-1 covers the ETRF2000 rectangle comprised by the following boundaries: $\lambda=7.80^\circ$ East and $\lambda=10.70^\circ$ East, $\phi=45.10^\circ$ North and $\phi=46.70^\circ$ North. It is gridded in geographical coordinates with a spatial resolution of 2×10^{-4} degrees. HD-1 has been corrected for lake areas and later a high resolution DTM has been used for additional correction of possible anomalies, outliers and discontinuities in the areas where it is available. The resulting DTM is named HD-2 and has been externally validated by RTK GNSS measures which confirm the good quality of the applied corrections.

At the present, HD-2 or later called HELI-DEM is compared with the ASTER/SRTM/GMTED2010 global models. The results obtained by these comparisons will be presented in the current paper.

Chapter 4

4 Geographic Resources Analysis Support System (GRASS GIS)

In this chapter the GRASS GIS software used to process the available elevation data and its main functionalities are explained. It is Free and Open Source software which allows reading, visualizing, editing and analyzing the information in a unique geographic platform.

4.1 Definition

GRASS GIS, commonly referred to as GRASS (Geographic Resources Analysis Support System), is a free and open source Geographic Information System (GIS) software suite used for geospatial data management and analysis, image processing, graphics and maps production, spatial modeling, and visualization. GRASS GIS is currently used in academic and commercial settings around the world, as well as by many governmental agencies including NASA, NOAA, USDA, DLR, CSIRO, the National Park Service, the U.S. Census Bureau, USGS, and many environmental consulting companies. GRASS GIS is an official project of the Open Source Geospatial Foundation (“GRASS GIS - General overview,” n.d.).

GRASS GIS contains over 350 modules to render maps and images on monitor and paper; manipulate raster, and vector data including vector networks; process multispectral image data; and create, manage, and store spatial data. GRASS GIS offers both an intuitive graphical user interface as well as command line syntax for ease of operations. GRASS GIS can interface with printers, plotters, digitizers, and databases to develop new data as well as manage existing data. GRASS libraries and core modules are written in C; other modules are written in C, C++, Python, UNIX shell, Tcl, or other scripting languages.

GRASS GIS can be used on multiple platforms, including Mac OS X (Mountain Lion), Linux (GNOME, Ubuntu) and other UNIX compliant platforms (32/64bit), additionally MS-Windows. It is Free (Libre) Software/Open Source released under GNU General Public License (GPL).

4.1.1 Free and Open Source meaning

Free and open-source software (FOSS) is computer software that can be classified as both free software and open-source software. That is, anyone is freely licensed to use, copy, study, and change the software in any way, and the source code is openly shared so that people are encouraged to voluntarily improve the design of the software. This is in contrast to proprietary

software, where the software is under restrictive copyright and the source code is usually hidden from the users (“Free and open-source software-Wiki,” n.d.).

The benefits of using FOSS can include decreasing software costs, increasing security and stability, protecting privacy, and giving users more control over their own hardware. Free, open-source operating systems such as Linux and descendents of BSD are widely utilized today, powering millions of servers, desktops, smartphones (e.g. Android), and other devices. Free software licenses and open-source licenses are used by many software packages.

The official website to download GRASS:

<http://grass.osgeo.org/download/software/>

(“GRASS GIS - Detailed Software Download,” n.d.)

4.1.2 Main capabilities

Raster analysis: Automatic rasterline and area to vector conversion, Buffering of line structures, Cell and profile dataquery, Colortable modifications, Conversion to vector and point data format, Correlation / covariance analysis, Expert system analysis , Map algebra (map calculator), Interpolation for missing values, Neighbourhood matrix analysis, Raster overlay with or without weight, Reclassification of cell labels, Resampling (resolution), Rescaling of cell values, Statistical cell analysis, Surface generation from vector lines

3D-Raster (voxel) analysis: 3D data import and export, 3D masks, 3D map algebra, 3D interpolation (IDW, Regularised Splines with Tension), 3D Visualization (isosurfaces), Interface to Paraview and POVray visualization tools

Vector analysis: Contour generation from raster surfaces (IDW, Splines algorithm), Conversion to raster and point data format, Digitizing (scanned raster image) with mouse, Reclassification of vector labels, Superpositioning of vector layers

Point data analysis: Delaunay triangulation, Surface interpolation from spot heights, Thiessen polygons, Topographic analysis (curvature, slope, aspect), LiDAR

Image processing: Support for aerial and UAV images, satellite data (optical, radar, thermal), Canonical component analysis (CCA), Color composite generation, Edge detection, Frequency filtering (Fourier, convolution matrices), Fourier and inverse fourier transformation, Histogram stretching, IHS transformation to RGB, Image rectification (affine and polynomial transformations on raster and vector targets), Ortho photo rectification, Principal component analysis (PCA), Radiometric corrections (Fourier), Resampling, Resolution enhancement (with RGB/IHS), RGB to IHS transformation, Texture oriented classification (sequential maximum a posteriori classification), Shape

detection, Supervised classification (training areas, maximum likelihood classification), Unsupervised classification (minimum distance clustering, maximum likelihood classification)

DTM-Analysis: Contour generation, Cost / path analysis, Slope / aspect analysis, Surface generation from spot heights or contours

Geocoding: Geocoding of raster and vector maps including (LiDAR) point clouds

Visualization: 3D surfaces with 3D query (NVIZ), Color assignments, Histogram presentation, Map overlay, Point data maps, Raster maps, Vector maps, Zoom / unzoom -function

Map creation: Image maps, Postscript maps, HTML maps

SQL-support: Database interfaces (DBF, SQLite, PostgreSQL, MySQL, ODBC)

Geostatistics: Interface to "R" (a statistical analysis environment), Matlab, etc.

Furthermore: Erosion modelling, Landscape structure analysis, Solution transport, Watershed analysis ("GRASS GIS - General overview," n.d.).

4.2 GRASS structure

The organization of GRASS data is based on a hierarchical structure and has been built in this efficient way in order to manage the access of the multiples users to the stored data.

Database: Contains all GRASS data.

Each GRASS project is organized in a "Location" directory with subsequent "Mapset" directories

Location: Defines a coordinate system and a rectangular boundary for a Project. Every location has a PERMANENT directory which stores some basic information about the whole location, and is a good place to park base files.

Mapset(s): Used to subdivide data by user names or subregions or access rights and each user has the possibility to edit data.

PERMANENT: Is a standard mapset that contains the definitions of the location.

Each location can have several "mapsets" that are used to subdivide the project into different topics, subregions, or workspaces for individual team members. Each mapset includes subdirectories for raster, vector, and attribute data, plus a working spatial extent definition file, named WIND. These subdirectories and files are hidden from the user while working in GRASS. When defining a new location, GRASS automatically creates a special mapset called PERMANENT,

which is used to store the default spatial extent, the coordinate system definitions and which may be used to also store geodata for the team.

The following figures sketch the GRASS structure for this study.



Figure 25 GRASS Structure in general

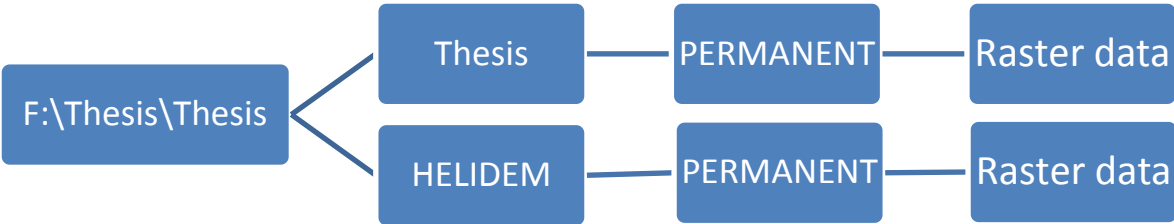


Figure 26 GRASS Structure in the current work

There are two kinds of data formats that can be read by GRASS: vectors and rasters. Each format has its own way to be stored in GRASS through different folders. In the current work is used only raster data.

4.2.1 Vector data

Each vector map is stored in its own directory: the directory has the same name of the vector map. Each vector map contains the following files:

- cidx: Contains the topological index.
- coor: Binary file that contains the features coordinates and categories.
- dbln: Contains information about database connection (driver, database, table, column, etc.).

- head: Contains the vector header.
- hist: Contains information about the vector history: author, date, executed commands, etc.
- topo: Binary file containing topology.

4.2.2 Raster data

RASTER maps are recorded in a matrix where each element represents a pixel with an integer or floating point value. Information about the raster maps is distributed in different files inside thematic subdirectories:

- tmp – holds temporary files
- cats – Contains category information
- cell – Contains binary files with the numerical matrix
- cellhd – Contains maps headers
- colr – Contains maps color information
- fcell – Contains binary files with the numerical matrix
- hist – Contains information about raster map history: author, date, executed commands, etc.

Chapter 5

5 Download of GDEMs, Start of a new project in GRASS, Import of GDEMs and Re-projection of HELI-DEM

This chapter explains step by step the process of downloading ASTER, SRTM and GMTED2010. Then are presented in details the first steps in defining a new project, creating locations and setting region extents in the GRASS platform so that further data management, analysis, processing, etc. could be initiated. Later, the way of importing the global and the local models into the GRASS platform is described. Here is indicated as well the sampling procedure for the HELI-DEM by decreasing its resolution until it reaches the ones of the global models. This action allows computations, comparisons and further analyses to be initiated. Three cases are going to be presented.

5.1 Download of global DEMs

5.1.1 Download of ASTER and SRTM data

The first needed sets of data are the global DEMs produced by ASTER and SRTM. They can be downloaded for free from the link down which is mentioned also in Chapter 2. Here is explained step by step the procedure.

<http://gdex.cr.usgs.gov/gdex/>

After opening the webpage a registration has to be done and some basic information as user profile details, user information, contact information and affiliation has to be fulfilled. Thereafter the log in, the access for downloading data is allowed. The area is defined by entering the boundaries in Lat/Lon, namely:

North Latitude $\varphi = 46.7^\circ$

South Latitude $\varphi = 45.1^\circ$

East Longitude $\lambda = 10.7^\circ$

West Longitude $\lambda = 7.8^\circ$

Once the area is defined and the DEM either ASTER or SRTM is chosen, the downloading process can be started by selecting the Download button.

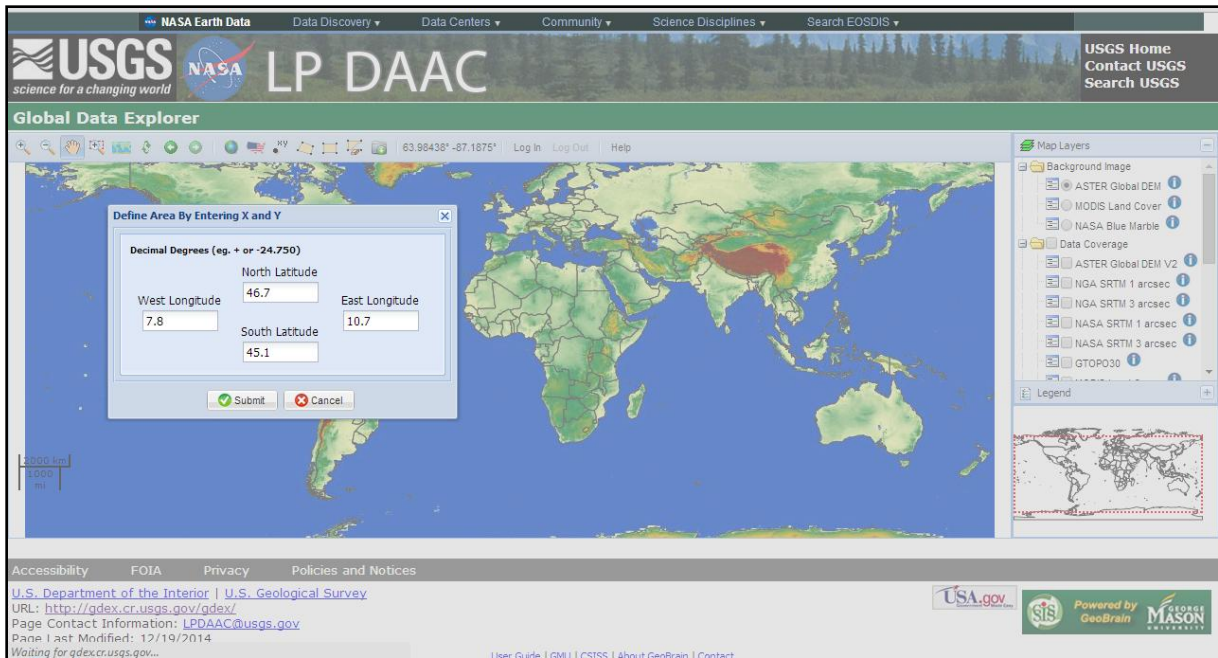


Figure 27. Website - ASTER and SRTM, defining boundaries

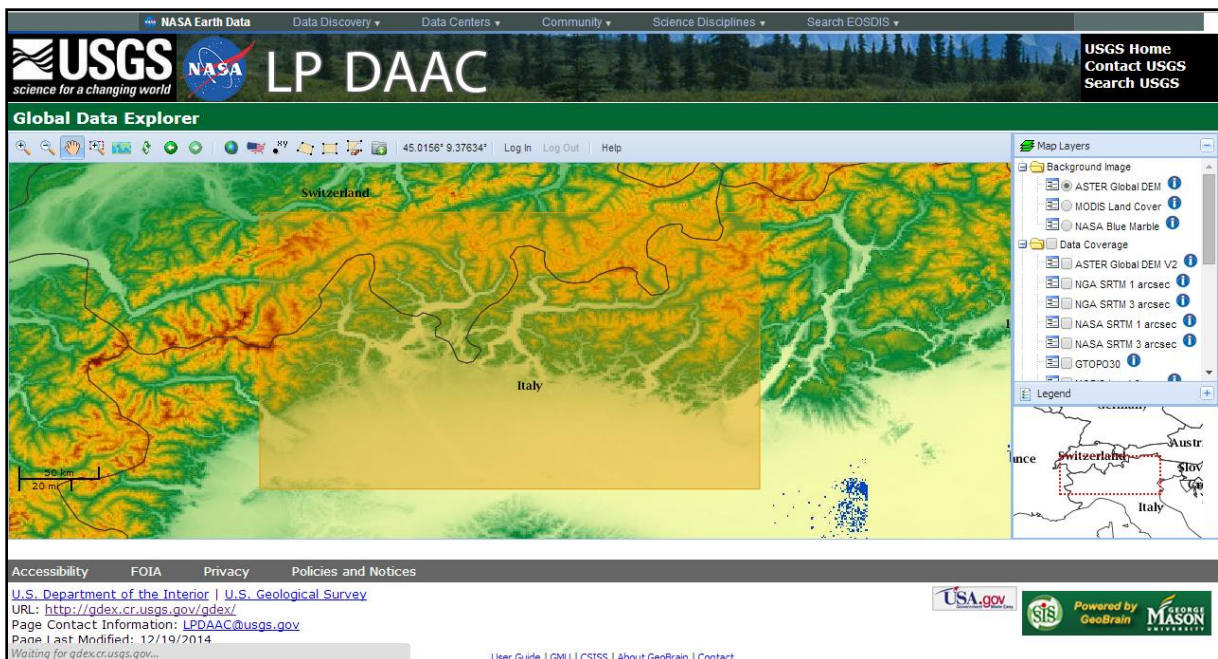


Figure 28. Website - ASTER and SRTM, region of interest

The type of format in which the DEM has to be stored (ArcASCII) is chosen and last but not least for the option of choosing a “Projection” Lat/Lon grid has to be selected. Here has to be mentioned that “Projection” option is not entered in a proper way because the available choices are types of coordinates but not different projections.

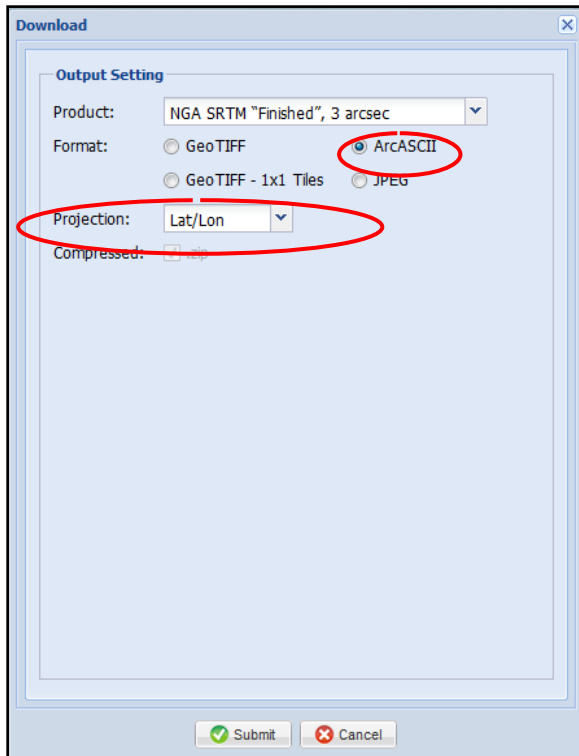


Figure 29 Download format - ASTER

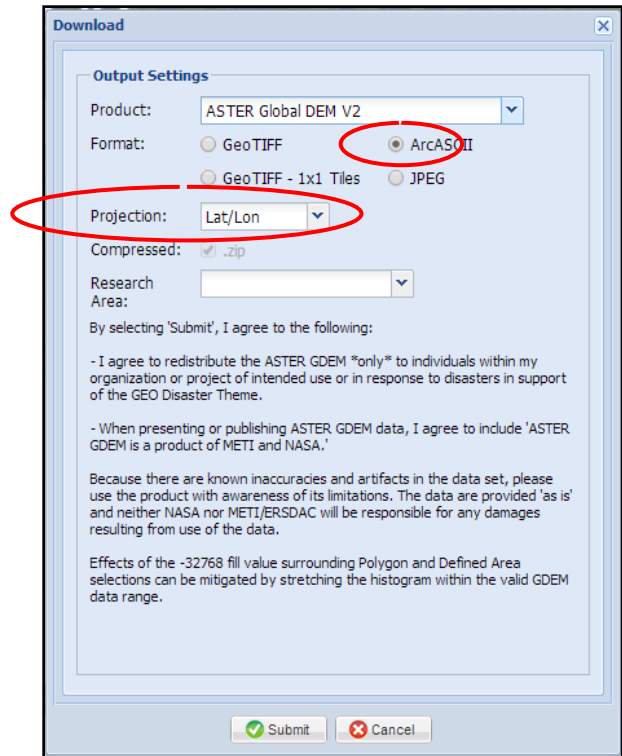


Figure 30 Download format - SRTM

Finally the DEMs are downloaded. There are two files for each model – the ASCII one and the .prj file which brings information about the coordinates and the datum. The DEMs present the following shape:

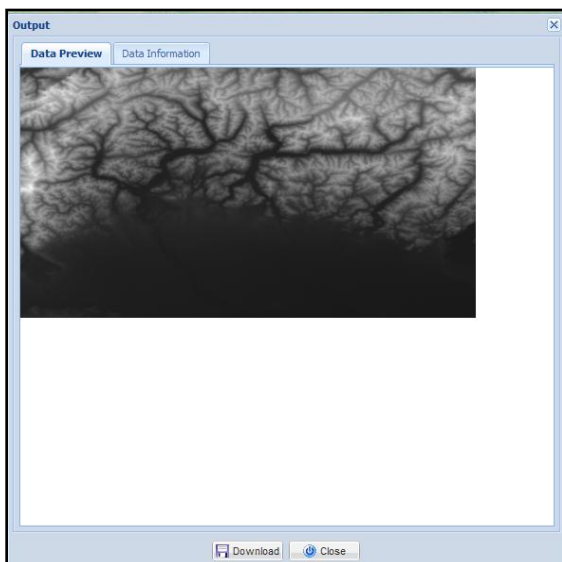


Figure 31 Website - ASTER output

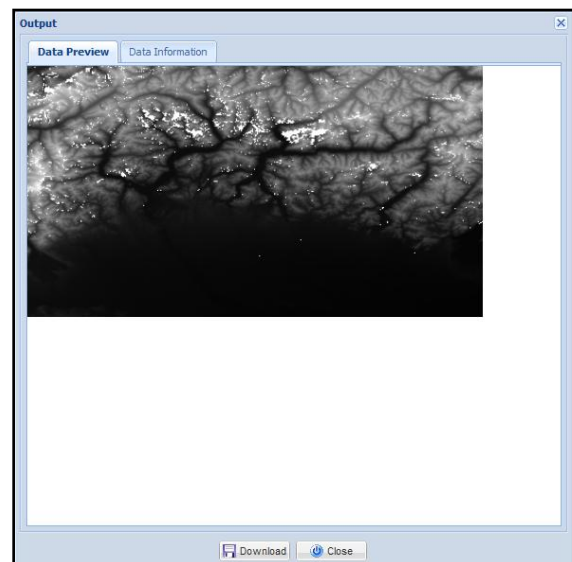


Figure 32 Website - SRTM output

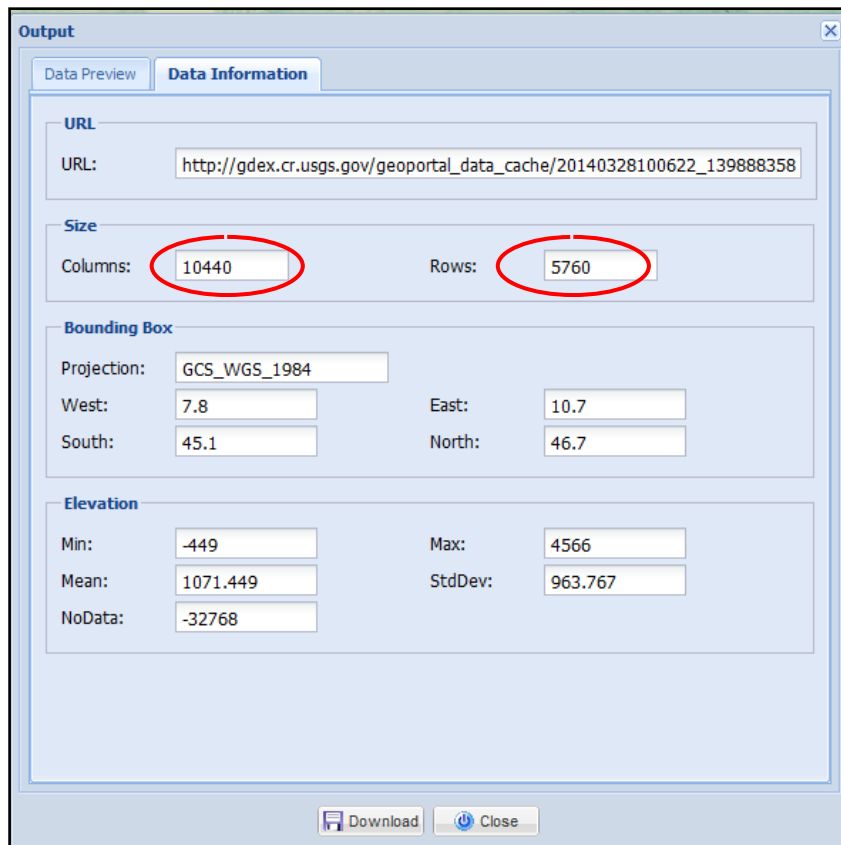


Figure 33 Output window for ASTER

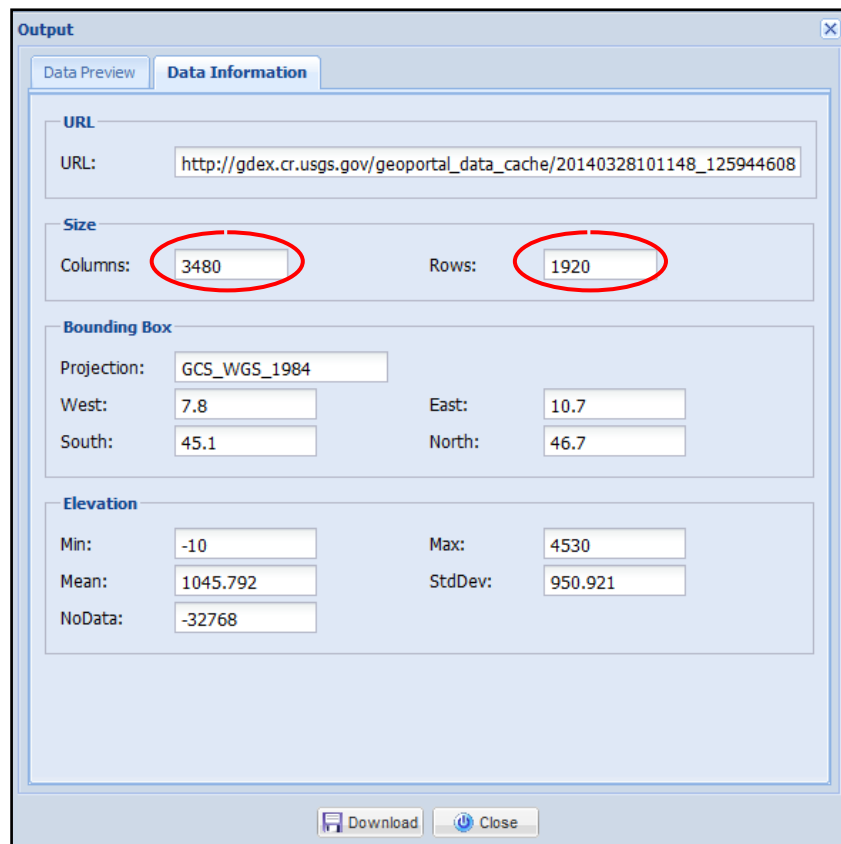


Figure 34 Output window for SRTM

During downloading the website shows an output window for each of the two models. They are presented in the figures above which visualize the difference in the resolution between the models through the amount of data. ASTER in 1 arc-second resolution has 60'134'400 (5760x10440) cells compared with SRTM in 3 arc-second resolution which contains 9 times less cells, exactly 6'681'600 (1920x3480). In the output are seen as well basic statistics which are analyzed later in the same chapter.

5.1.2 Download of GMTED2010 data

The last needed DEM is the GMTED 2010 which will be downloaded for free almost in the same way as the previous ones.

After opening the webpage below a registration has to be done and some basic information as login information, user affiliation/data usage information and personal information has to be fulfilled. Thereafter a conformation, a new account is activated, the sign in is possible and the access for downloading data is now allowed. It is time that the boundaries of the region which are the same as for ASTER and SRTM have to be set in the first step "Search Criteria". The coordinates stated in the previous lines are in decimal indices but the website allows to be fulfilled in degrees as well. The area is defined and on the next step the "Data Set" has to be selected from the "Digital Elevation" menu tree, namely GMTED2010.

<http://earthexplorer.usgs.gov/>

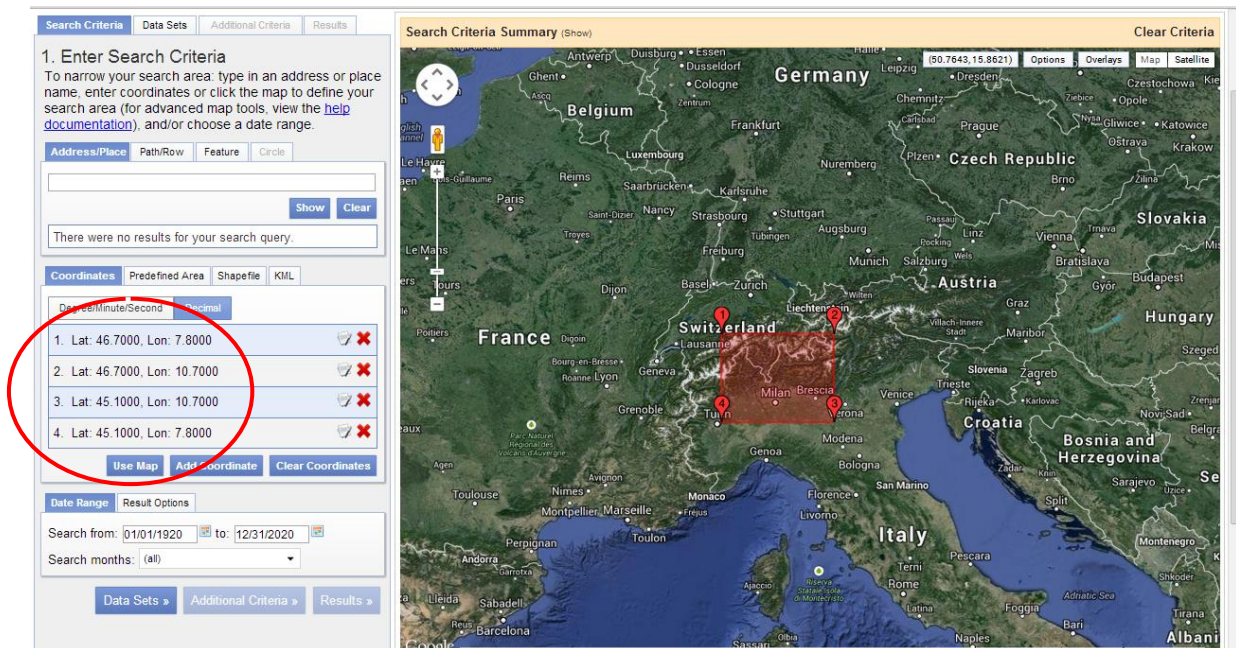


Figure 35 Defining rectangular border for GMTED by coordinates

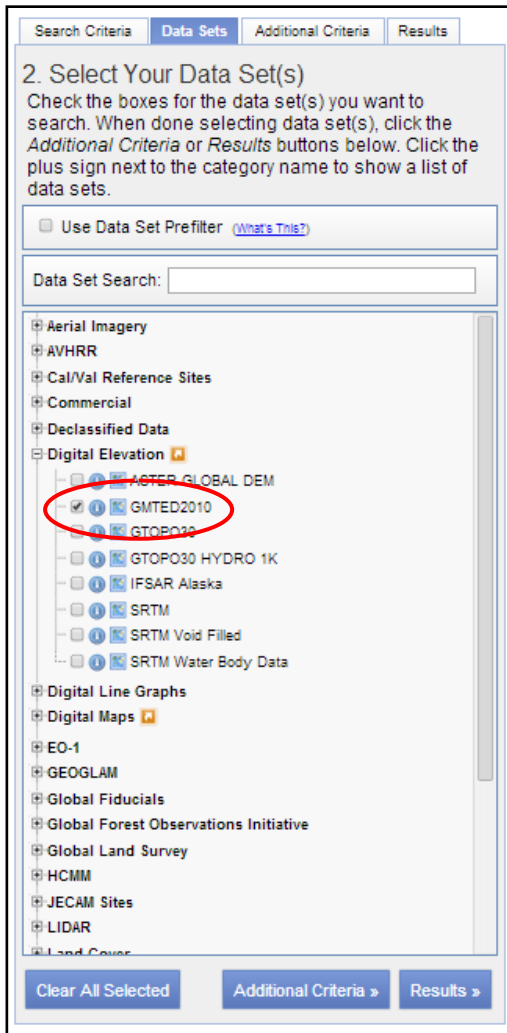


Figure 36 Choosing GMTED2010 for downloading

The last step is accessing the “Results” and selecting the button “Download”. Also the resolution has to be set: as is mentioned in the Chapter 2, GMTED 2010 has 3 different resolutions, for this study is used the higher resolution which means 7.5 arc-second.

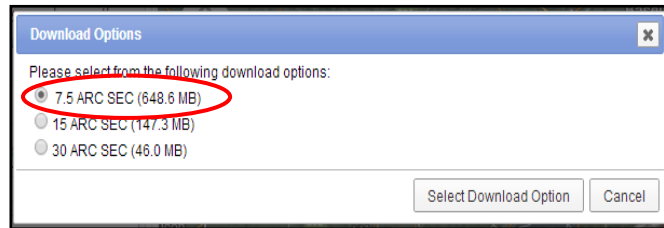


Figure 37 Selecting resolution 7.5 arc-second

Finally GMTED2010 is downloaded. There are seven files in GeoTIFF format (minimum, maximum, mean, median, standard deviation, systematic subsample and break-line emphasis) as is explained in details about this DEM in Chapter 2.

5.2 Start of a new project

5.2.1 Creating a Location for the Global DEMs

Once the GRASS is started a new project has to be defined and inside it the location “Thesis” will be the first one created, taking into account a projection for it.

A GRASS location is referenced with a single projection and coordinate system (or unreferenced as XY location). When creating a new location from an existing raster or vector map using the tools available from the startup screen or the map import commands, projection and coordinate system are defined. To

change the projection of maps, a new location has to be created and the desired maps have to be reprojected into it from the source location (“Projections in GRASS GIS,” n.d.).

For all coordinate reference systems that use geographical coordinates (gridded in Lat/Lon) GRASS uses a Plate Carrée projection (i.e. equirectangular or equidistant cylindrical projection with standard parallel 0°) which in essence just interprets the angular units of the geographic coordinates as linear units of a Cartesian coordinate system (Synder, 2011).

The software needs gridded geographical coordinated to perform that operation i.e. to read projection and datum terms from a .wkt or .prj file. As mentioned previously, during the downloading process of ASTER and SRTM GDEMs, two files for each of the models have been obtained: the ASCII one and the projection file. All the three global models are posted on a Lat/Lon grid and referenced to the WGS84 datum. In this case, since a .prj file is available, not the projection but the datum will be read from the .prj file referring to ASTER.

Here is explained the procedure of creating a new location in the platform step by step.

At first from the bottom “Browse” choose a directory for the data and then from “Location wizard” create a new Location. A new window appears in which “Project Location” and “Location Title” should be named.

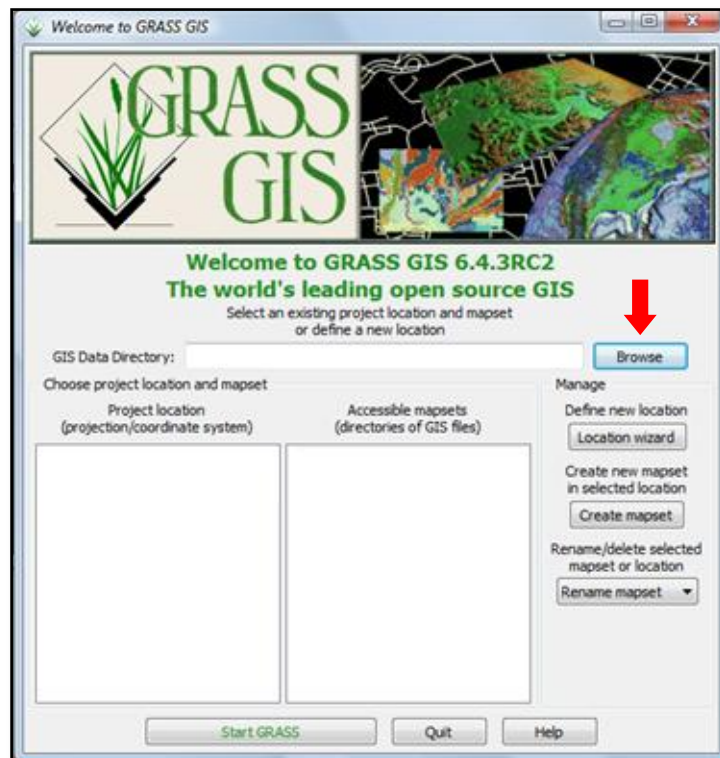


Figure 38 Creating a new location into the GRASS platform

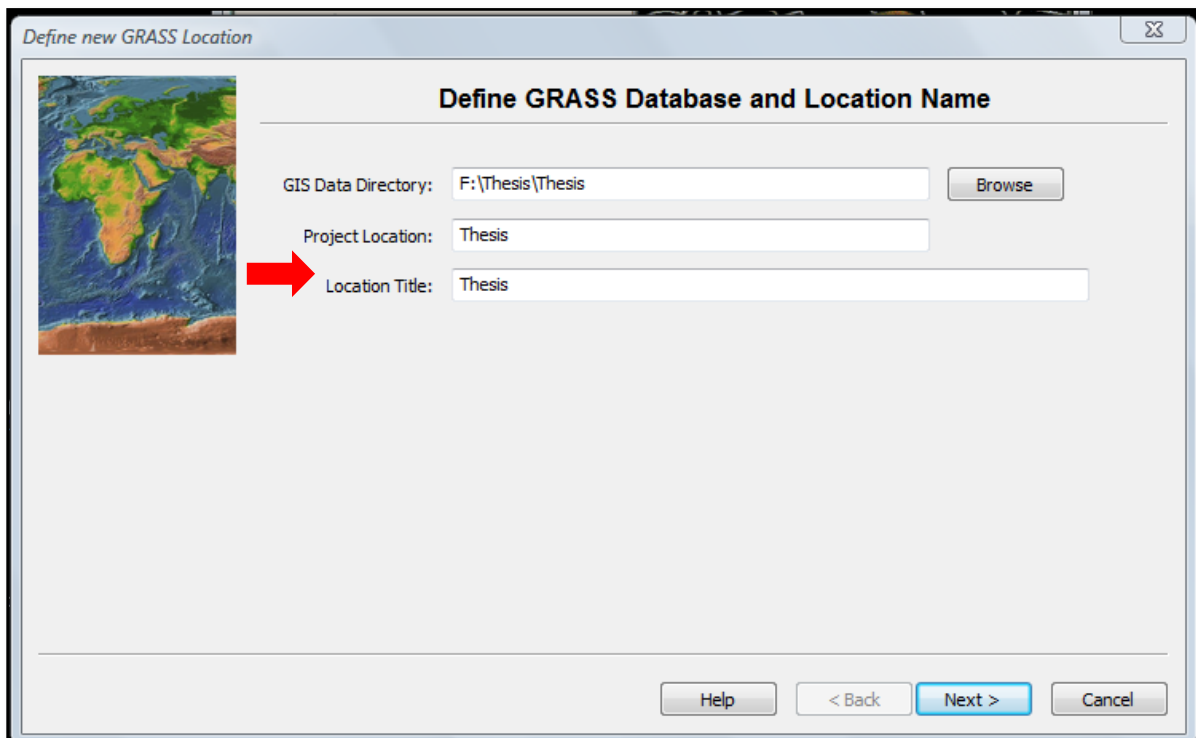


Figure 39 Giving a directory and a name of the new location

Then on the next step a projection file, from which the datum will be read, has to be chosen. In this case the projection will be read from the .prj file referring to ASTER DEM.

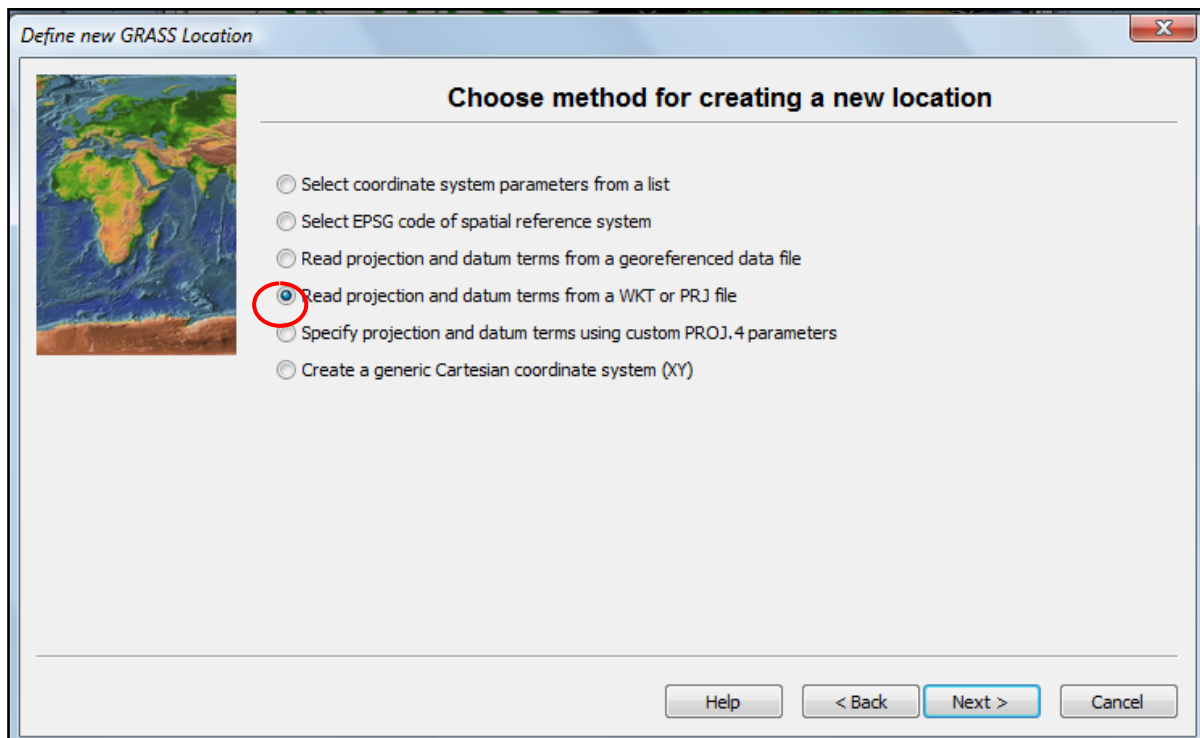


Figure 40 Choosing a method for creating a new location

(Read projection and datum term from a WKT or PRJ file)

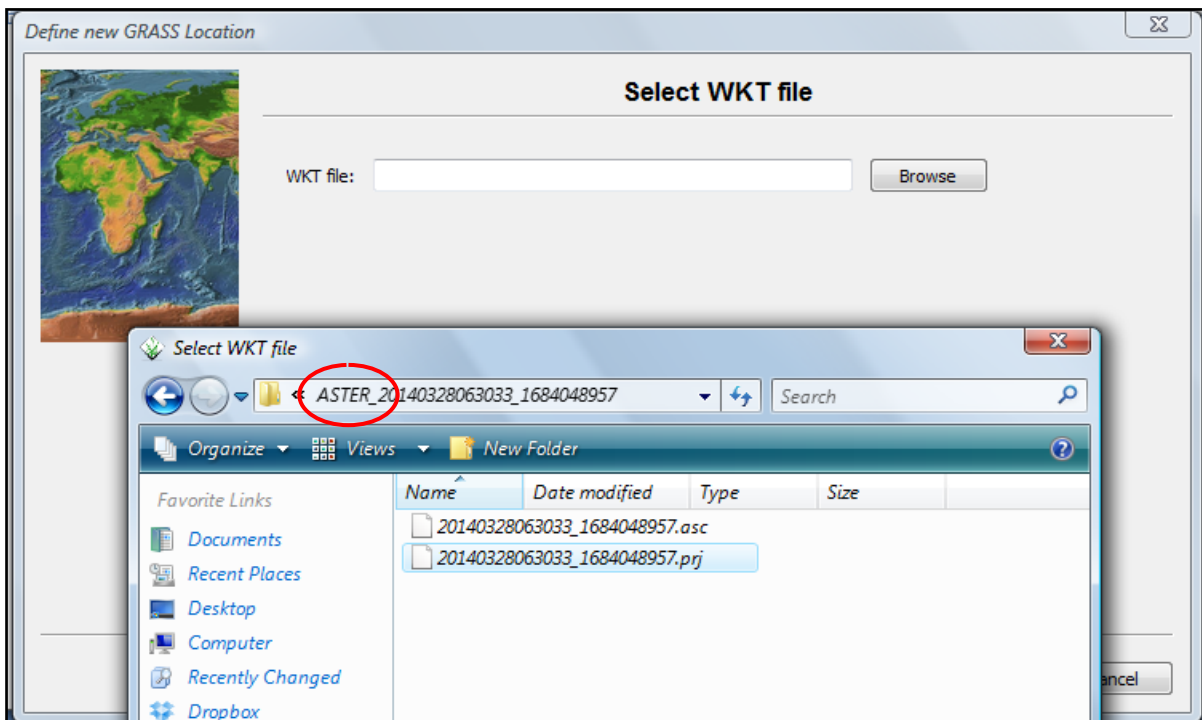


Figure 41 Choosing ASTER projection file

After the Location “Thesis” has been created, a new window appears and it is time default region extents to be set. The boundaries are the same as stated before in the beginning of this chapter:

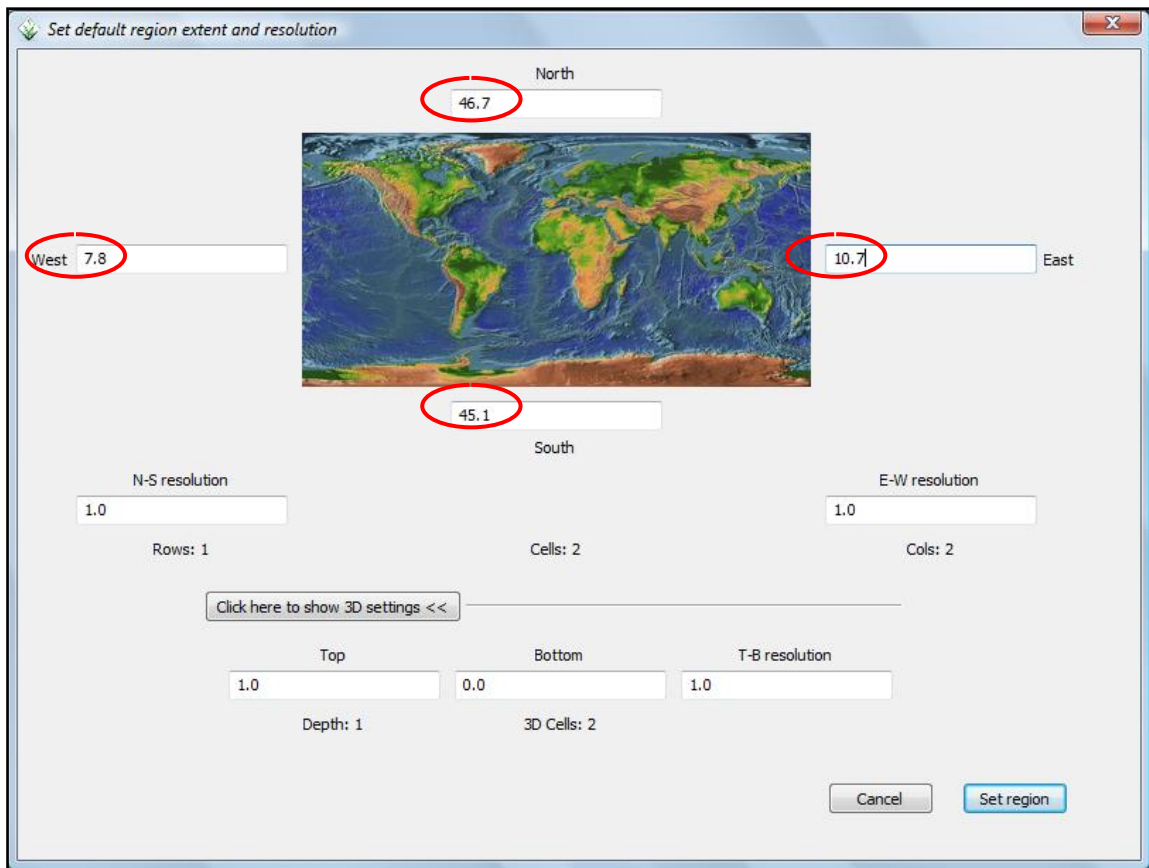


Figure 42 Set default region extents

Together with the location Thesis also a mapset called PERMANENT has been created into it and this is the default mapset that will be used as explained already in Chapter 4 referring to GRASS GIS software.

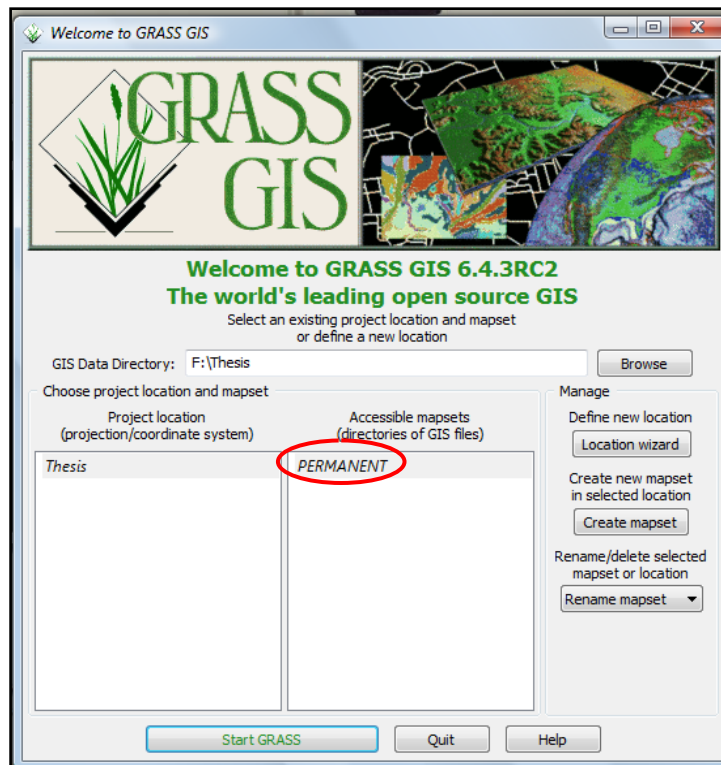


Figure 43 Created new location and the corresponding mapset

5.2.2 Creating a Location for the Local DEM

Now a new location is needed to be added since the local model HELI-DEM is not referenced to the same datum WGS84 despite that it is in geographical coordinates as the global models. In this case that information will be read by the program directly from the file of the model.

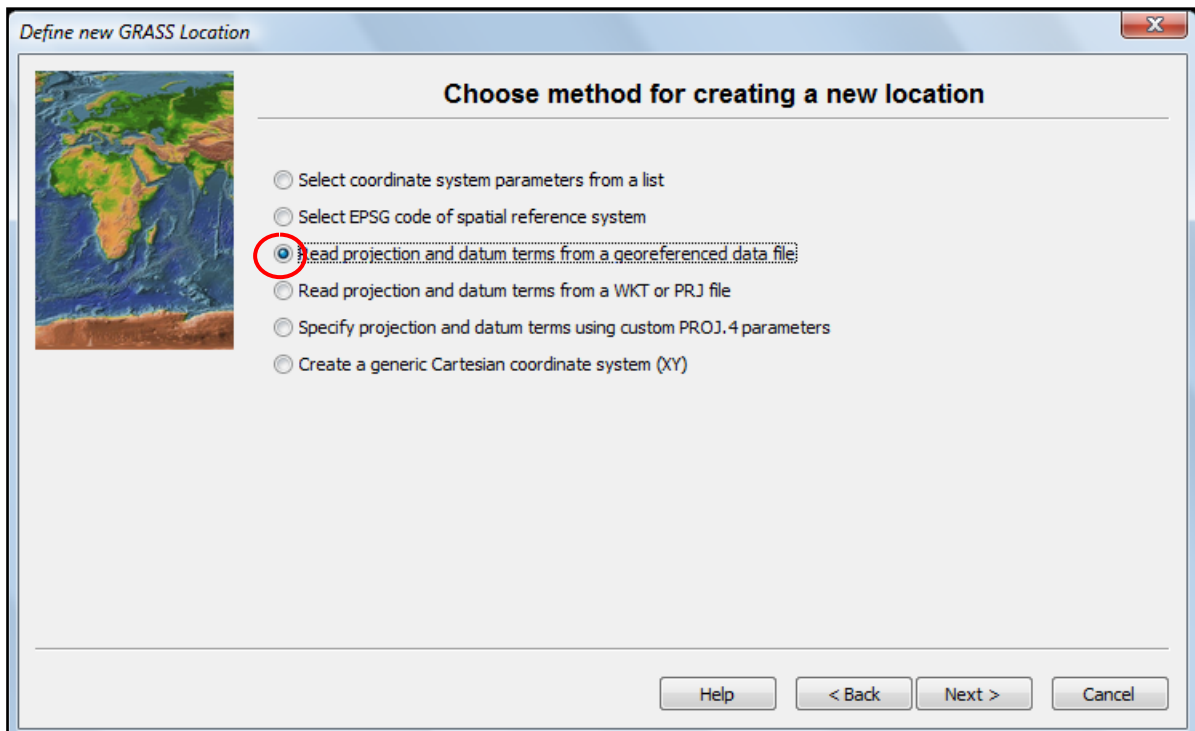


Figure 44 Choosing method for creating HELIDEM location

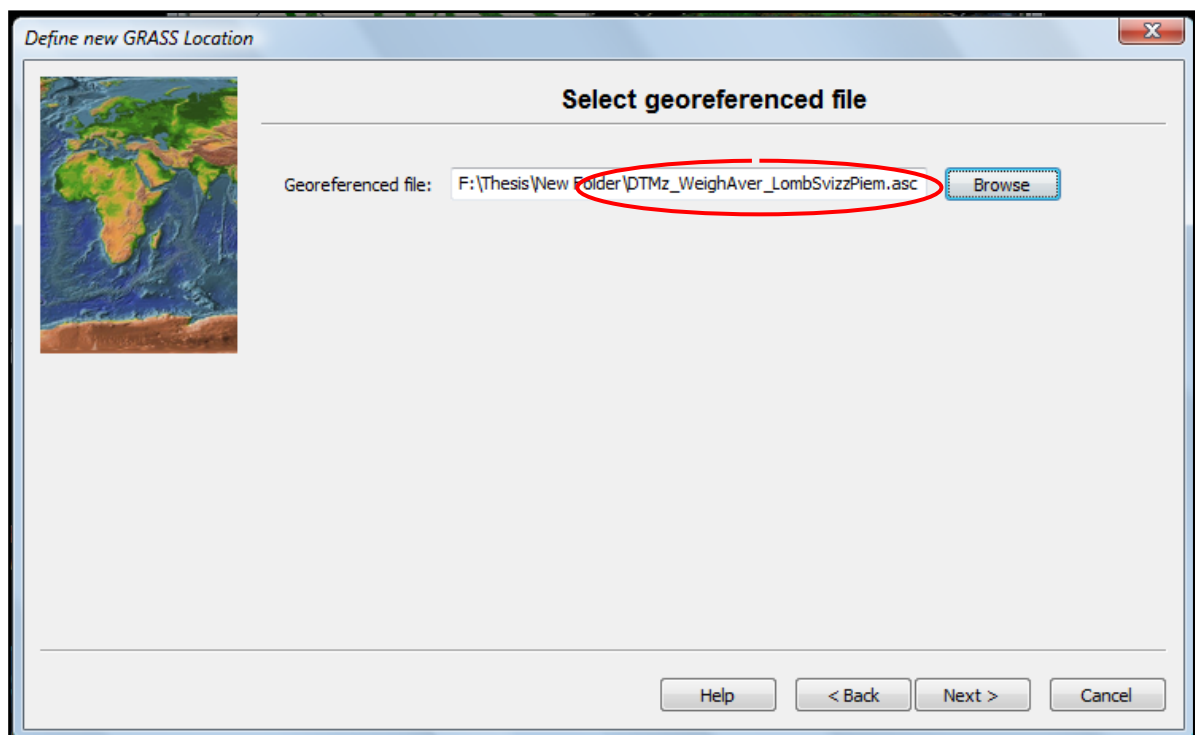


Figure 45 Selecting georeferenced file

Again default region extents have to be set and they are the same as the ones for the location Thesis.

Finally going to the starting window also the location HELIDEM appears next the location Thesis.

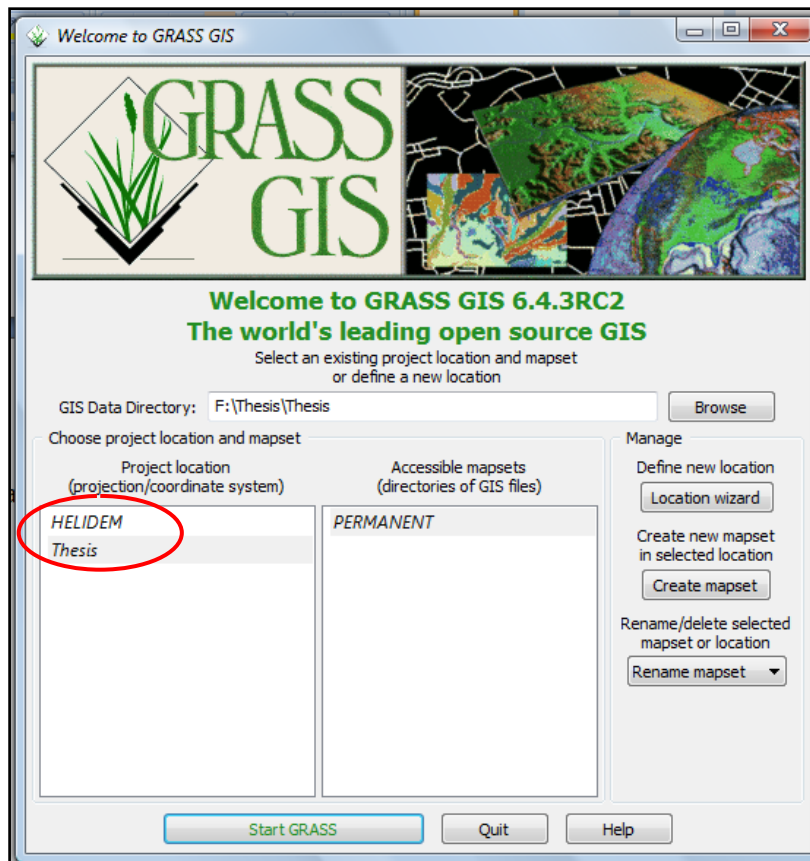


Figure 46 GRASS Locations available

5.3 Import of global DEMs

Once the Global DEMs are downloaded, they have to be imported in the GRASS platform in Location “Thesis” in projection read by projection file referring to ASTER DEM as it is mentioned in the beginning of the present chapter.

5.3.1 Import of ASTER and SRTM data

The operation is realized from the menu as following:

File → Import raster data → Common formats import
or directly by the command r.in.gdal.

When the command is executed, a new window appears. In it through the bottom browser it is possible to select the raster location file, in this case ASTER. By default, the type of format of the browser window is GeoTIFF, taking into account that ASTER is not in this format but ASCII and then the parameter “All files” is selected.

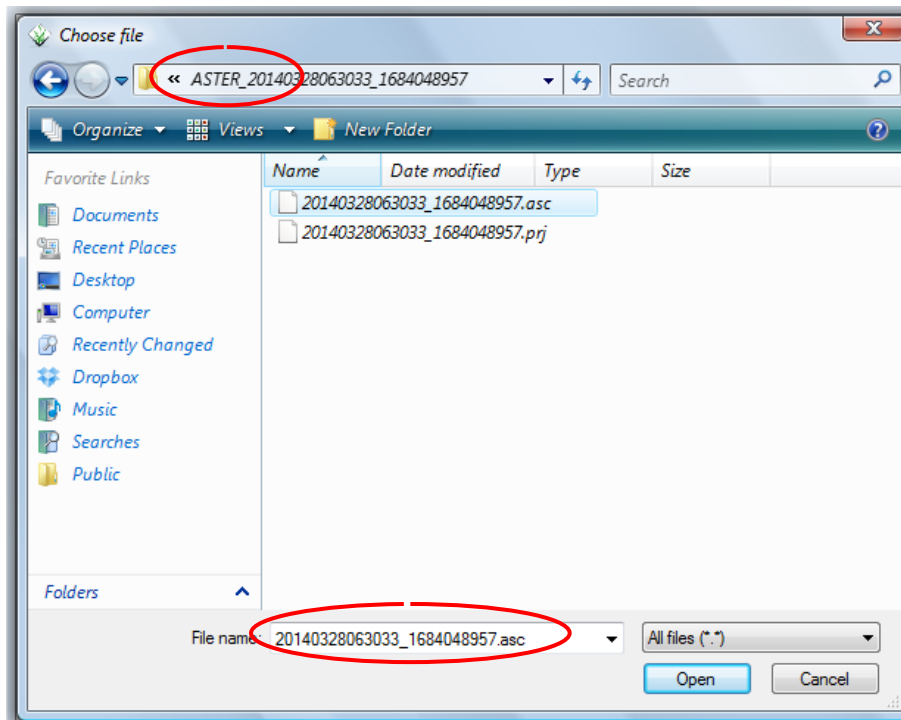


Figure 47 Selecting ASTER ascii file for import

The last but not the least step, in the main import window tick “Override projection” which uses location’s projection. If the user wishes to ignore the difference between the apparent coordinate system of the source data and the current location, they may pass the -o flag to override the projection check. In the previous part of the present chapter is already explained that for Location’s projection is used the projection file referring to ASTER and since the three DEMs use the same projection is better that the “Override projection” tick is done, moreover, when there is no projection file referring to GMTED.

After choosing the “Import” the operation is done.

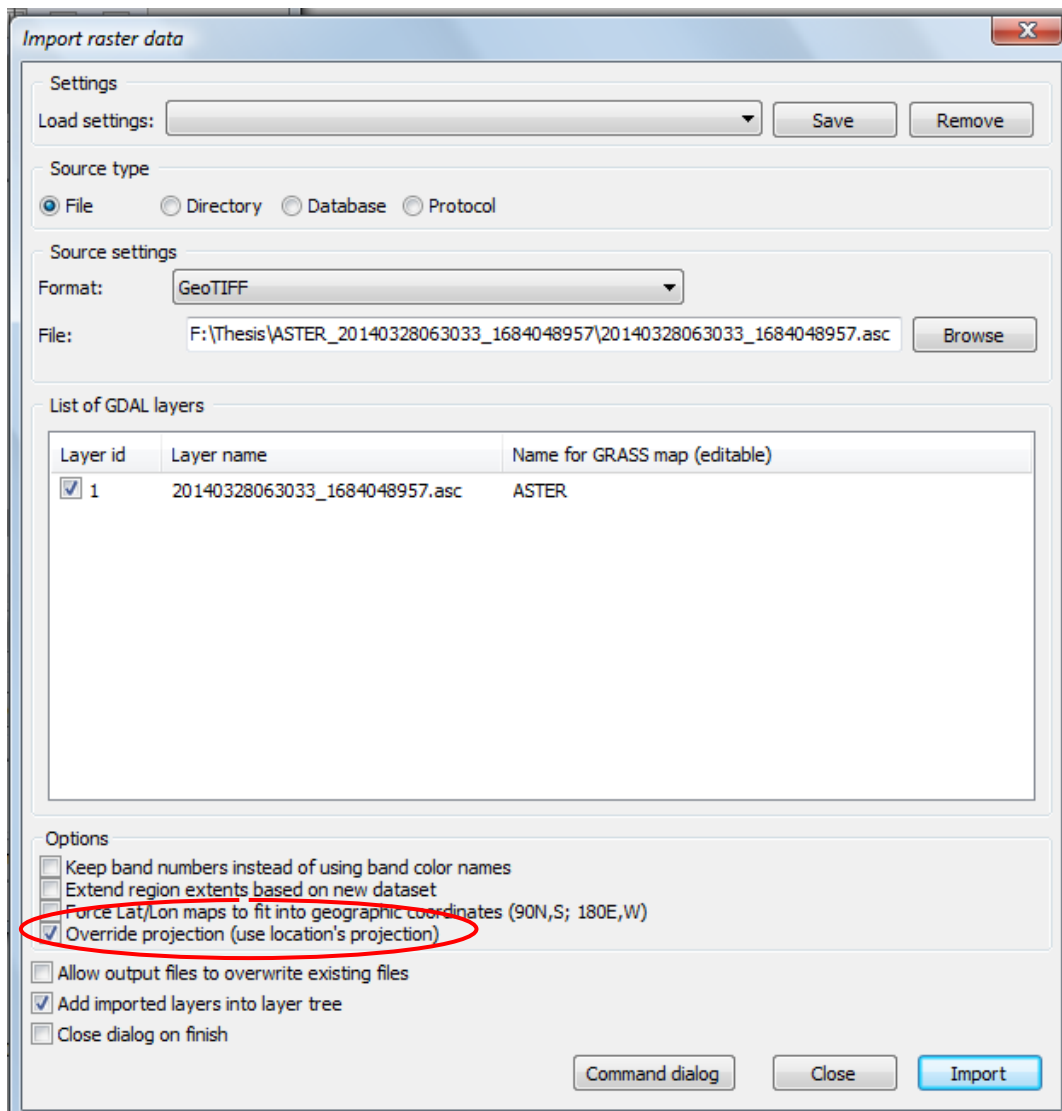


Figure 48 Importing ASTER

Resuming:

r.in.gdal → browser → type of format = All format → ASTER → Overwrite projection → Import

The same procedure is repeated for importing SRTM DEM.

5.3.2 Import of GMTED2010 data

The same steps are followed, just with a small variation in the type of format. In addition, it is worth noting the data that have been downloaded contains 7 files inside the DEM folder, just recalling something that was mentioned in Chapter 2. Thus, from these 7 files only the raster map corresponding to the mean is going to be used.

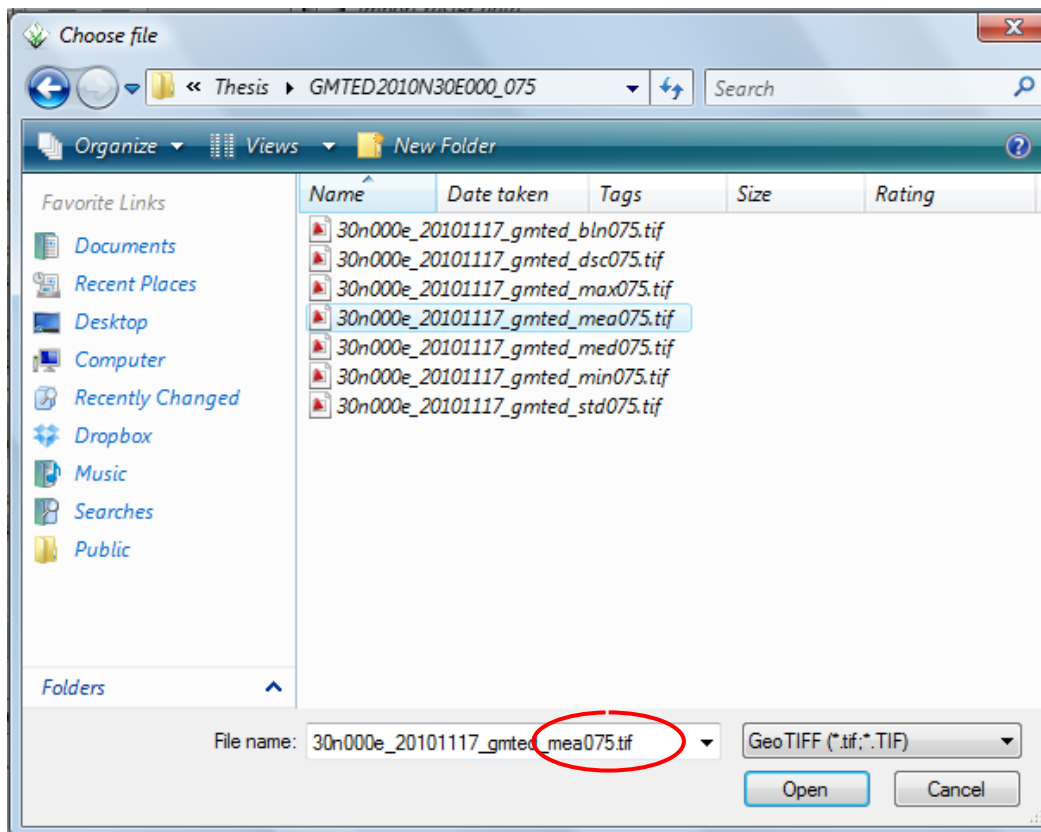


Figure 49 Selecting GMTED mean value file for import

Finally, the three global DEMs are shown by calling them with the command “Add multiple raster or vector map layers” shown on the figure below.

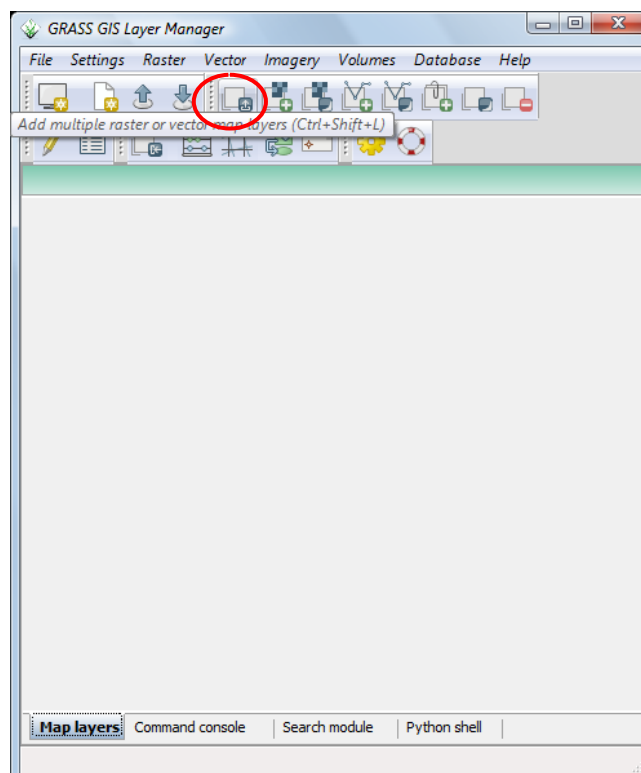


Figure 50 Add multiple raster or vector map layers

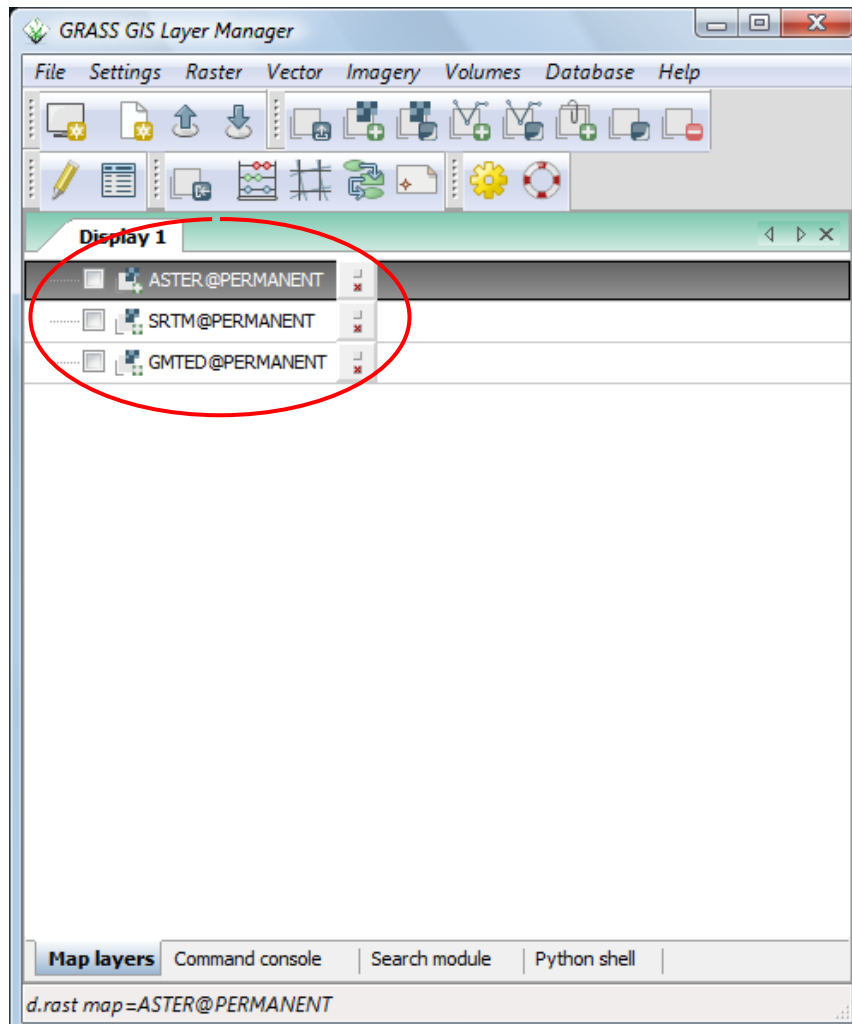


Figure 51 Displayed raster maps

The displayed raster maps of the global DEMs are shown on the figures in the next pages.

Figure 52 ASTER

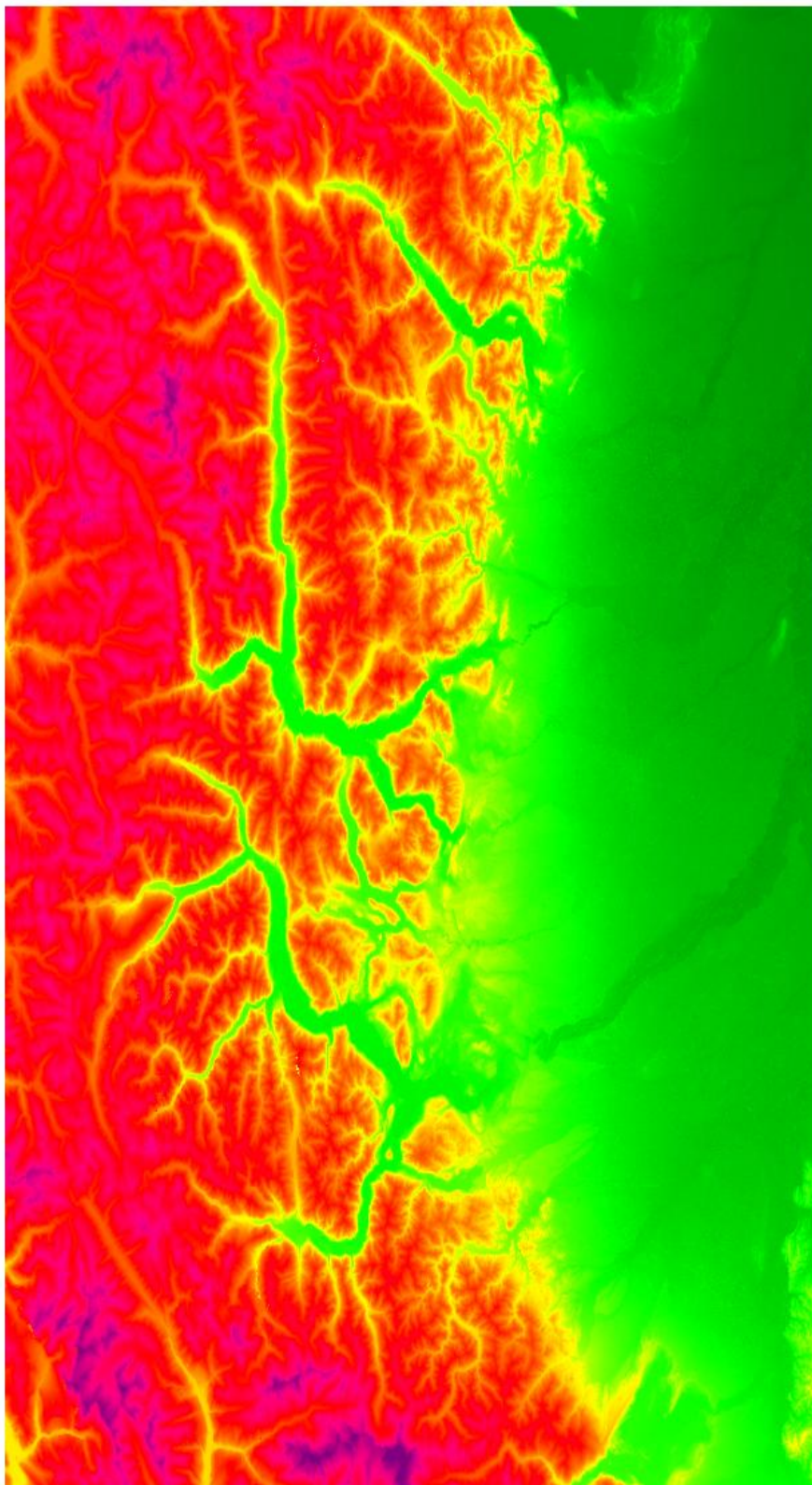
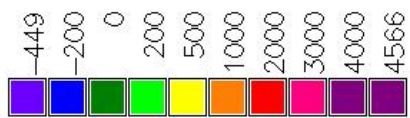


Figure 53 SRTM

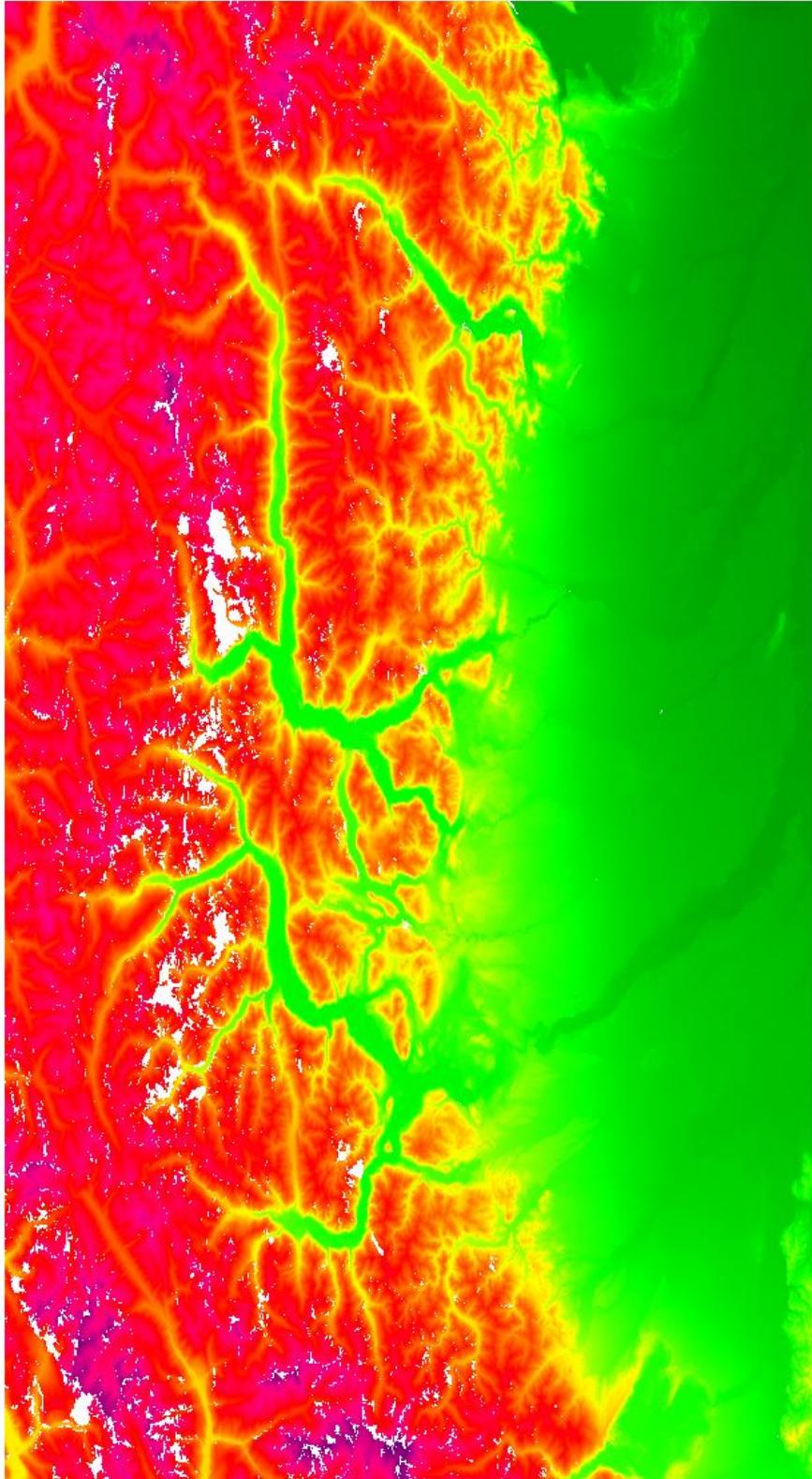
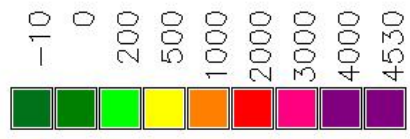
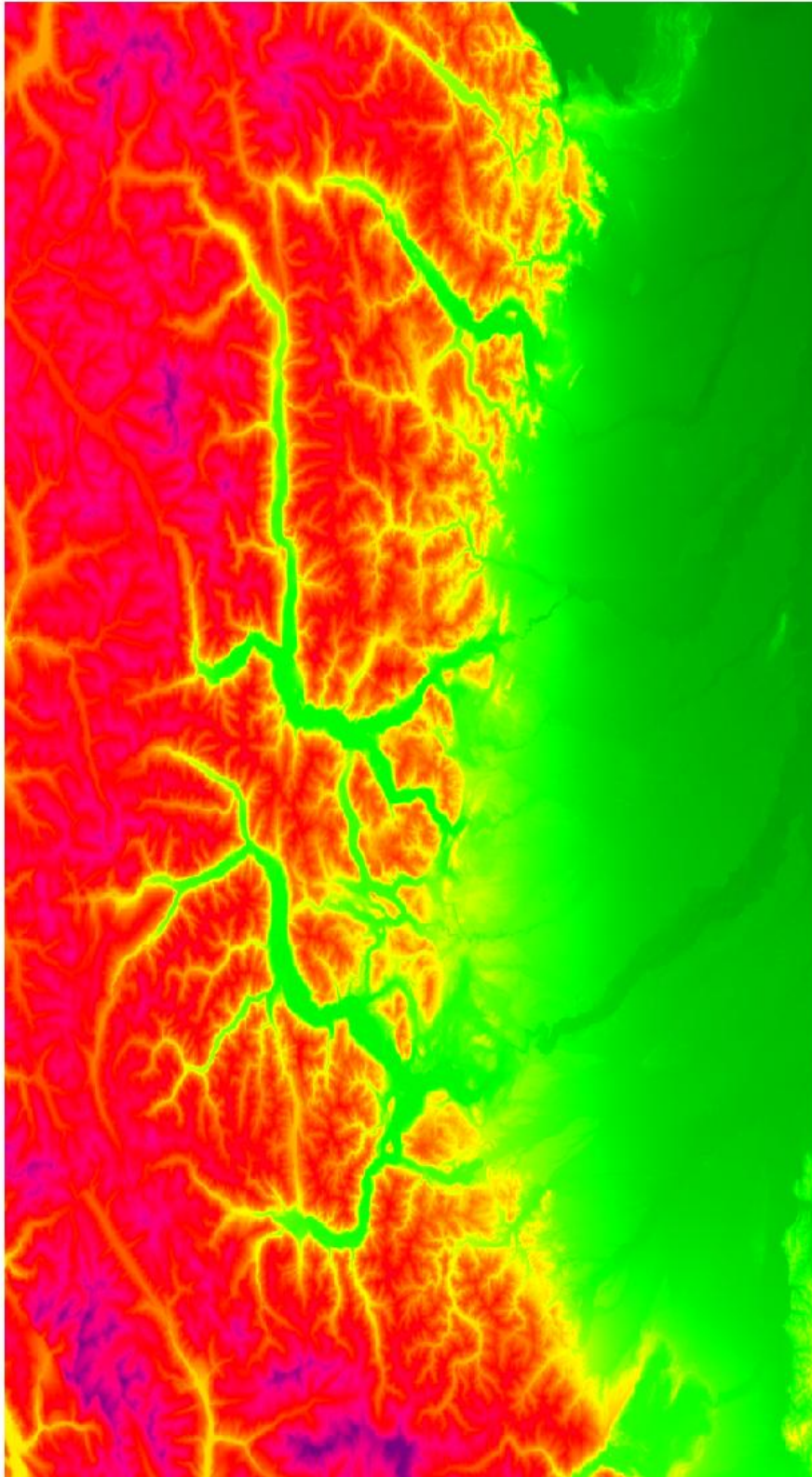
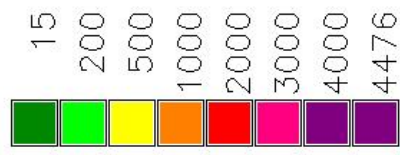


Figure 54 GMTED



5.4 Import of HELI-DEM

HELI-DEM has to be imported in Location HELIDEM because it is not referenced to the WGS84 datum as the global models are, even though it is in geographical coordinates.

From the starting window the correct location is chosen and the import follows as for the global DEMs. Easier way to change location is directly from the menu as follows:

Settings → GRASS working environment → Change location and mapset

Then a new window appears and the location “HELIDEM” is chosen.

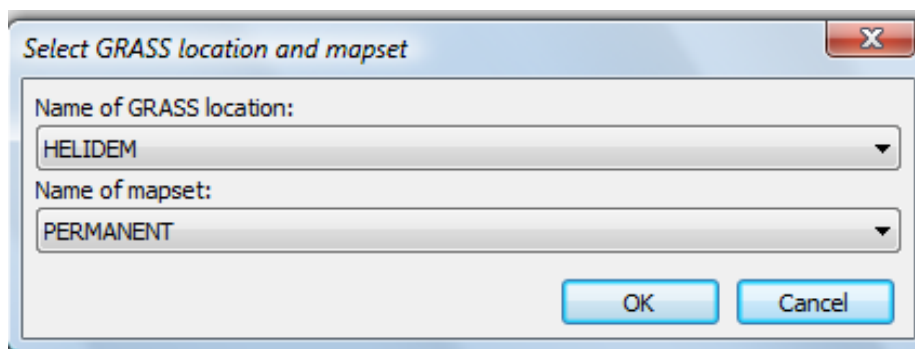


Figure 55 Changing current location

To import the file again the command `r.in.gdal` is used.

A new window appears where the file is chosen and renamed to “HELIDEM” for easier usage. A tick has to be put in the box “Override projection (use location’s projection)” so that GRASS will use the already georeferenced file to project the model.

The import window and the display of the raster in the platform are shown on the next two figures followed by the visualization of the raster map of HELI-DEM.

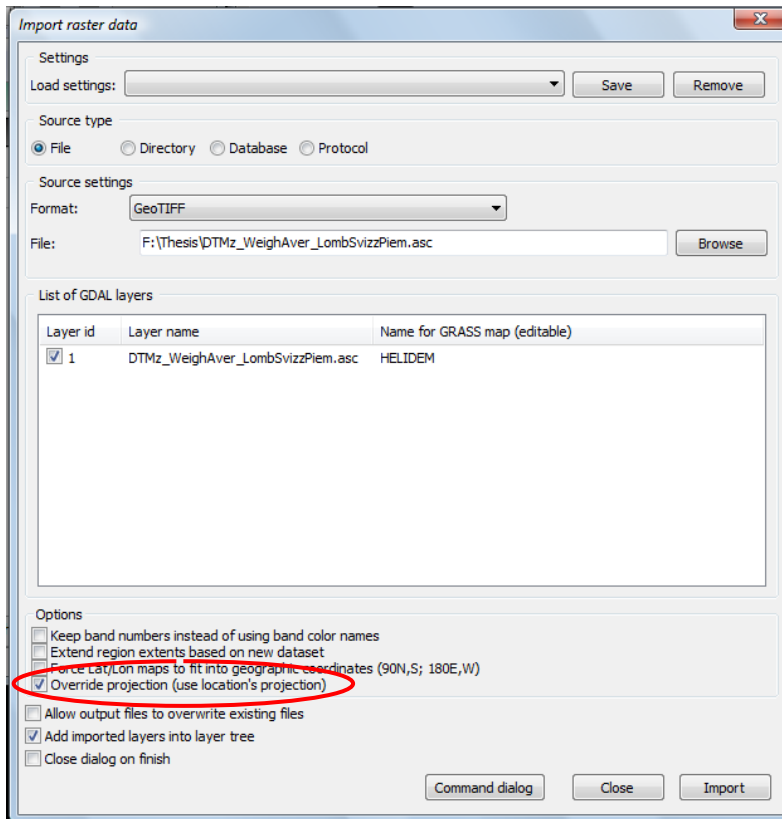


Figure 56 Importing HELIDEM

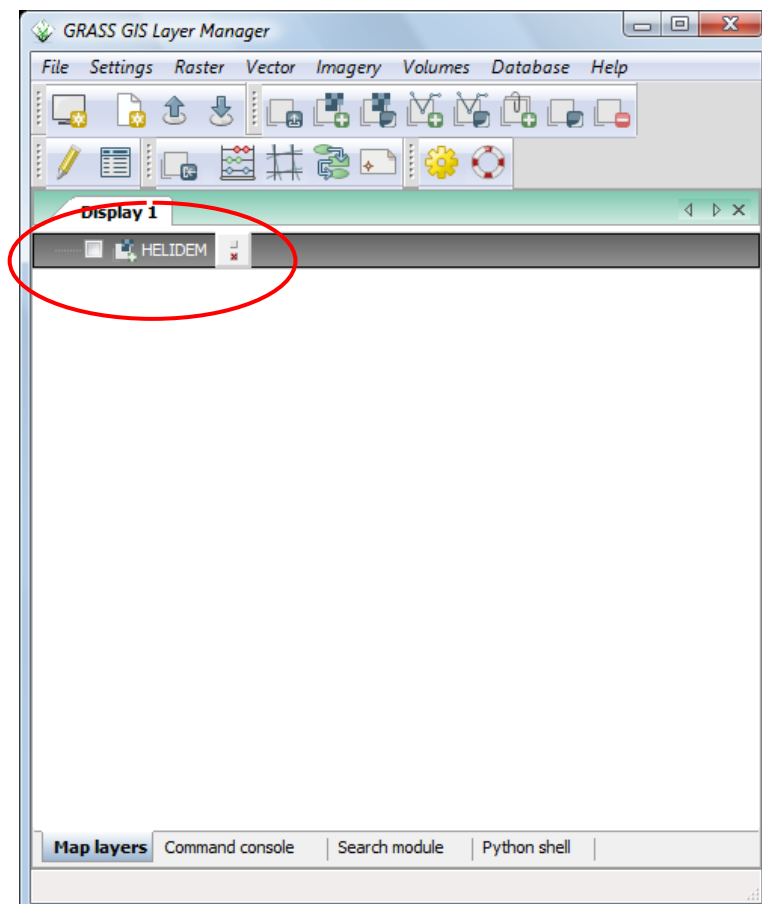
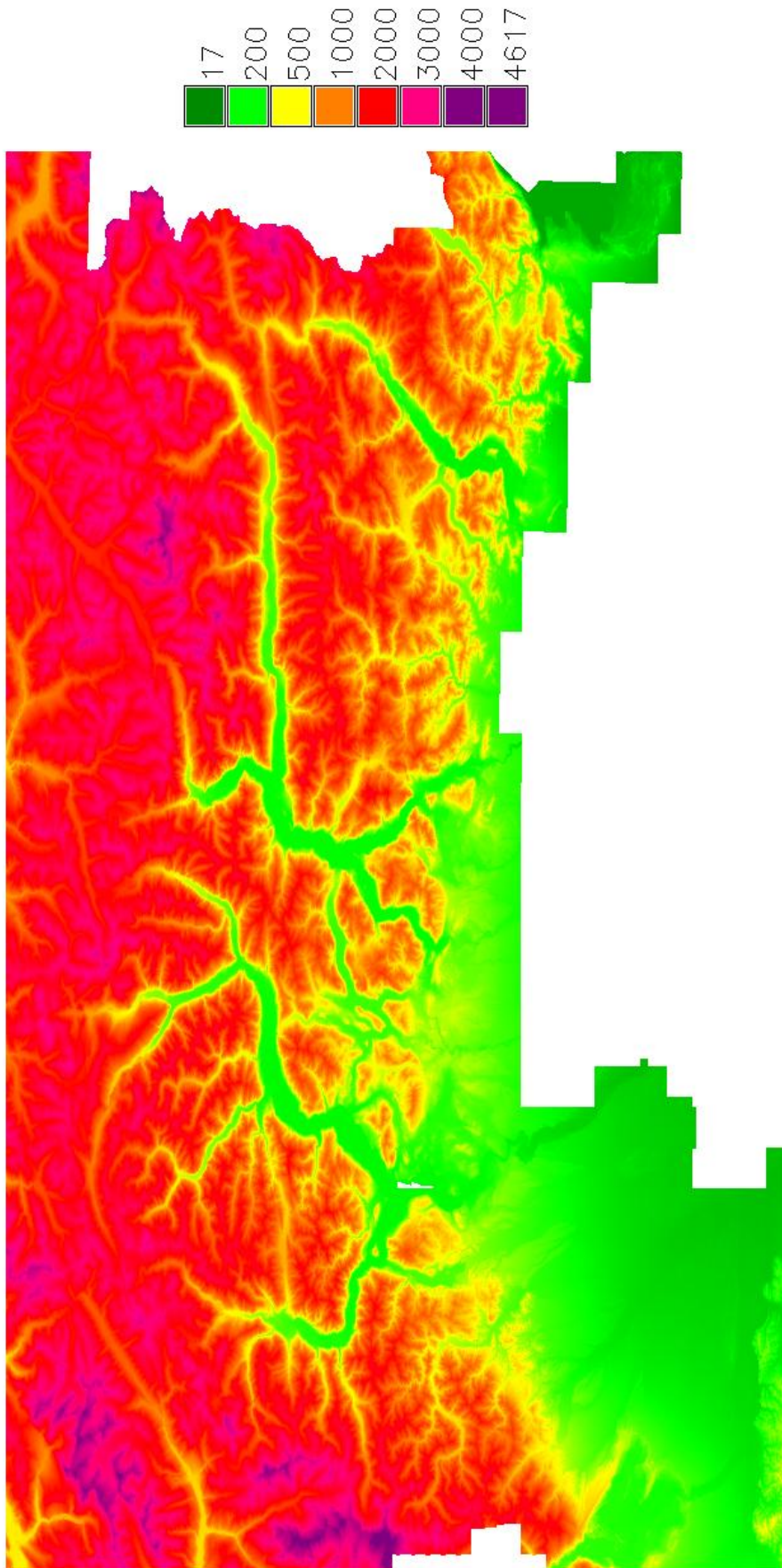


Figure 57 HELIDEM display

Figure 58 HELIDEM



5.5 Statistics of Data

To perform any operation in GRASS is required to select a temporary region by the command `g.region rast` which takes the area of this raster and the operations are done only inside the region.

Note: In GRASS, a “region” refers to a geographic area with some defined boundaries, based on a specific map coordinate system and map projection. Each region also has associated with it the specific east-west and north-south resolutions of its smallest units (rectangular units called "cells"). Typically all raster and display modules are affected by the current region settings (“GRASS GIS manual: g.region,” n.d.). Thus, a new region is selected as follows:

```
g.region rast = ASTER@PERMANENT
```

Details about the region could be reported with the command: `g.region -p`

The region could be set as default with: `g.region -s`

In order to have an overview of the data, some statistics are calculated. The next table presents the results that have been obtained. They are extracted directly with the command `r.univar`.

Statistics about HELIDEM are calculated in the same way as before by `r.univar` and a region HELIDEM is set in advance again by the command `g.region`.

	ASTER	SRTM	GMTED	HELIDEM
total non-null cells	60'134'400	6'532'017	1'069'056	88'477'603
minimum, (h) , m	-449	-10	15	17
maximum, (h) , m	4566	4530	4476	4617
mean, $\mu (h)$, m	1071,45	1045,79	1072,57	1300,55
standard deviation, $\sigma (h)$, m	963,77	950,92	959,86	920,10

Table 6 Statistics global and local DEMs

The first comment is done about the number of pixels, clearly, the number of pixels of the ASTER model is bigger the rest of the models due to the higher resolution that ASTER has with respect to SRTM and GMTED resolution. The same applies for the HELI-DEM which has even higher resolution than ATER.

It is seen that the maximum, the mean and the standard deviation are similar but it could be clearly recognized that the ASTER model has extremely lower minimum value compared with the other models and that behavior will be analyzed in the next chapters. In general, there is a good agreement in general statistics.

5.6 Re-projection of HELI-DEM

The local model is already imported but a technical problem arises – the HELI-DEM data is in another location and the resolution of the model is better than any of the global ones so it is needed an additional transformation step.

Note: Raster maps are backward projected in GRASS. This means that the user has to run the raster projection command (`r.proj`) in the target location and "pull" the map from the source location. Both locations need to have a projection defined (“Projections in GRASS GIS,” n.d.).

HELIDEM has to be sampled by decreasing the resolution until it reaches the ones of the global models. The new raster maps have to be saved in the same Location “Thesis” where there are the global DEMs so that computations, comparisons and further analyses could be initiated. Three cases are going to be presented.

The first task needed to be done before starting the projection is to set a specific region depending on the current global model (ASTER/SRTM/GMTED).

Case a = ASTER@PERMANENT

Case b = SRTM@PERMANENT

Case c = GMTED@PERMANENT

Once the region has been chosen, HELIDEM raster map is transformed from: Raster → Develop raster map → Reproject raster map

or directly from the command `r.proj`.

The command reads a map from a different location, in this case “HELIDEM”, re-projects it and writes it out in the current location “Thesis”.

There is some input information that has to be fulfilled as:

- Location containing input raster map
- Name of input raster map to re-project
- Mapset containing input raster map
- Path to GRASS database of input location
- Name of output raster map
- Interpolation method to use (cubic)
- Resolution of output map (here is put the calculated parameter)

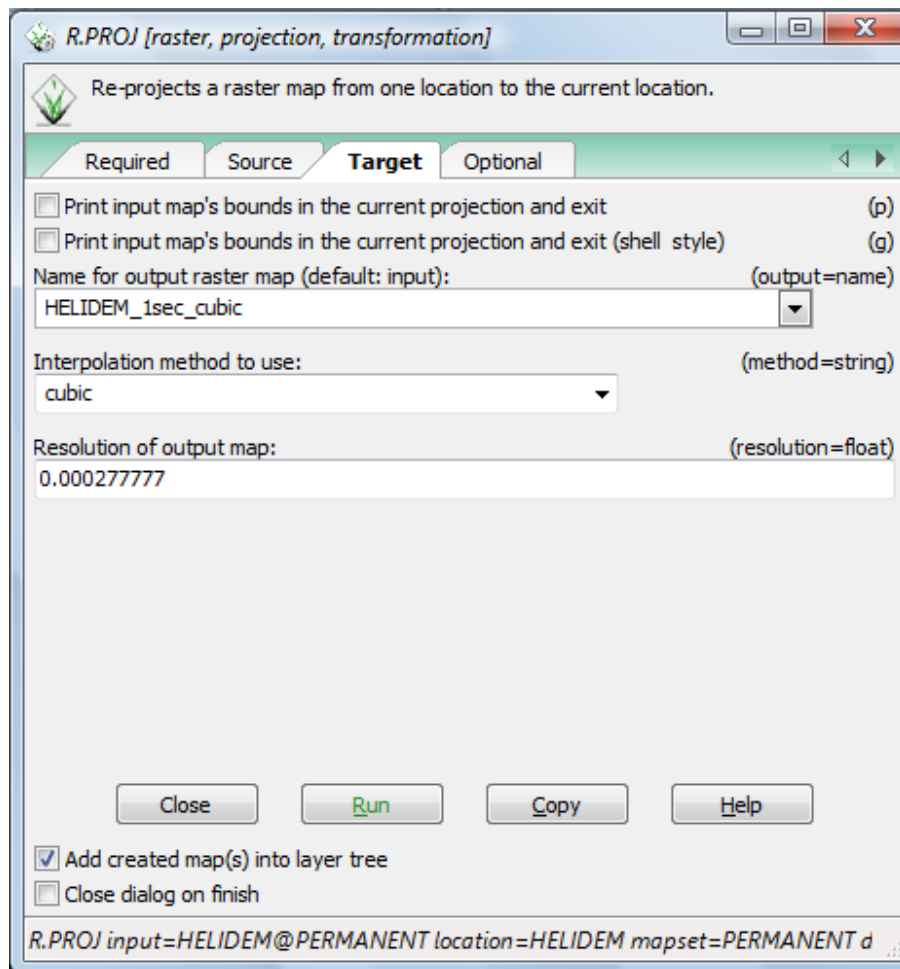


Figure 59 Reprojection of HELIDEM

The command georeferences the raster map in the datum already defined for the current location (WGS84) and decreases the resolution level from the HELIDEM resolution (0.72 arc-second (about 20m) to the global models resolution (1 arc-second (about 30m), 3 arc-second (about 90m) and 7,5 arc-second (about 250m)) using different interpolation methods that GRASS gives as options: nearest, bilinear and cubic. For this study is chosen the **cubic** method which is described in Chapter 1. This method generally is considered as better because it gives more reliable results than the other two methods so it is chosen to be used for this study.

The values can be obtained by dividing the number of arc-seconds into 3600 and the results are respectively:

Case a: $1/3600 = 0.000277777$ (1 arc-second, the same resolution as ASTER)

Case b: $3/3600 = 0.000833333$ (3 arc-second, the same resolution as SRTM)

Case c: $7.5/3600 = 0.002083333$ (7.5 arc-second, the same resolution as GMTED)

Finally the commands executed and the corresponding results are:

1 arc-second resolution:

```
r.proj input=HELIDEM location=Thesis mapset=PERMANENT
dbase=F:\Thesis\Thesis output=HELIDEM_1sec_cubic method=cubic
resolution=0.000277777
```

3 arc-second resolution:

```
r.proj input=HELIDEM location=Thesis mapset=PERMANENT
dbase=F:\Thesis\Thesis output=HELIDEM_3sec_cubic method=cubic
resolution=0.000833333
```

7.5 arc-second resolution:

```
r.proj input=HELIDEM location=Thesis mapset=PERMANENT
dbase=F:\Thesis\Thesis output=HELIDEM_7.5sec_cubic method=cubic
resolution=0.002083333
```

Cols	14500
Rows	8000
North	46.7
South	45.1
West	7.8
East	10.7
EW-res	0.0002
NS-res	0.0002

Table 7 HELIDEM input raster map

	HELIDEM_1sec	HELIDEM_3sec	HELIDEM_7.5sec
Cols	10440	3480	1392
Rows	5760	1920	768
North	46.7	46.7	46.7
South	45.1	45.1	45.1
West	7.8	7.8	7.8
East	10.7	10.7	10.7
EW-res	0.000278	0.000833	0.002083
NS-res	0.000278	0.000833	0.002083

Table 8 HELIDEM Output raster maps

At the end the generated files are:

HELIDEM_1sec_cubic@PERMANENT

HELIDEM_3sec_cubic@PERMANENT

HELIDEM_7.5sec_cubic@PERMANENT

For the statistics seen in next table are taken only cells with non-null values and could be seen that the numbers are different from the ones of the output raster maps presented in the tables on the previous page.

	HELIDEM_1sec	HELIDEM_3sec	HELIDEM_7.5sec
total non-null cells	45'821'175	5'093'341	815'198
minimum, (h) , m	15,88	15,88	58,68
maximum, (h) , m	4614,17	4608,85	4558,83
mean, $\mu (h)$, m	1300,60	1300,71	1300,42
standard deviation, $\sigma (h)$, m	919,87	919,87	919,95

Table 9 Statistics of HELIDEM data in different resolutions

The figures on the next pages visualize the new created raster maps presenting HELI-DEM model in the tree different resolutions.

Figure 60 HELIDEM_1sec_cubic

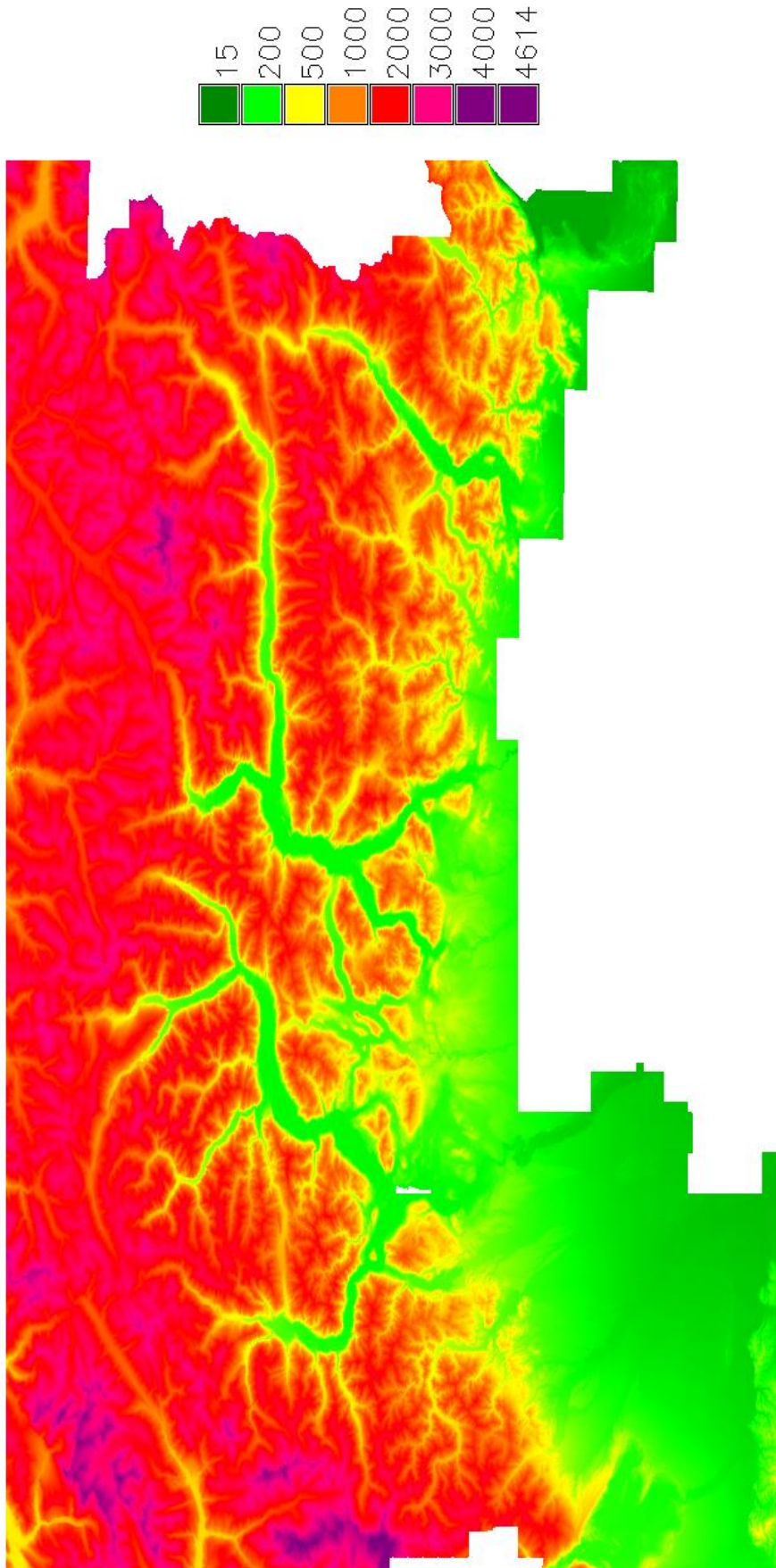


Figure 61 HELIDEM_3sec_cubic

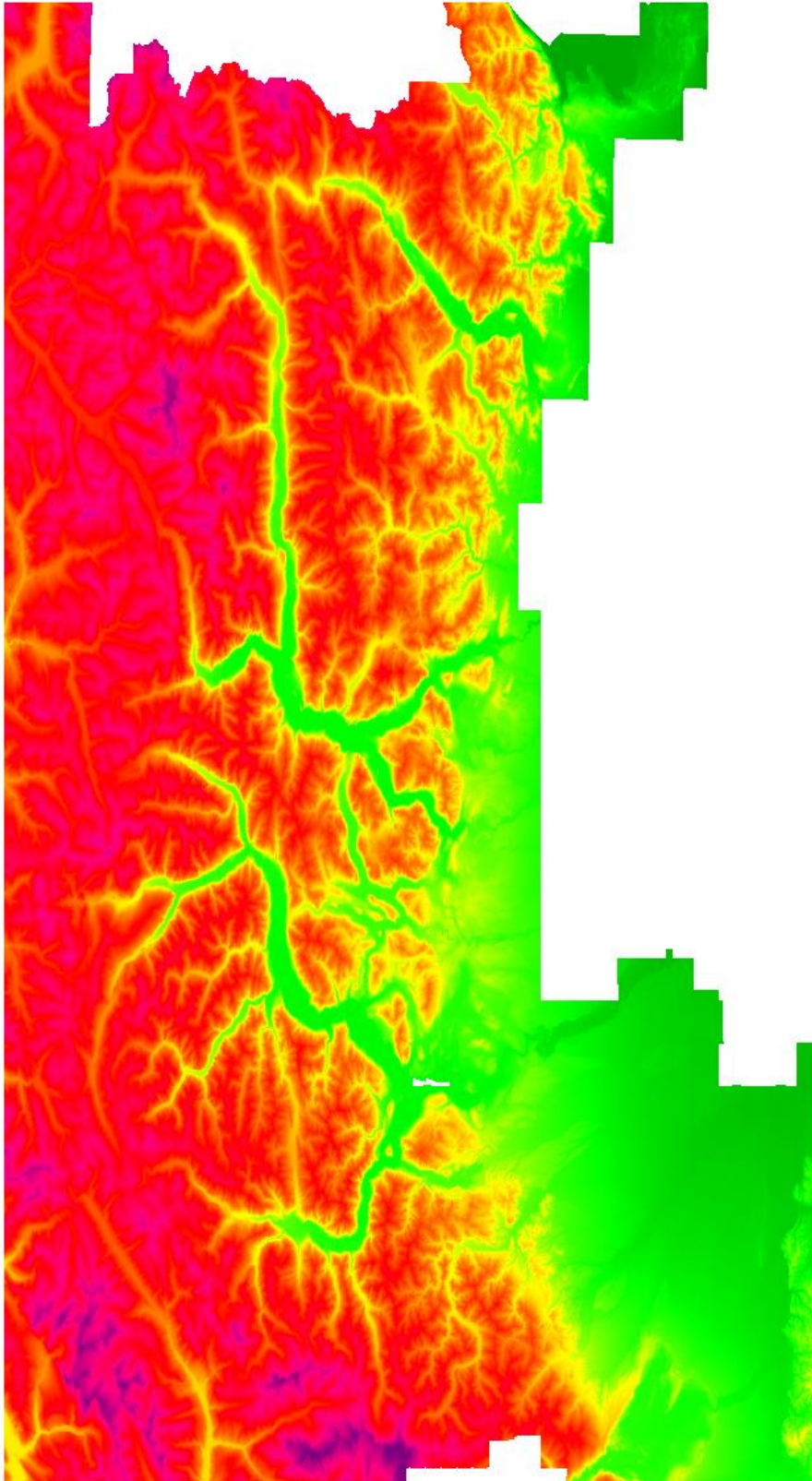
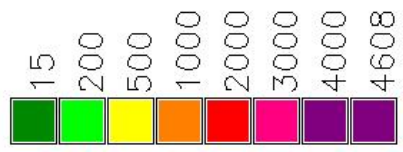
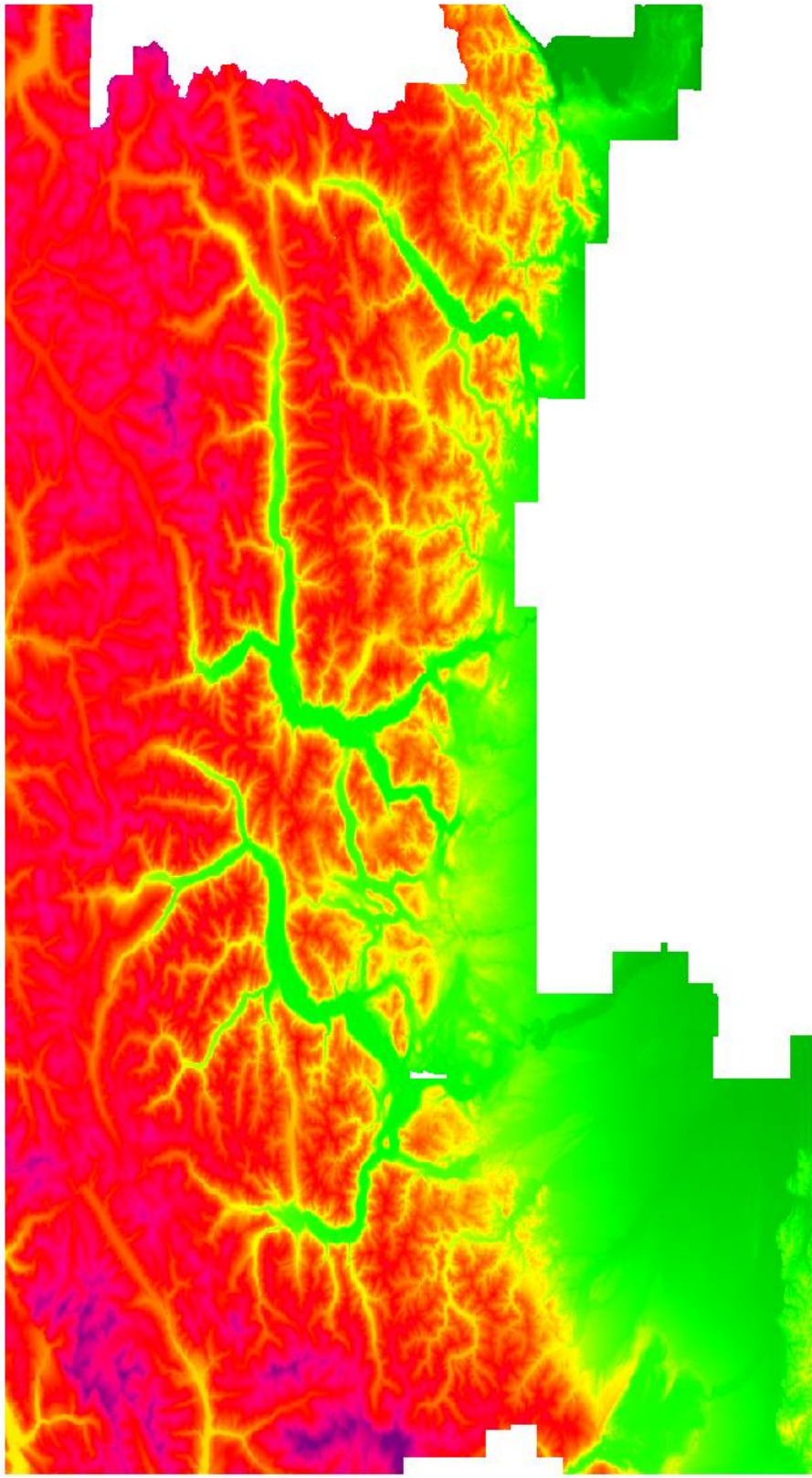
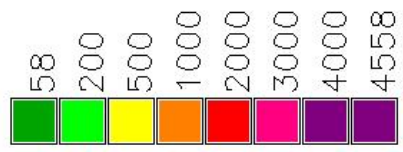


Figure 62 HELIDEM_7.5sec_cubic



Chapter 6

6 Comparison between ASTER Global DEM and HELI-DEM Local DEM

In this chapter a final map of the differences between the local model HELI-DEM and the global model ASTER is produced and analyzed. Histogram with the empirical and the normal distribution is presented. Furthermore, a correlation index between the height (h) of the local model and the difference of heights between the two models (Δh) is calculated as well as the correlation index between the slope of HELI-DEM and again the difference of heights between the two models (Δh). The analysis is finished with converting all negative differences into positive and recalculating the two correlation indices. The general analysis is completed by computing the same correlation indices but this time using the absolute values of the differences.

6.1 Analysis of the differences between ASTER and HELIDEM

Once the models are imported into GRASS GIS platform and the transformation process for the local model is carried out as explained in Chapter 5, other further actions can be initiated now.

As mentioned also in previous lines, before any operation a region should be set by the command `g.region rast`. Thus, the region set in this case is `ASTER@PERMANENT`.

By the command `r.mapcalc` is calculated the difference between the global and the local DEMs. This command works with two inputs raster maps `ASTER@PERMANENT` and `HELIDEM_1sec_cubic@PERMANENT`. The output is the produced final raster map `Diff_ASTER_HELIDEM_1sec_cubic` which is the algebraic difference between the input maps. It is illustrated in the next figure.

```
r.mapcalc Diff_ASTER_HELIDEM_1sec_cubic =  
ASTER@PERMANENT - HELIDEM_1sec_cubic@PERMANENT
```

Figure 63 Diff_ASTER_HELIDEM_1sec_cubic



It is important to verify the outcomes in order to work with accurate data and without outliers so to do that some statistical tools will be calculated such as minimum, maximum, mean and standard deviation. The command `r.univar` is applied to obtain these basic statistics.

```
r.univar map=Diff_ASTER_HELIDEM_1sec_cubic@PERMANENT
```

Diff_ASTER_HELIDEM_1sec_cubic	
total non-null cells	45'821'175
minimum, (Δh), m	-2164.07
maximum, (Δh), m	1023.00
mean, μ (Δh), m	4.14
standard deviation, σ (Δh), m	25.41

Table 10 Statistics of Diff_ASTER_HELIDEM_1sec_cubic

According to the results, it is noticeable the presence of very big negative and positive differences, which shows likely a rare behavior on one of the models either the global or the local one. These are clearly anomalous values and their behavior will be analyzed in the following pages.

6.2 Histogram of the differences between ASTER and HELIDEM and classification of the outliers

For the extracted statistics also the respective histogram is obtained. After it is cut for better visualization in the center where are concentrated the majority of the values (Δh from -300 till 300 meters), it is also produced the histogram with a Gaussian distribution calculated with the same mean and standard deviation as the data. The figure bellow presents the comparison between the relative frequency of the empirical distribution of the data and the normal one. It is visible that the empirical distribution is negligibly right-skewed and has a narrower shape compared to the normal one.

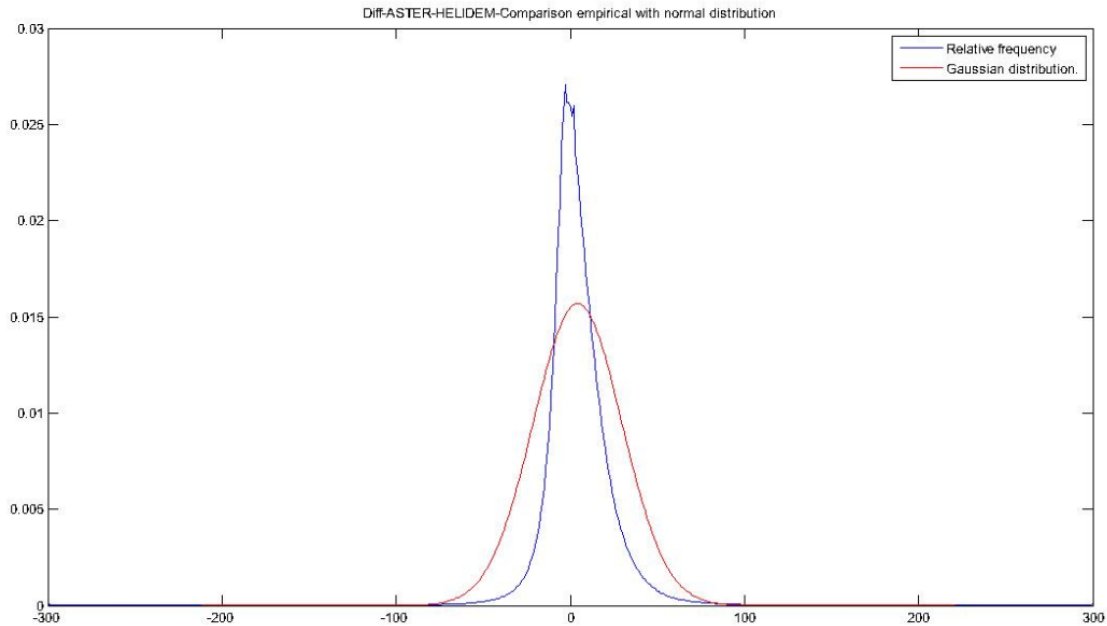


Figure 64 Diff_ASTER_HELIDEM_1sec_cubic – Comparison empirical with normal distribution

By analyzing the statistics and the histogram is observed that the mean values are comparatively close to zero and the standard deviation is of 25 m which is less than the resolution of the input raster maps ASTER and HELIDEM_1sec_cubic, i.e. about 30 m. That means that the majority of the differences are satisfactory. However, it is observed that some outliers exist and it is clean in the minimum and the maximum values.

To verify the amount of outliers, a simple computation is done. The value of three times the standard deviation ($\sigma = 25.41$ m) is used as a threshold and it is equal to 76.23 m. The number of the cells whose values are bigger than it is 346'153 and their percentage of the total number of non-null cells is 0.76%, which is statistically negligible. In additional, a further classification of these values is done and reported in the table.

Diff_ASTER_HELIDEM_1sec_cubic		
Classification	Number of cells	Percent of all non-null cells, %
$3\sigma \leq \Delta h < 100$	171485	0,37
$100 \leq \Delta h < 500$	160881	0,35
$500 \leq \Delta h < 1000$	10165	0,02
$ \Delta h \geq 1000$	3622	0,01

Table 11 Classification of outliers in Diff_ASTER_HELIDEM_1sec_cubic

6.3 Spatial identification of severe outliers

Clearly the previous statistics show outliers; in principal could be generated in the data acquisition or in the data interpolation either in ASTER or/and in HELI-DEM. However, HELI-DEM has been validated against other data sources therefore problems are almost surely in ASTER and it is interesting to identify to investigate their spatial behavior.

Excluding isolated points, there are three areas with differences exceeding 1000 m. They are shown on the following figures:

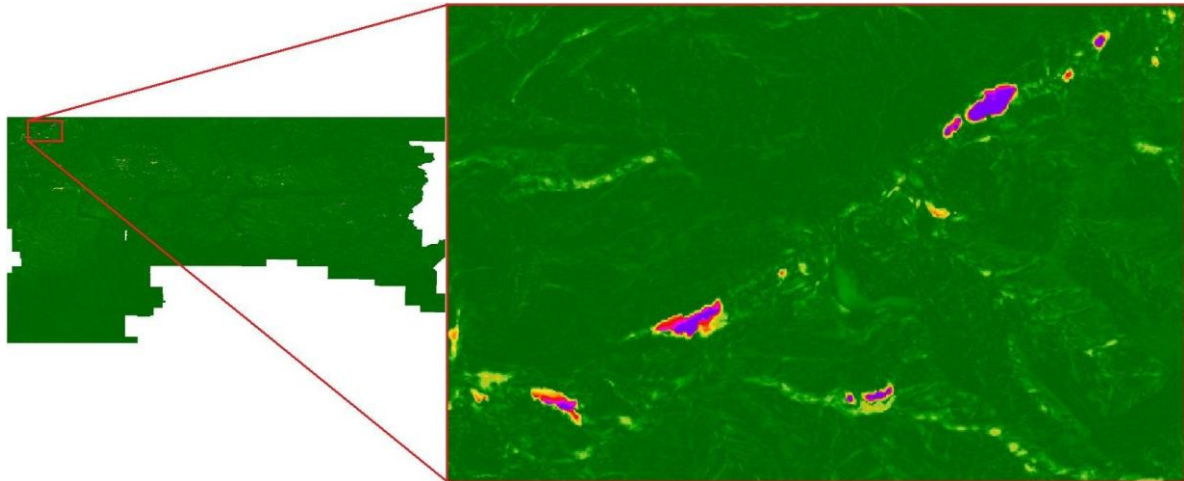


Figure 65 Zoom of area 1 presenting outliers in Diff_ASTER_HELIDEM_1sec_cubic

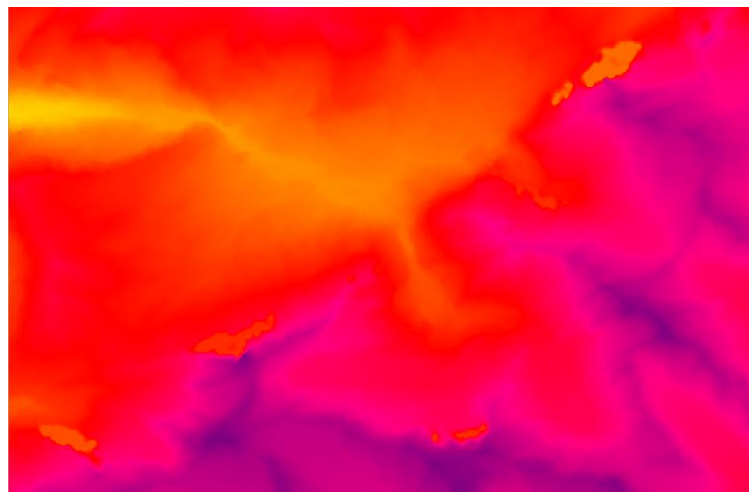


Figure 66 Zoom of area 1 in ASTER

The first one, called Area 1 has extensions: from 46.32 N to 46.40 N in latitude and from 7.55 E to 8.10 E in longitude; it is in very high mountain region with elevation between 1000 and 4000 m. On Figure 66 is shown the same extent but in ASTER model. It is visible that the same outliers exist also there. These points of ASTER accept constant values; the majority of them: 1177, 1405, 1675 and some of them: 1372 and 1827.

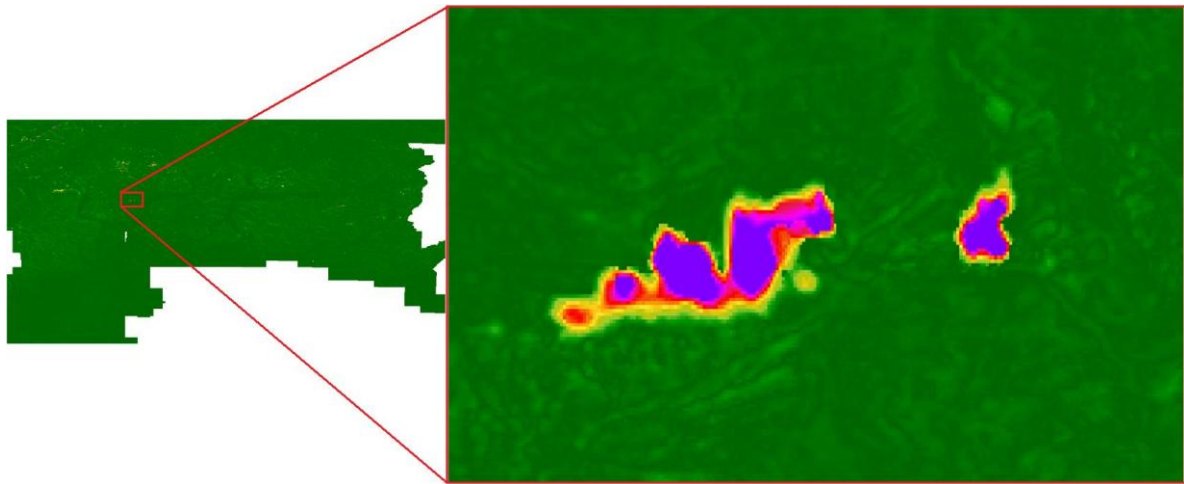


Figure 67 Zoom of area 2 presenting outliers in Diff_ASTER_HELIDEM_1sec_cubic

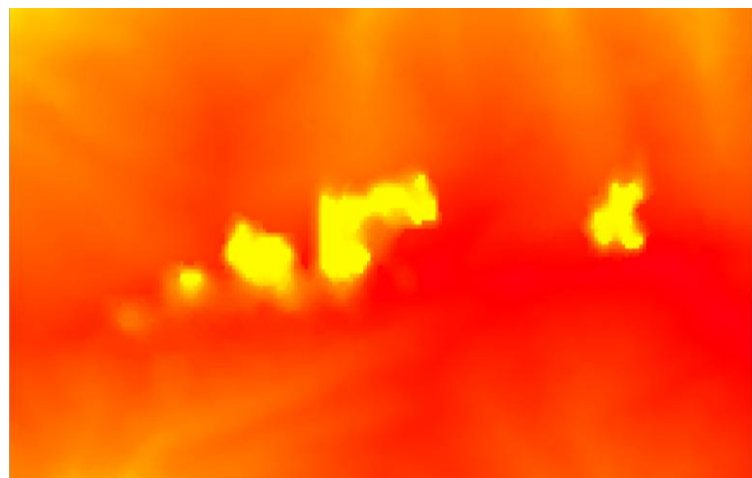


Figure 68 Zoom of area 2 in ASTER

Area 2 has extensions: from 46.06 N to 46.08 N in latitude and from 8.35 E to 8.39 E in longitude. It is in a mountain region where the elevations are between 1000 and 2000 m. On Figure 68 is shown the same extent but in ASTER model. It is visible that the same outliers exist also there. The majority of these points of ASTER accept the constant value 513 and just some of them are equal to 526.

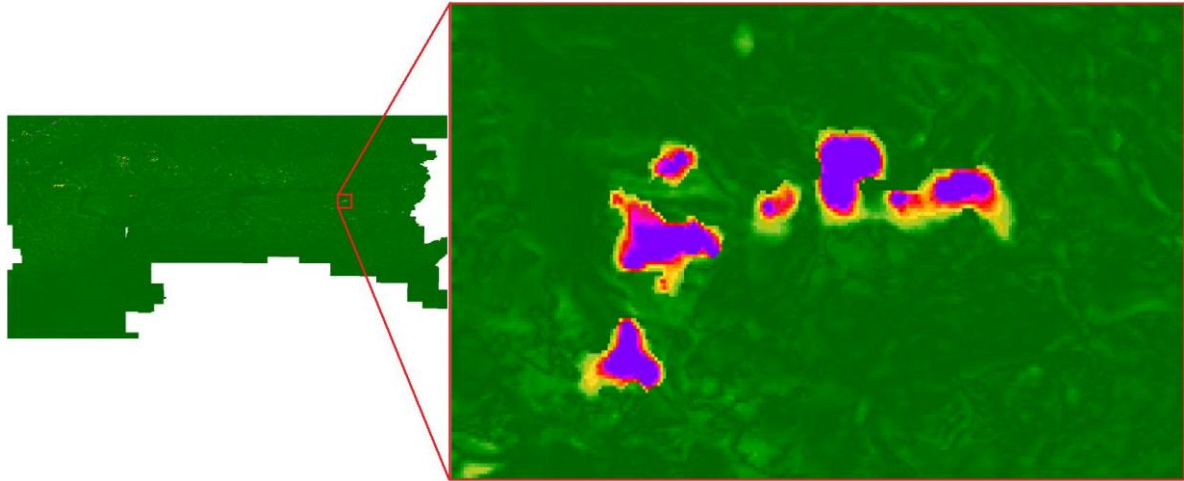


Figure 69 Zoom of area 3 presenting outliers in Diff_ASTER_HELIDEM_1sec_cubic

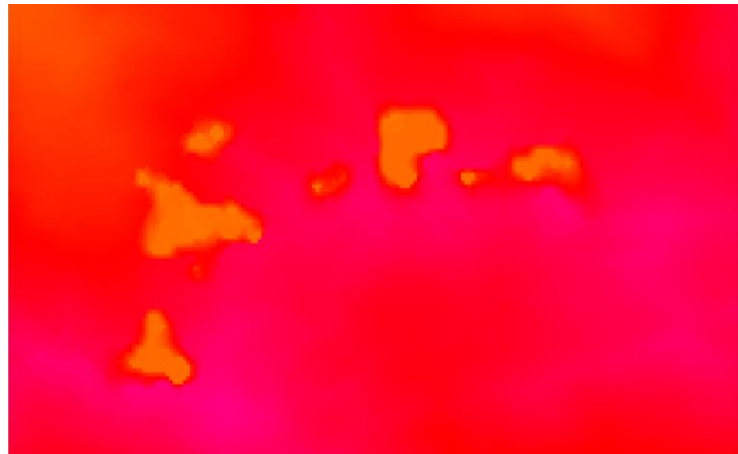


Figure 70 Zoom of area 3 in ASTER

The boundaries of Area 3 are the following: from 46.04 N to 46.05 N in latitude and from 9.59 E to 10.02 E in longitude. It is in a mountain region where the elevations are between 1500 and 3000 m. On Figure 70 is shown the same extent but in ASTER model. It is visible that the same outliers exist also there. The majority of these points of ASTER accept the constant values: 1122, 1152, 1182 and just some of them: 1130 and 1157.

6.4 Identification of correlation between the heights of HELIDEM and their differences with ASTER

To complete this general analysis, two new parameters are calculated:

- Correlation coefficient between the HELI-DEM elevation (h) and the differences ASTER/HELI-DEM (Δh): The goal of using this coefficient is to verify if the differences between ASTER and HELI-DEM models depend on the terrain height.

GRASS GIS has a useful command, namely, `r.covar` which returns the covariance matrix and implicitly the correlation value.

```
r.covar -r map=HELIDEM_1sec_cubic@PERMANENT,
Diff_ASTER_HELIDEM_1sec_cubic@PERMANENT
```

The matrix is obtained:

$$\begin{vmatrix} 1 & 0.02 \\ 0.02 & 1 \end{vmatrix}$$

The value 0.02 indicates null correlation, meaning that the differences between the two models do not depend on the height. That is present also on the following scatter plot, on which in some parts is seen as well a linear relation regarding only the constant values of the outliers in the areas where they exist.

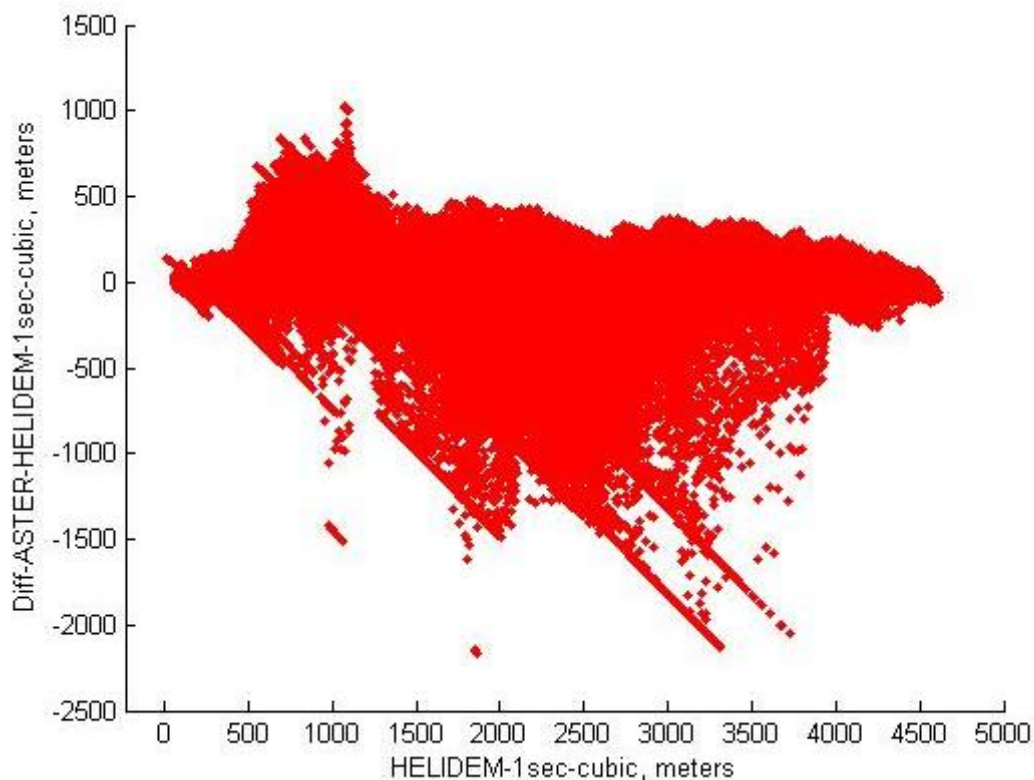


Figure 71 HELIDEM_1sec_cubic vs. Diff_ASTER_HELIDEM_1sec_cubic

Further analysis is done by computing the correlation index again but using the absolute values of the differences.

```
r.covar -r map=HELIDEM_1sec_cubic@PERMANENT,
Diff_ASTER_HELIDEM_1sec_cubic_color@PERMANENT
```

Getting:

$$\begin{vmatrix} 1 & 0.13 \\ 0.13 & 1 \end{vmatrix}$$

The new obtained value is 0.13 and as expected it is higher than the previous one but still does not indicate a significant correlation. The same partial linear relation regarding the constant values of the outliers and the terrain presented by HELIDEM is seen on the figure:

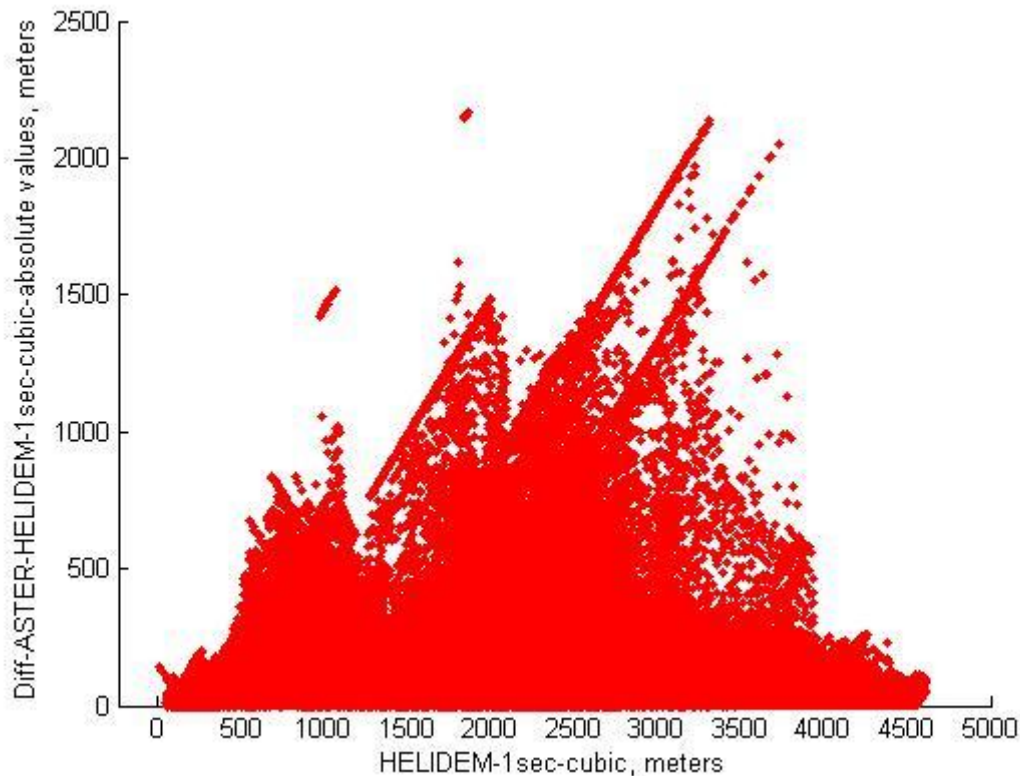


Figure 72 HELIDEM_1sec_cubic vs. Diff_ASTER_HELIDEM_1sec_cubic_absolute values

6.5 Identification of correlation between the slopes of HELIDEM and the differences between ASTER and HELIDEM

The correlation coefficient can be used to present as well a non linear dependence on the slope.

- Correlation coefficient between the HELI-DEM slope (degrees) and the differences ASTER/HELI-DEM (Δh): The goal of using this coefficient is to verify if the differences between ASTER and HELI-DEM models depend on the terrain slope.

The first step is to be produced a slope raster map by the command `r.slope.aspect`.

As an input the name of the raster map whose slope is going to be computed is needed; moreover the name of the output raster map is input. The command produces an aspect raster map as well.

```
r.slope.aspect elevation=ASTER@PERMANENT
slope=ASTER_slope aspect=ASTER_aspect
```

The command is used to be produced the slope raster map for ASTER DEM as well as for the local HELI-DEM DEM in the corresponding resolution of 1 arc-second. The following figures on the next pages are the outputs of the operation. It is also computed their difference by executing the command used before r.mapcalc:

```
r.mapcalc Diff_ASTER_slope_HELIDEM_1sec_cubic_slope =
ASTER_slope@PERMANENT -
HELIDEM_1sec_cubic_slope@PERMANENT
```

Figure 73 ASTER_slope

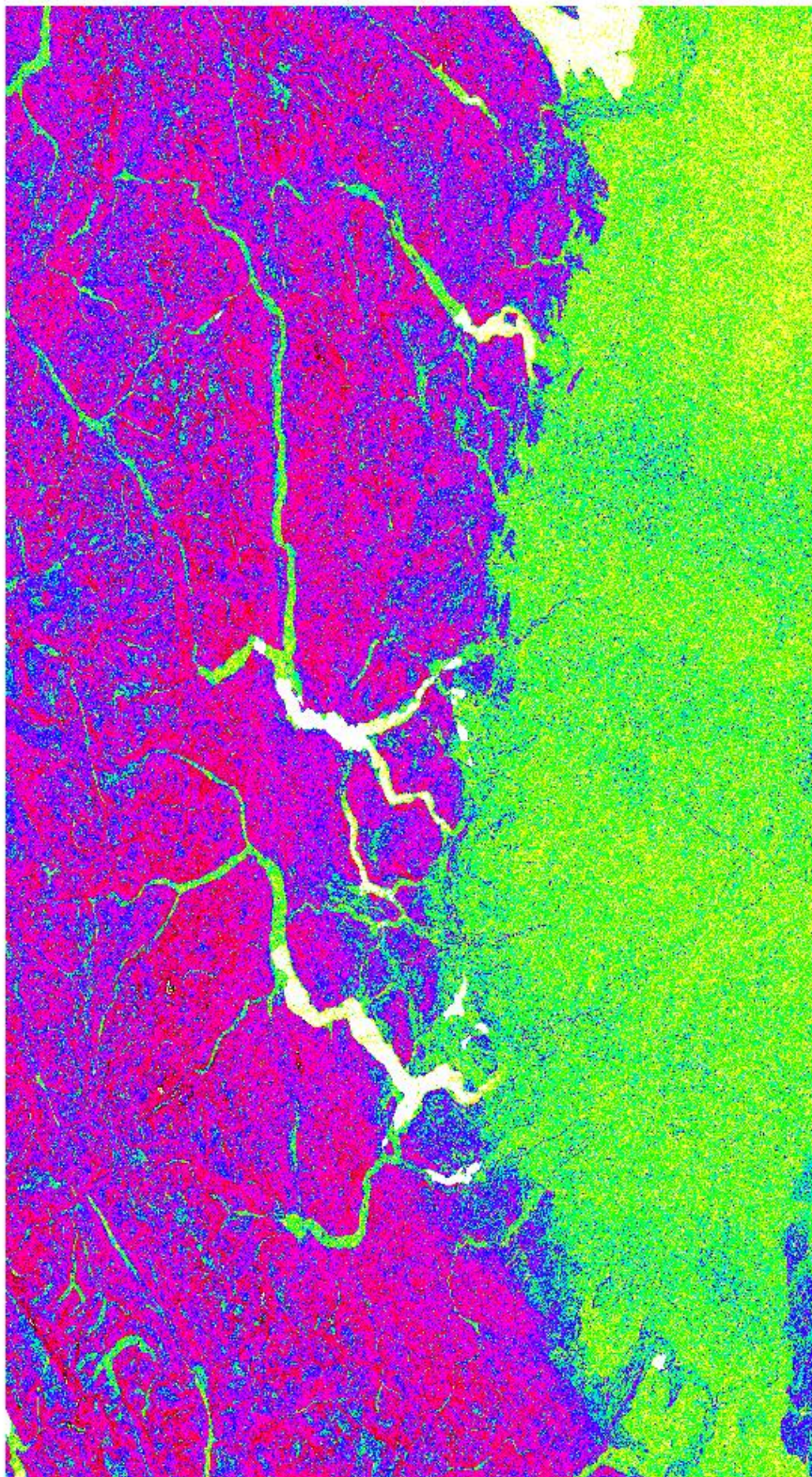
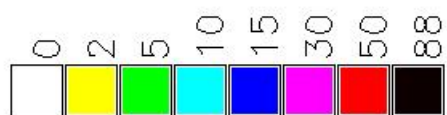


Figure 74 HELIDEM_1sec_cubic_slope

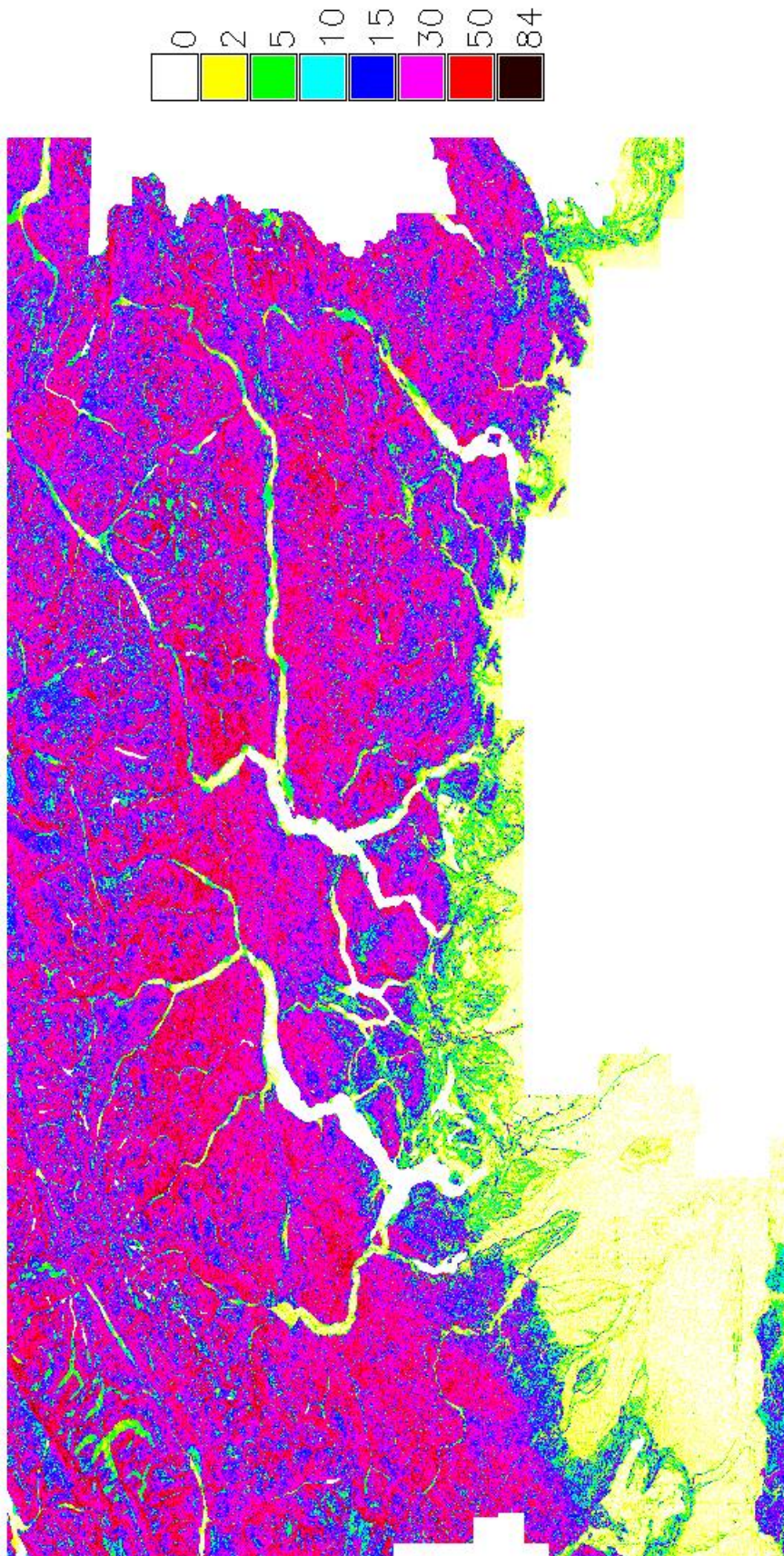
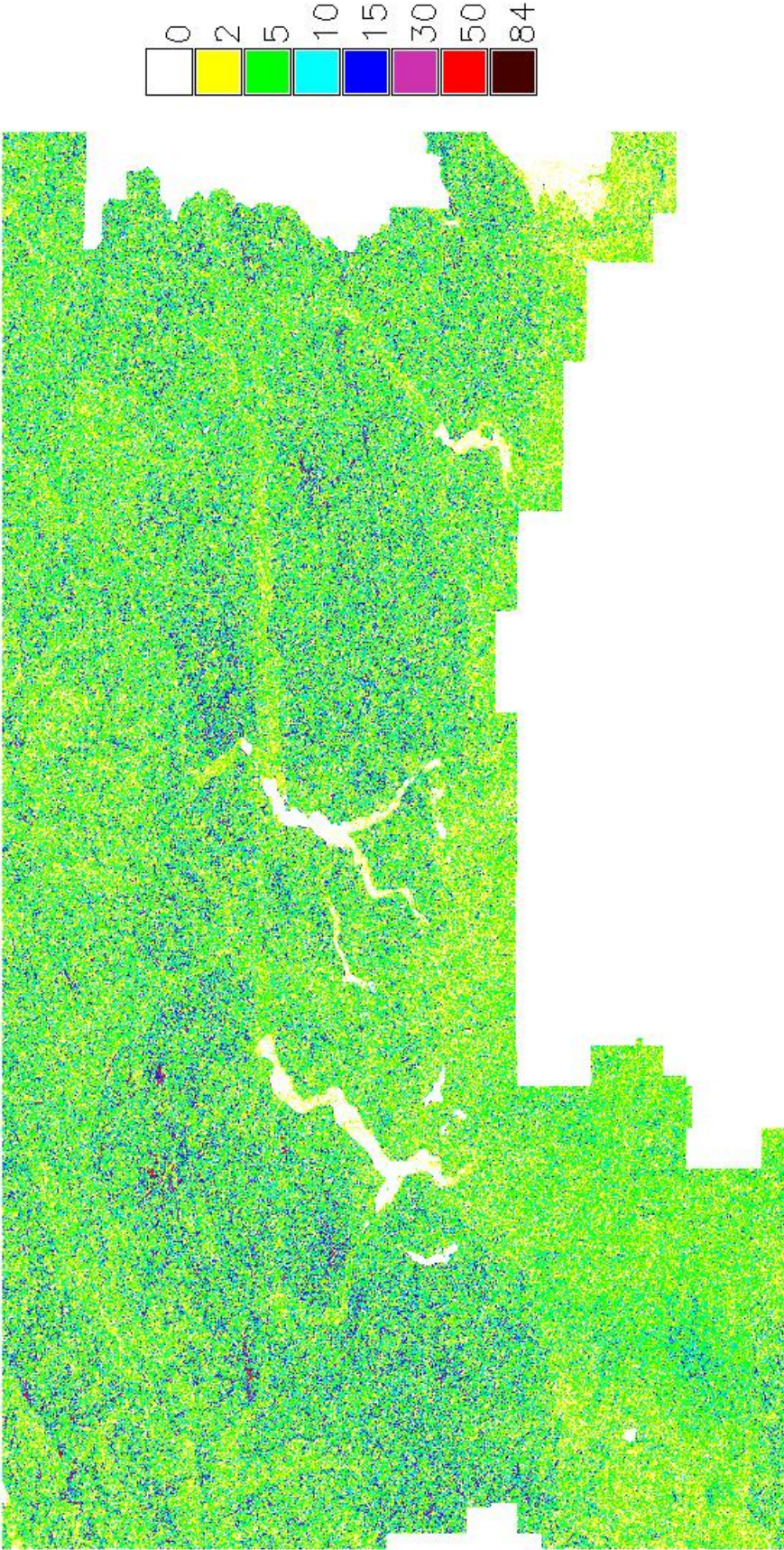


Figure 75 Diff_ASTER_slope_HELIDEM_1sec_cubic_slope_Absolute Values



The next table illustrates some general statistics about the slopes and their differences in absolute values.

	ASTER_slope	HELIDEM_1sec_cubic_slope	Diff_ASTER_slope_HELIDEM_1sec_cubic_slope_abs.val
total non-null cells	60'102'004	45'777'538	45'777'538
minimum, deg	0	0	0
maximum, deg	88,61	84,04	84,52
mean, deg	18,59	22,39	5,39
standard deviation, deg	14,80	15,74	5,19

Table 12 Statistics of ASTER_slope, HELIDEM_1sec_cubic_slope and their difference in absolute values

The maximum value of the differences of the slopes indicates an anomalous behavior which could be understood as possible increase of the depression with the slope. This assumption is going to be confirmed or rejected by the analysis of the correlation index which finally obtained by performing the command:

```
r.covar -r map=HELIDEM_1sec_cubic_slope@PERMANENT,
Diff_ASTER_HELIDEM_1sec_cubic@PERMANENT
```

Getting:

$$\begin{vmatrix} 1 & 0.11 \\ 0.11 & 1 \end{vmatrix}$$

The results obtained by the covariance matrix present a correlation coefficient equal to 0.11 which indicates a not significant relationship between these two parameters. It visualized by the following figure.

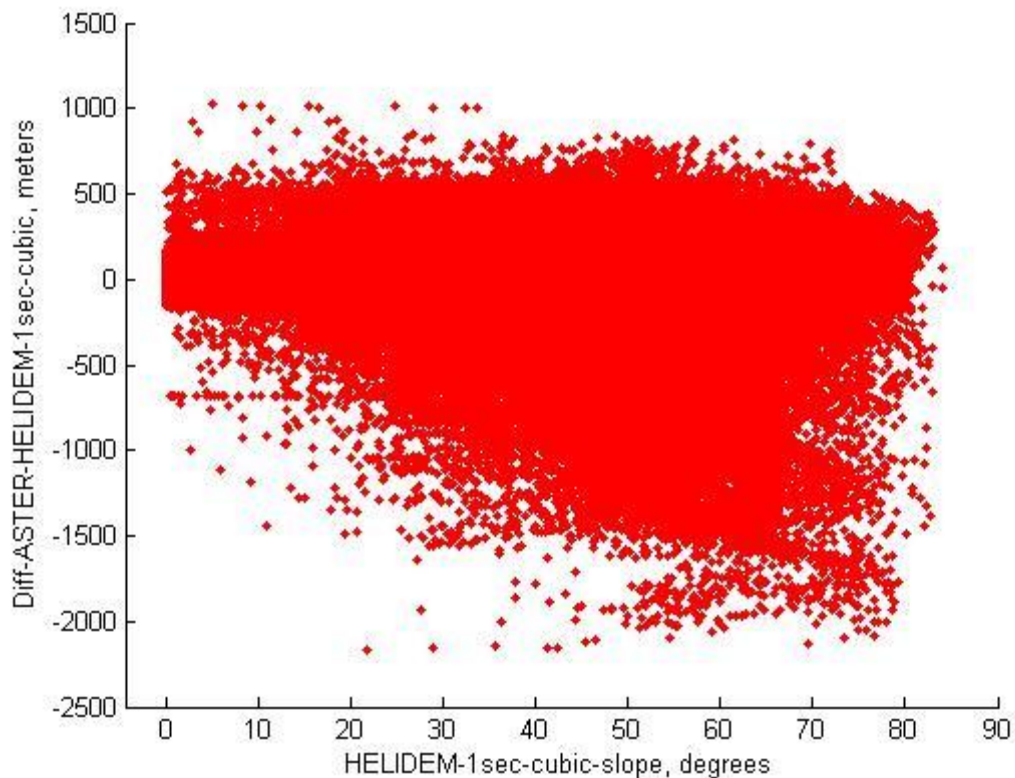


Figure 76 HELIDEM_1sec_cubic_slope vs. Diff_ASTER_HELIDEM_1sec_cubic

One step more consists in converting all the negative differences into positive and recalculation of the correlation.

```
r.covar -r map=HELIDEM_1sec_cubic_slope@PERMANENT,
Diff_ASTER_HELIDEM_1sec_cubic_color@PERMANENT
```

Getting:

$$\begin{vmatrix} 1 & 0.30 \\ 0.30 & 1 \end{vmatrix}$$

The new value is 0.30. It is clear that this new correlation increases significantly but still there is not a strict relation between the study parameters. As on the figure below is seen that with the increase of the slope also an increase of the dispersion is present.

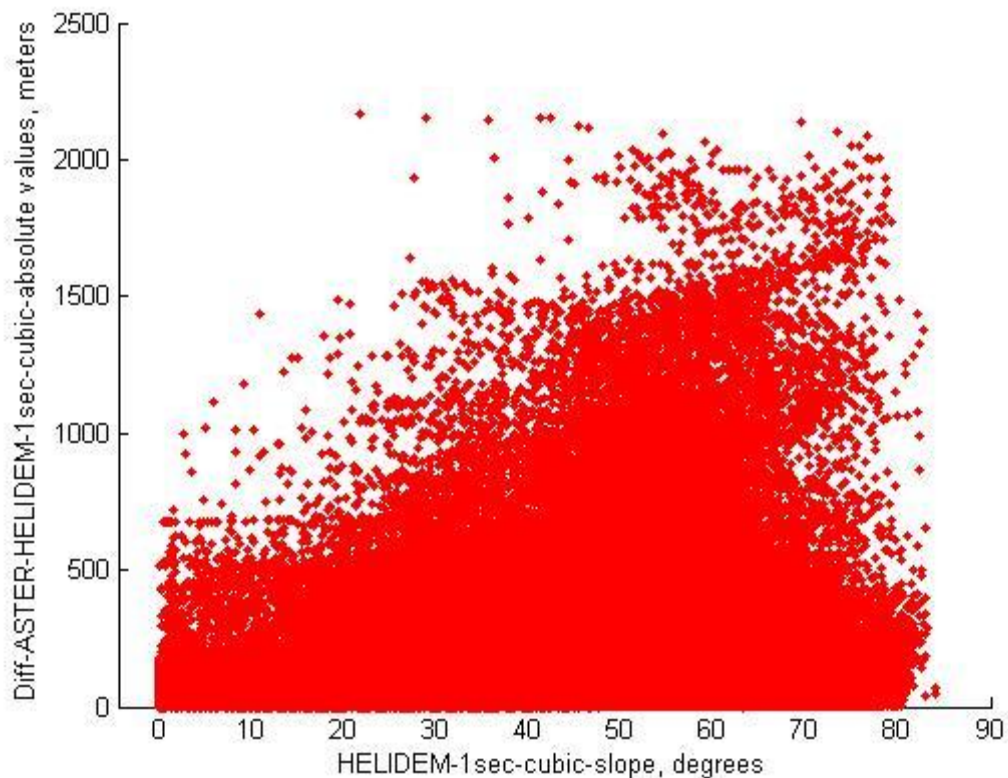


Figure 77 HELIDEM_1sec_cubic_slope vs. Diff_ASTER_HELIDEM_1sec_cubic_absolute values

As a final point, the analysis of the differences between the ASTER and the HELI-DEM DEMs shows presence of outliers concentrated mainly in three areas. Going more detailed through histograms and correlation indices could be said that doesn't exist dependence between the height (h) of the local model and the difference of heights between the local and the global models (Δh); it is present a linear relation regarding only the constant values of the outliers in the areas where they exist and the terrain. Whereas, is present an increase of the dispersion of the difference between ASTER and HELI-DEM (Δh) with the increase of the slope of HELI-DEM.

Chapter 7

7 Comparison between SRTM Global DEM and HELI-DEM Local DEM

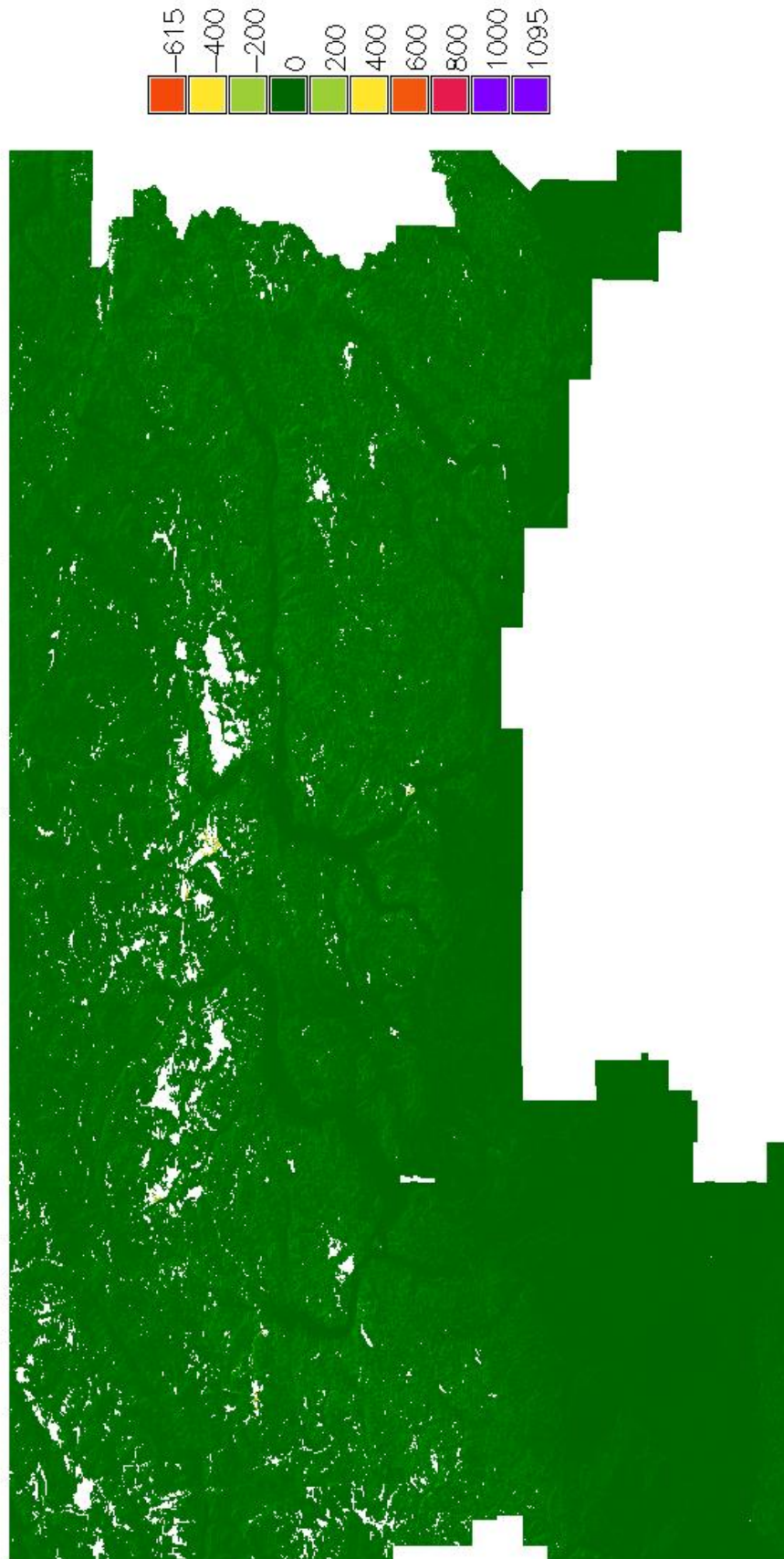
In this chapter a final map of the differences between the local model HELI-DEM and the global model SRTM is produced and analyzed. Histograms with the empirical and the normal distribution are presented. Furthermore, a correlation index between the height (h) of the local model and the difference of heights between the two models (Δh) is calculated as well as the correlation index between the slope of HELI-DEM and again the difference of heights between the two models (Δh). The analysis is finished with converting all negative differences into positive and recalculating the two correlation indices. The general analysis is completed by computing the same correlation indices but this time using the absolute values of the differences.

7.1 Analysis of the differences between SRTM and HELIDEM

The models are already imported into GRASS GIS platform and the transformation process for the local model is carried out, as already explained in Chapters 5.

At first, a region is set having the extensions of SRTM@PERMANENT raster map. Then a raster map called Diff_SRTM_HELIDEM_3sec_cubic is produced as the algebraic difference between SRTM@PERMANENT and HELIDEM_3sec_cubic@PERMANENT. It is illustrated in the next figure.

Figure 78 Diff_SRTM_HELIDEM_3sec_cubic



As for the differences between ASTER and HELIDEM_1sec as well here some basic statistics are obtained. They are reported in the next table.

Diff_SRTM_HELIDEM_3sec_cubic	
total non-null cells	4'948'764
minimum, $max(\Delta h)$, m	-615.33
maximum, $min(\Delta h)$, m	1094.98
mean, $\mu(\Delta h)$, m	1.57
standard deviation, $\sigma(\Delta h)$, m	22.32

Table 13 Diff_SRTM_HELIDEM_3sec_cubic

According to the results, it is noticeable the presence of very big positive differences but the values are not as high as the ones seen in the previous comparison in Chapter 6. It still shows likely a rare behavior on one of the models either the global or the local one. These are clearly anomalous values and their behavior will be analyzed in the following pages.

7.2 Histogram of the differences between SRTM and HELIDEM and classification of the outliers

For the extracted statistics again the respective histogram is obtained. It is cut in the interval of differences from -200 to 200 meters and it is compared with the Gaussian distribution, as shown on the figure. It is seen that the empirical distribution has spiked shape and it is narrower than the normal one.

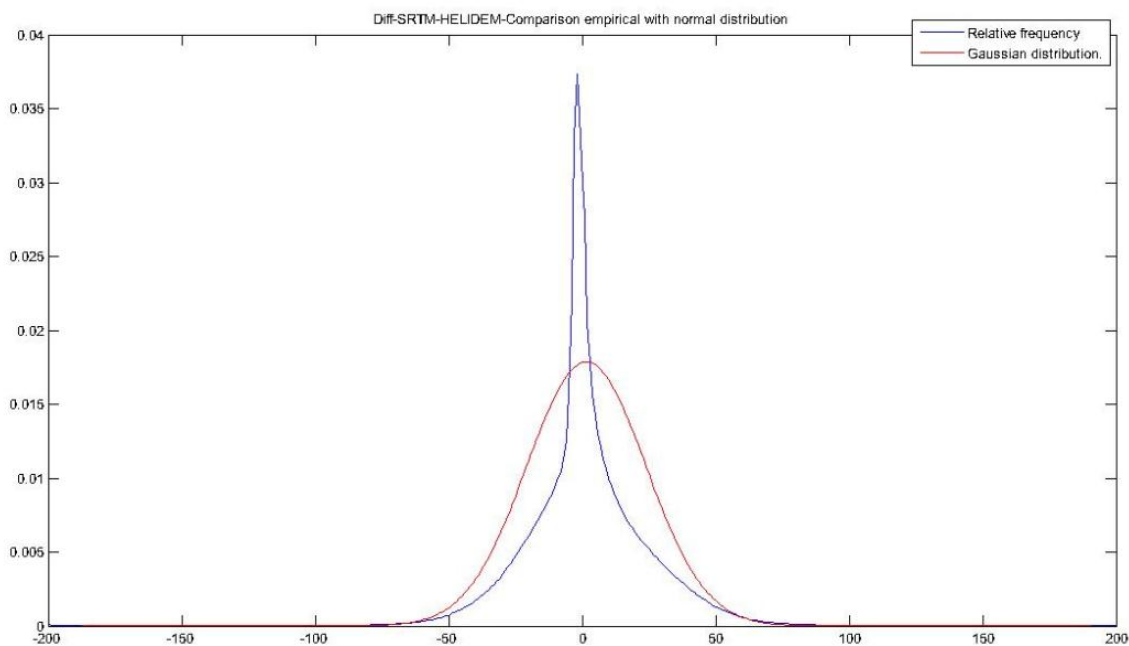


Figure 79 Diff_SRTM_HELIDEM_3sec_cubic – Comparison empirical with normal distribution

By analyzing the statistics and the histogram is observed that the mean values are close to zero and the standard deviation is about 22 m which is significantly less than the resolution of the input raster map, i.e. about 90 m. In general the obtained results are better than the ones generated in the previous comparison. Still some outliers exist which is clean in the minimum and the maximum values.

Their amount is verified by a simple computation as before. The value of three times the standard deviation ($\sigma = 22.32$ m) is used as a threshold and it is equal to 66.96 m. The number of the cells whose values are bigger than it is 49'383 and their percentage of the total number of non-null cells is 1%, which is statistically negligible. The classification of these values is reported in the table:

Diff_SRTM_HELIDEM_3sec_cubic

Classification	Number of cells	Percent of all non-null cells, %
$3\sigma \leq \Delta h < 100$	40688	0,82
$100 \leq \Delta h < 500$	8613	0,17
$500 \leq \Delta h < 1000$	81	0,002
$ \Delta h \geq 1000$	1	0

Table 14 Classification of outliers in Diff_SRTM_HELIDEM_3sec_cubic

It is seen that just one cell exceeds 1000 m so it is isolated cell. Moreover, the cells between 500 and 1000 m are only 81 and their number is negligible especially compared with the differences between ASTER and HELIDEM_1sec, where their percentage of all non-null cells was ten times bigger than now.

7.3 Spatial identification of severe outliers

Clearly the previous statistics show outliers; in principal could be generated in the data acquisition or in the data interpolation either in SRTM or/and in HELIDEM. As mentioned before, HELI-DEM has been validated against other data sources therefore problems are almost surely in SRTM.

Excluding isolated points, there are two small areas with values exceeding the regular differences with more than 500 m. From the following figures is seen that the presence of outliers is times small compared with the ones appearing in the differences between ASTER and HELIDEM_1sec.

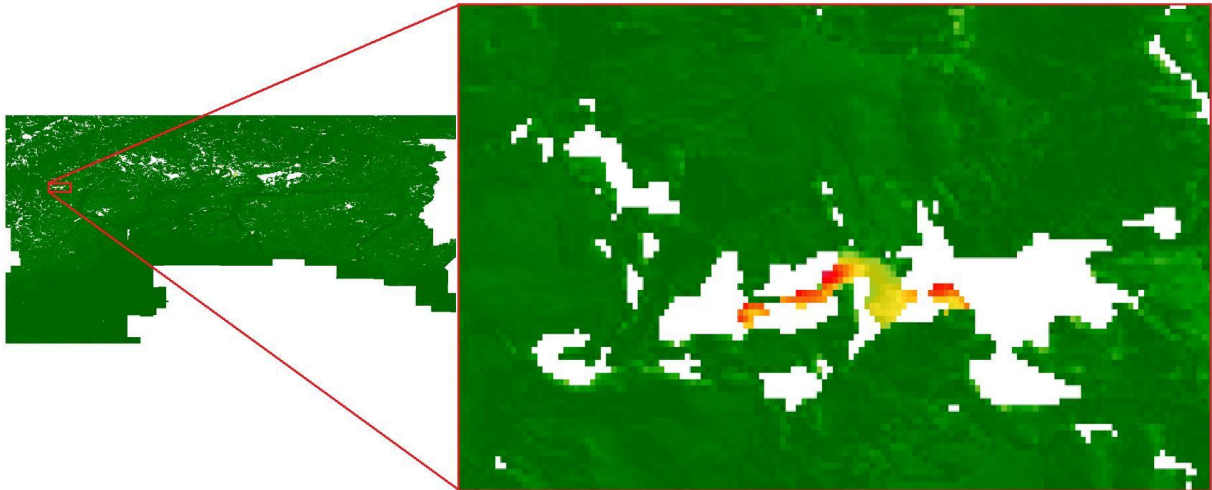


Figure 80 Zoom of area 1 presenting outliers in Diff_SRTM_HELIDEM_3sec_cubic

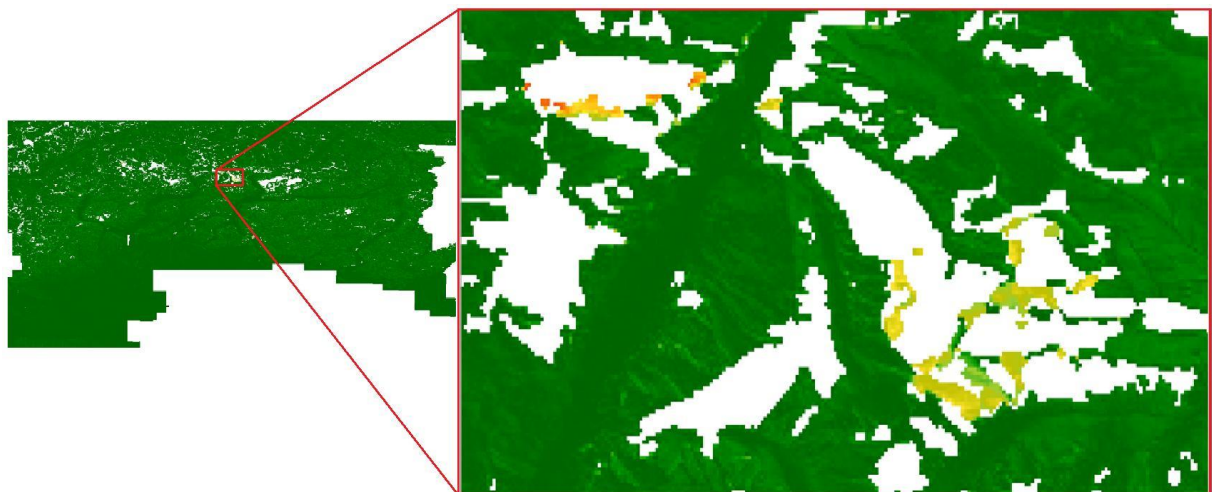


Figure 81 Zoom of area 2 presenting outliers in Diff_SRTM_HELIDEM_3sec_cubic

The first one, called Area 1 has extensions: from 46.10 N to 46.12 N in latitude and from 8.06 E to 8.09 E in longitude. The boundaries of Area 2 are the following: from 46.15 N to 46.21 N in latitude and from 9.08 E to 9.18 E in longitude. Both areas are in mountain regions where the elevation is between 1000 and 2000 m.

These errors are significant but relevant to the areas in which the global model presents voids therefore the outliers are due to acquisition problems existing in SRTM.

7.4 Identification of correlation between the heights of HELIDEM and their differences with SRTM

Again two new parameters are calculated in order to complete the general analysis:

- Correlation coefficient between the HELI-DEM elevation (h) and the differences SRTM/HELI-DEM (Δh): The goal of using this coefficient is to verify if the differences between SRTM and HELI-DEM models depend on the terrain height.

The matrix is obtained:

$$\begin{vmatrix} 1 & -0.09 \\ -0.09 & 1 \end{vmatrix}$$

The value -0.09 indicates a no significant correlation, meaning that the differences between the two models do not depend on the height. That is presented also on the following scatter plot:

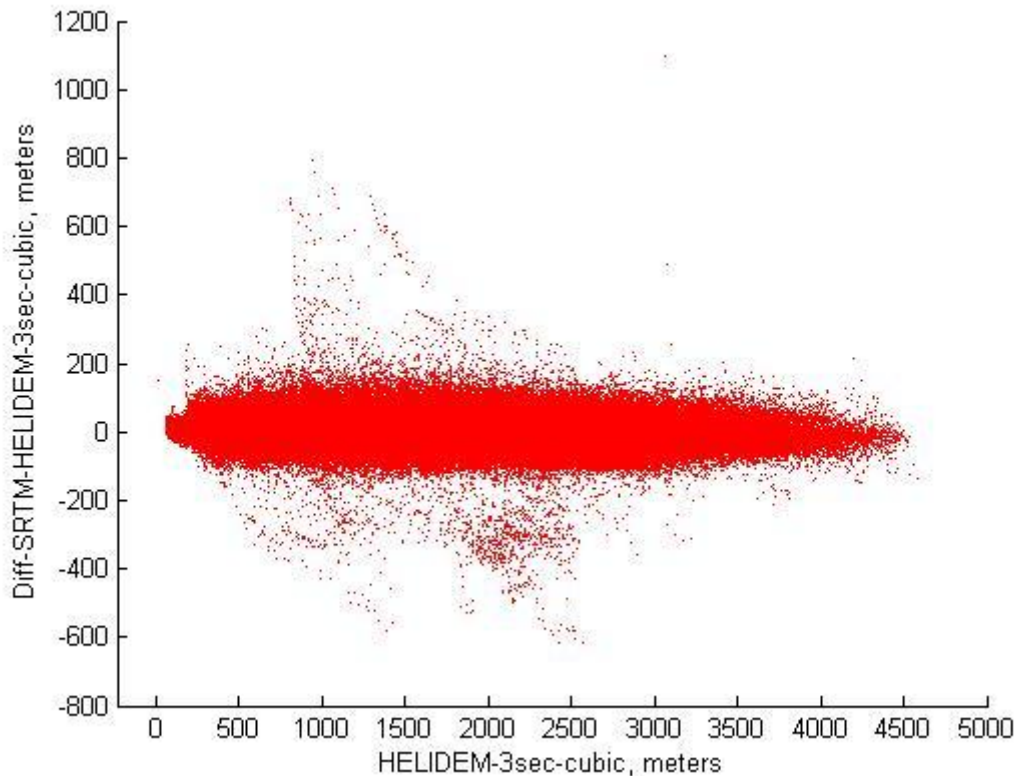


Figure 82 HELIDEM_3sec_cubic vs. Diff_SRTM_HELIDEM_3sec_cubic

Further analysis is done by computing the correlation index again but using the absolute values of the differences.

Getting:

$$\begin{vmatrix} 1 & 0.25 \\ 0.25 & 1 \end{vmatrix}$$

The new obtained value is 0.25 and as expected it is higher than the previous one but still there is not a relation between the study parameters. The correlation is shown on the figure:

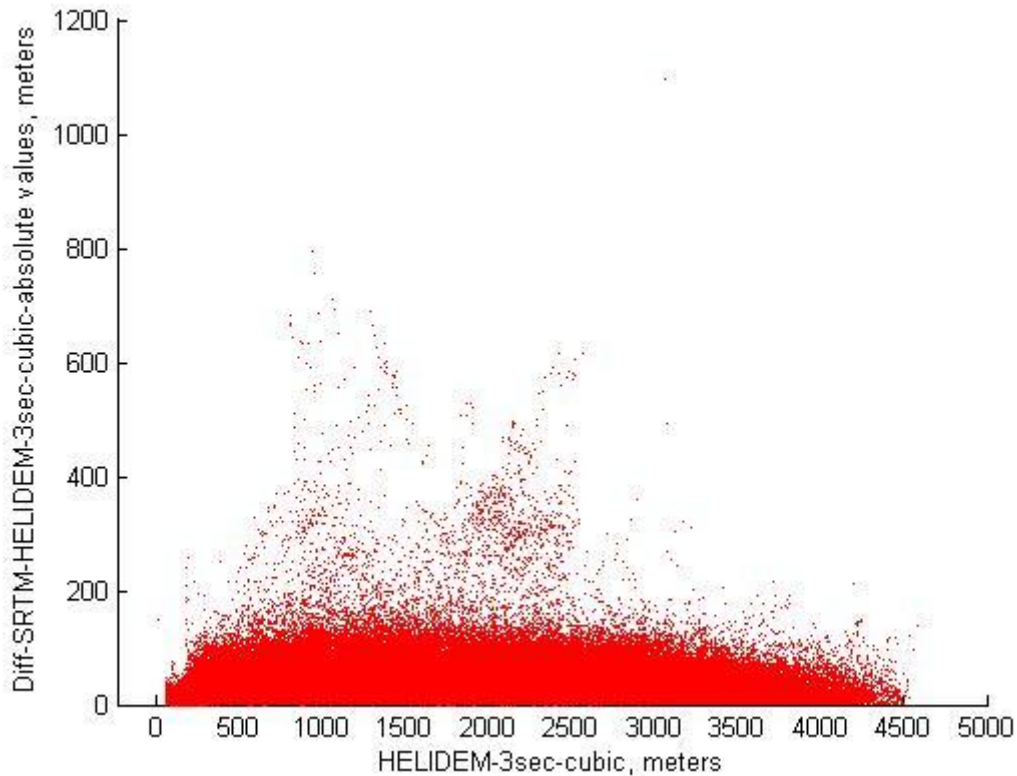


Figure 83 HELIDEM_3sec_cubic vs. Diff_SRTM_HELIDEM_3sec_cubic_absolute values

7.5 Identification of correlation between the slopes of HELIDEM and the differences between SRTM and HELIDEM

As before, a correlation coefficient can be used to present as well a non linear dependence on the slope.

- Correlation coefficient between the HELI-DEM slope (degrees) and the differences SRTM/HELI-DEM (Δh): The goal of using this coefficient is to verify if the differences between SRTM and HELI-DEM models depend on the terrain slope.

In order to be computed this correlation index again at first two new raster maps are produced: the ones corresponding to the slopes of SRTM and HELIDEM_3sec. It is also computed their difference. The following figures on the new pages are the outputs of the operation.

Figure 84 SRTM_slope

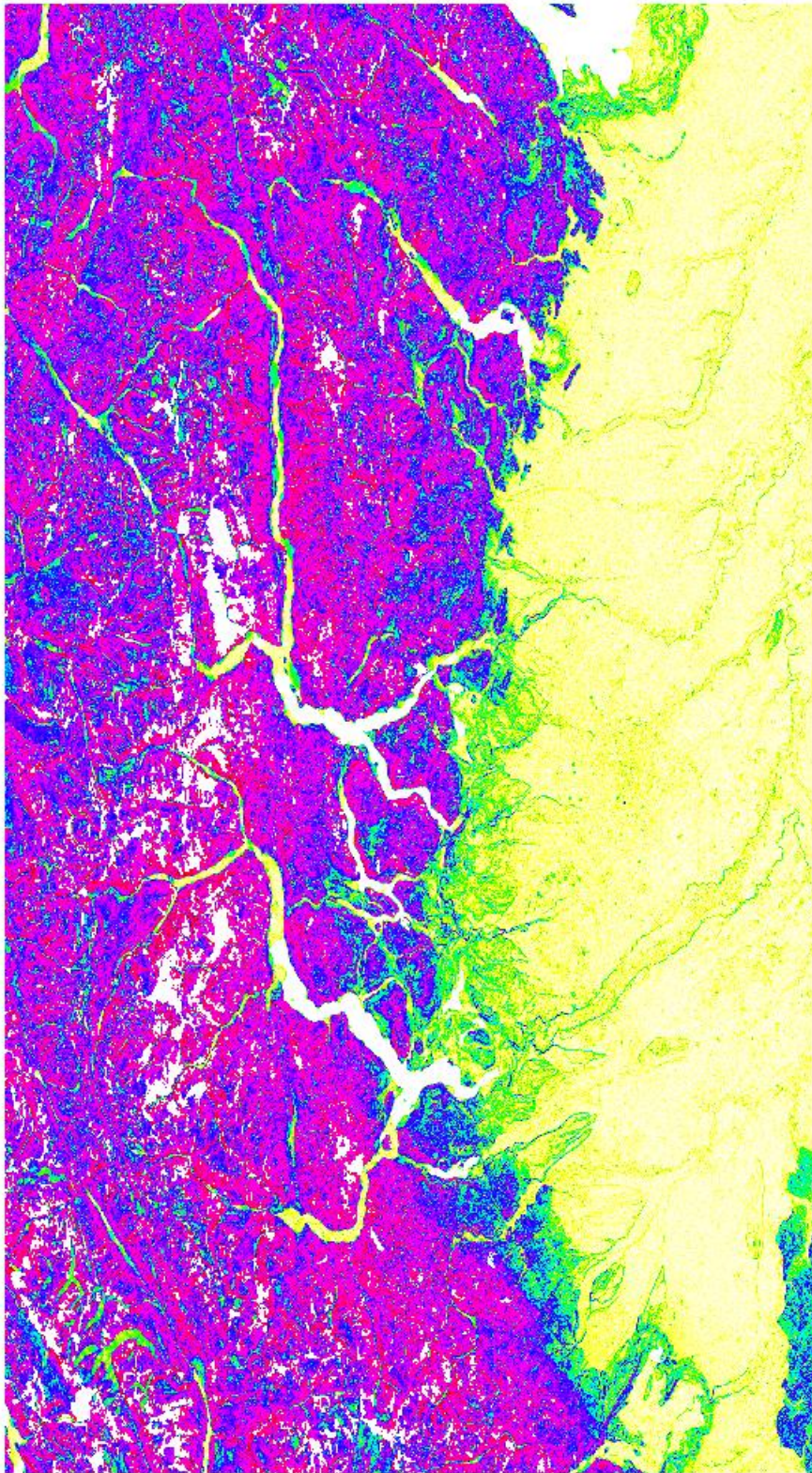
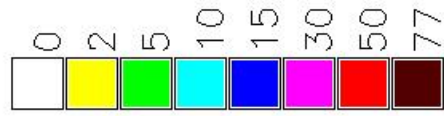


Figure 85 HELIDEM_3sec_cubic_slope

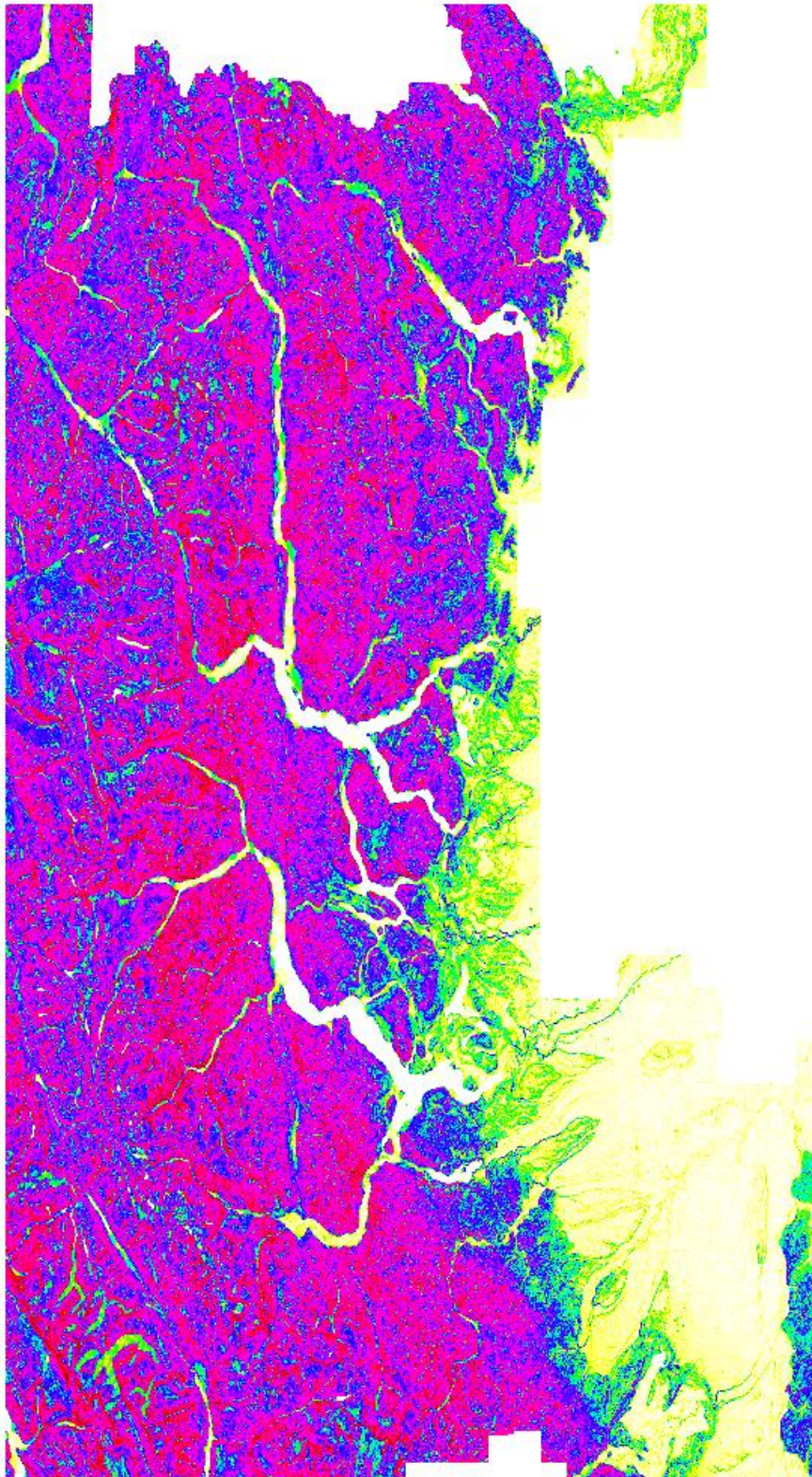
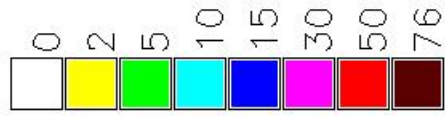
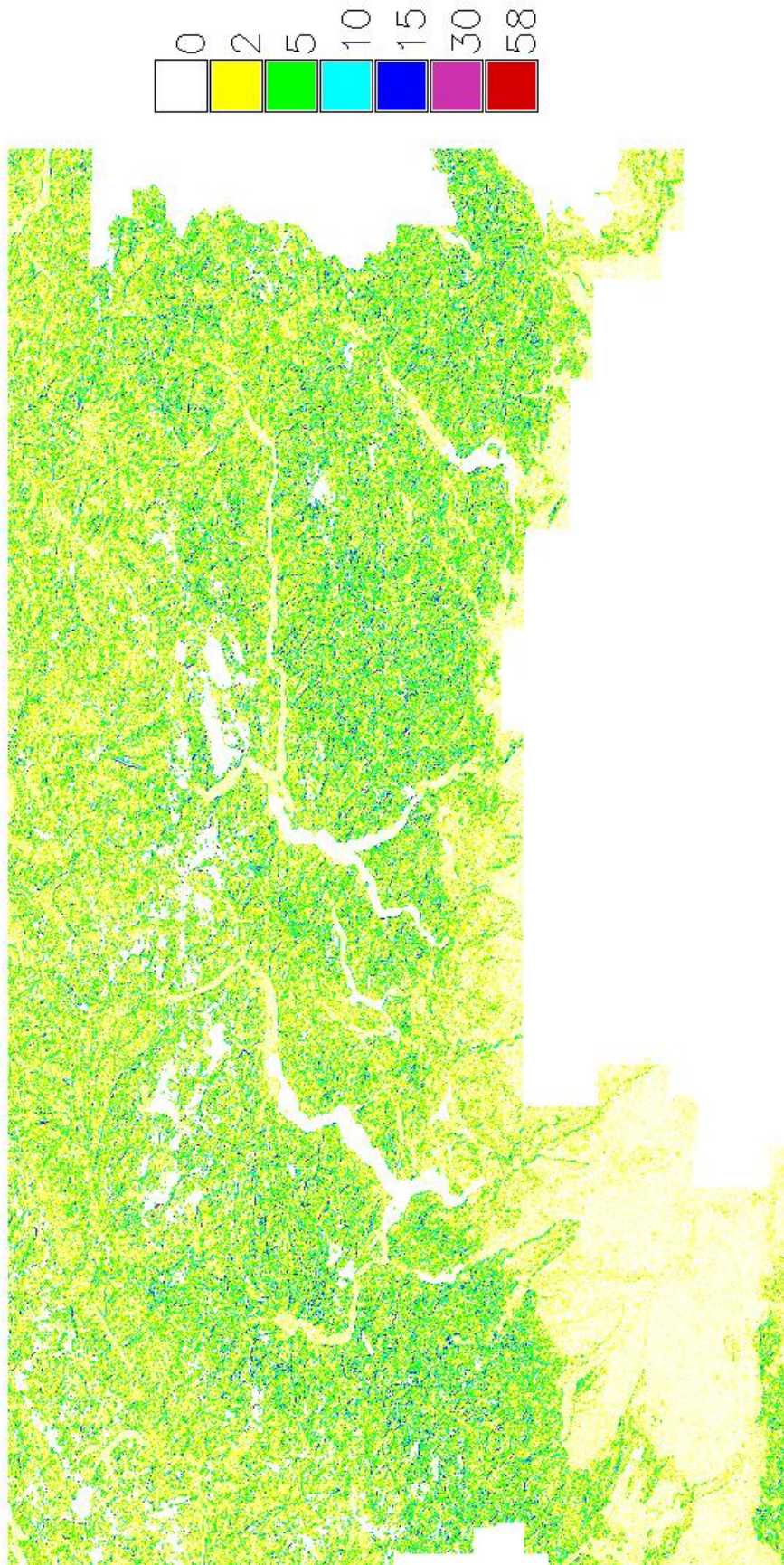


Figure 86 Diff_SRTM_slope_HELIDEM_3sec_cubic_slope_Absolute Values



The next table illustrates some general statistics about the slopes and their differences in absolute values.

	SRTM_slope	HELIDEM_3sec_cubic_slope	Diff_SRTM_slope_HELIDEM_3sec_cubic_slope_abs.val
total non-null cells	6'387'604	5'078'804	4'807'437
minimum, deg	0	0	0
maximum, deg	77,38	76,78	58,55
mean, deg	15,42	20,77	2,54
standard deviation, deg	14,18	14,52	3,03

Table 15 Statistics of SRTM_slope, HELIDEM_3sec_cubic_slope and their difference in absolute values

The maximum value of the differences of the slopes, as in the previous comparison, indicates an anomalous behavior but it is not so high. Again it could be understood as possible increase of the depression with the slope but that is going to be shown in the value of the next computed correlation index:

$$\begin{vmatrix} 1 & 0.06 \\ 0.06 & 1 \end{vmatrix}$$

The results obtained by the covariance matrix present a correlation coefficient equal to 0.06 which indicates a null significant relationship between these two parameters. It is visualized by the following figure.

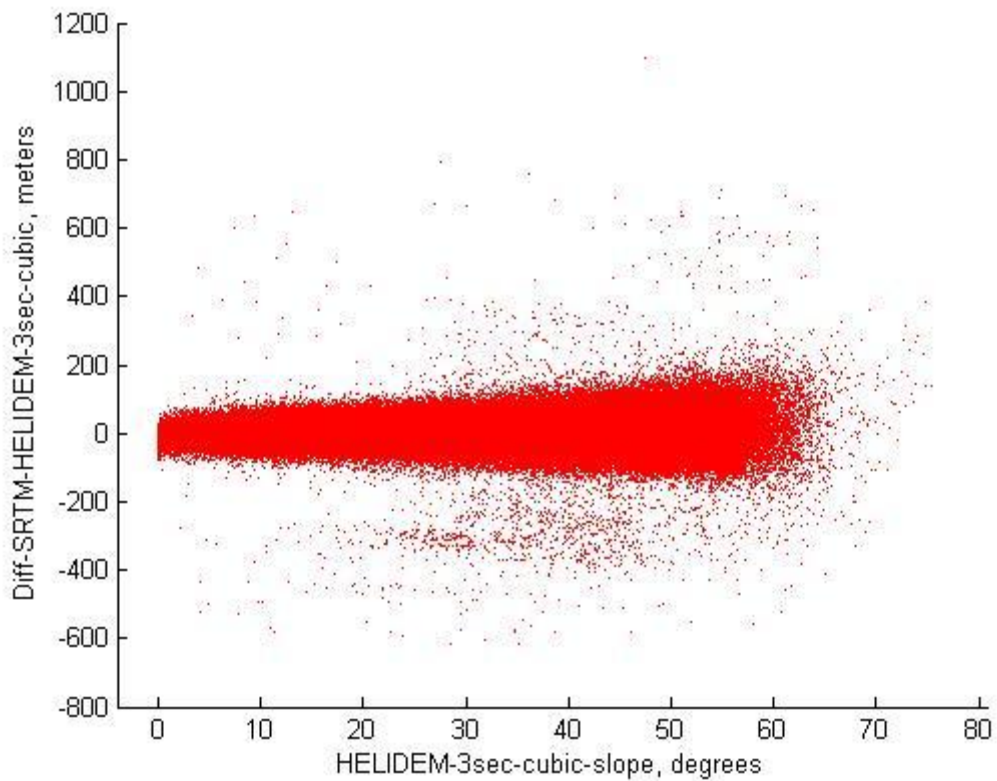


Figure 87 HELIDEM_3sec_cubic_slope vs. Diff_SRTM_HELIDEM_3sec_cubic

One step more consists in converting all the negative differences into positive and recalculation of the correlation.

Getting:

$$\begin{vmatrix} 1 & 0.56 \\ 0.56 & 1 \end{vmatrix}$$

It is clear that this new value of 0.56 increases significantly and it is almost ten times higher than the previous one. Still there is not a strict correlation between the study parameters. As it is seen on the figure below, with increase of the slope also an increase of the dispersion of the differences is present.

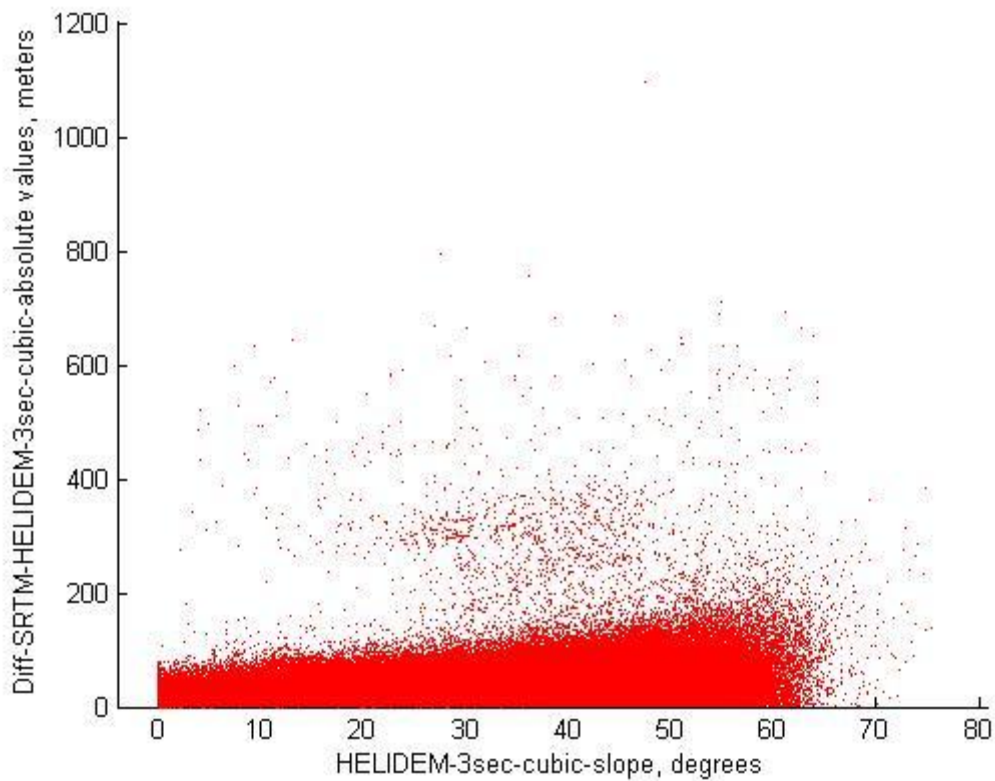


Figure 88 HELIDEM_3sec_cubic_slope vs. Diff_SRTM_HELIDEM_3sec_cubic_absolute values

As a final point, the analysis of the differences between the SRTM and the HELI-DEM DEMs shows presence of outliers concentrated in two areas. Going more detailed through histograms and correlation indexes could be said that the difference of heights between SRTM and HELI-DEM (Δh) and the height (h) of HELI-DEM are not related. The analysis shows an increase of the dispersion of the differences between the two models with the increase of the slope of the local one.

Chapter 8

8 Comparison between GMTED2010 Global DEM and HELI-DEM Local DEM

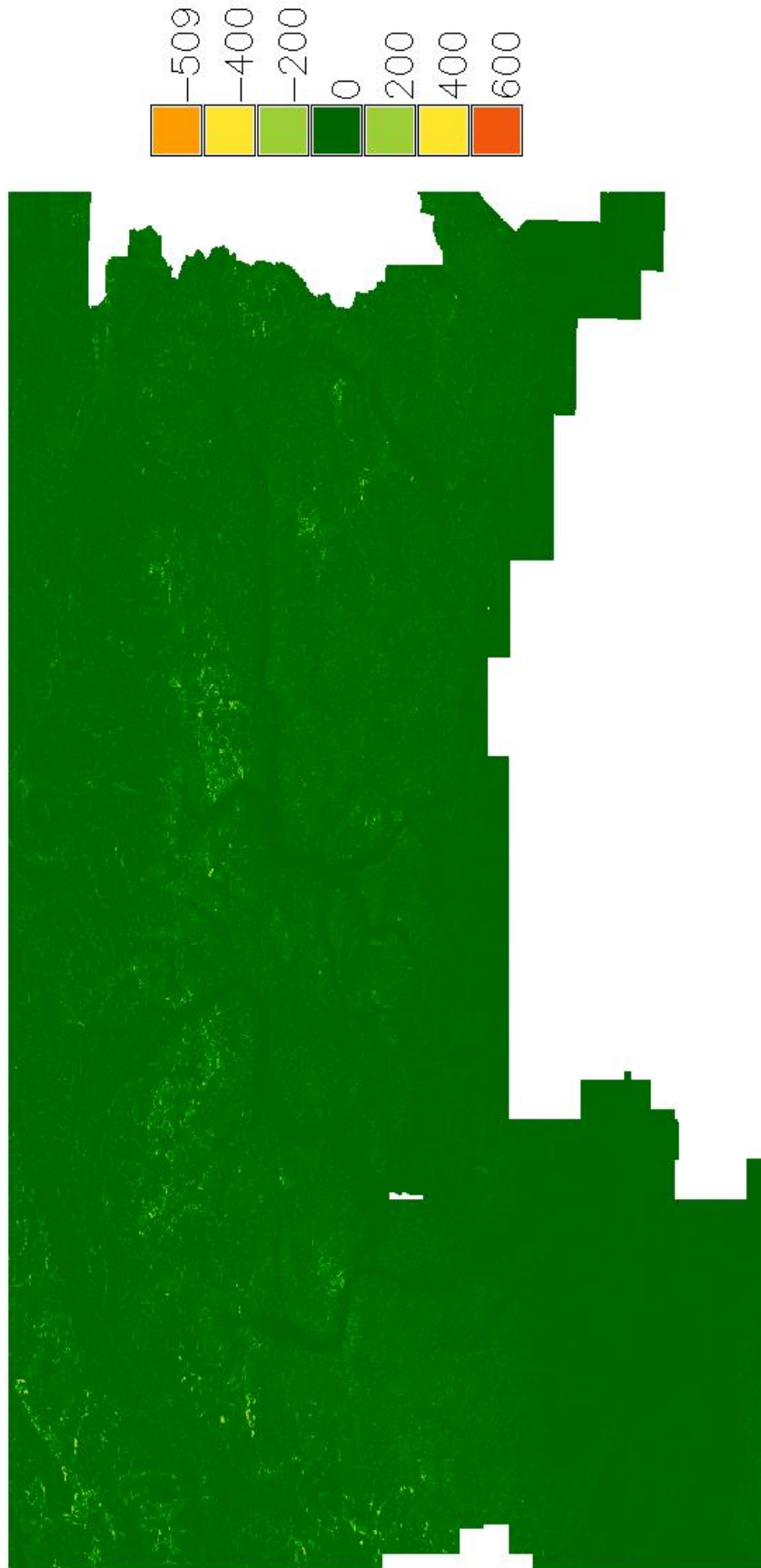
In this chapter a final map of the differences between the local model HELI-DEM and the global model GMTED is produced and analyzed. Histogram with the empirical and the normal distribution is presented. Furthermore, a correlation index between the height (h) of the local model and the difference of heights between the two models (Δh) is calculated as well as the correlation index between the slope of HELI-DEM and again the difference of heights between the two models (Δh). The analysis is finished with converting all negative differences into positive and recalculating the two correlation indices. The general analysis is completed by computing the same correlation indices but this time using the absolute values of the differences.

8.1 Analysis of the differences between GMTED and HELIDEM

As before, since the needed raster maps of GMTED and the sampled HELIDEM in 7.5 resolution are already imported in the platform, all the actions of their comparison and further analysis can be initiated.

The region is set with the same extensions as the GMTED raster map. Then Diff_GMTED_HELIDEM_7.5sec_cubic raster map is produced in the same way as in the previous two chapters as the algebraic difference between the inputs which in this case are GMTED and HELIDEM_7.5sec_cubic. The output is illustrated in the next figure.

Figure 89 Diff_GMTED_HELIDEM_7.5sec_cubic



In additional, some basic statistics are calculated and reported in the next table:

Diff_GMTED_HELIDEM_7.5sec_cubic	
total non-null cells	815'198
minimum, $max(\Delta h)$, m	-509,77
maximum, $min(\Delta h)$, m	600,87
mean, $\mu(\Delta h)$, m	1,67
standard deviation, $\sigma(\Delta h)$, m	19,29

Table 16 Diff_GMTED_HELIDEM_7.5sec_cubic

According to the results, it is noticeable the presence of big negative and positive differences but the values are smaller than in the previous two comparisons.

8.2 Histogram of the differences between GMTED and HELIDEM and classification of the outliers

For the extracted statistics also the respective histogram is obtained. It is cut in the range between -200 and 200 m and compared with the Gaussian distribution, as shown on the next figure. The shape of the empirical distribution, as in the two cases before, is narrower than the one of the normal. It is spiked and symmetric.

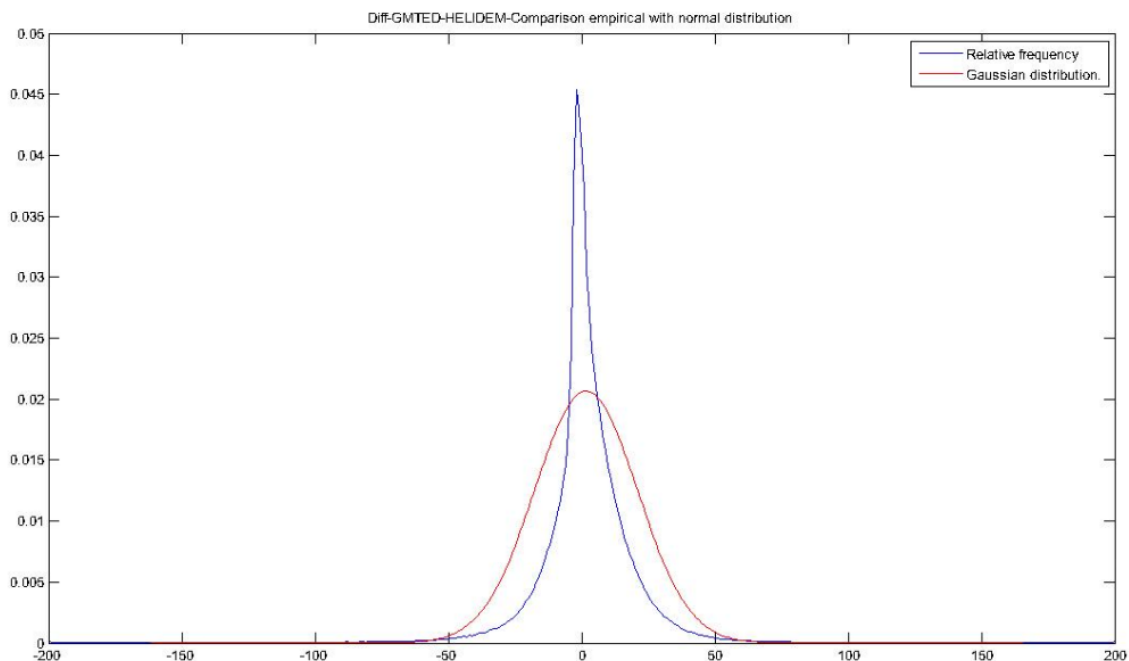


Figure 90 Diff_GMTED_HELIDEM_7.5sec_cubic – Comparison empirical with normal distribution

The mean values are close to zero and the standard deviation is about 20 m which means that the obtained results are satisfactory since the resolution of the input maps (about 250 m) is times lower. Still some outliers exist and it is seen in the minimum and the maximum values from the obtained statistics.

To verify their amount, a simple computation is done, using the value of three times the standard deviation ($\sigma = 19.29$ m) as a threshold, which is equal to 57.87 m. The number of the cells whose values are bigger than it is 13'455 and their percentage of the total number of non-null cells is 1.65%. This value of less than two per cent could be defined as slight but a further classification is done:

Diff_GMTED_HELIDEM_7,5sec_cubic

Classification	Number of cells	Percent of all non-null cells, %
$3\sigma \leq \Delta h < 100$	9583	1,18
$100 \leq \Delta h < 500$	3866	0,47
$ \Delta h \geq 500$	6	0,001

Table 17 Classification of outliers in Diff_GMTED_HELIDEM_7.5sec_cubic

It is seen that the number of nodes whose values exceed 500 m is only six and it's negligible, moreover because it does not correspond to the same area of concentrated outliers, visualized previously, but it presents some isolated points.

8.3 Spatial identification of severe outliers

The previous statistics show outliers; in principal could be generated in the data acquisition or in the data interpolation either in GMTED or/and in HELI-DEM. However, HELI-DEM has been validated against other data sources therefore problems are almost surely in GMTED.

There are some isolated points exceeding the regular differences with but the only area where are concentrated more than four of these nodes is shown on the figure below.

This area has extensions: from 46.34 N to 46.35 N in latitude and from 7.59 E to 8.00 E in longitude and it is in very high mountain region.

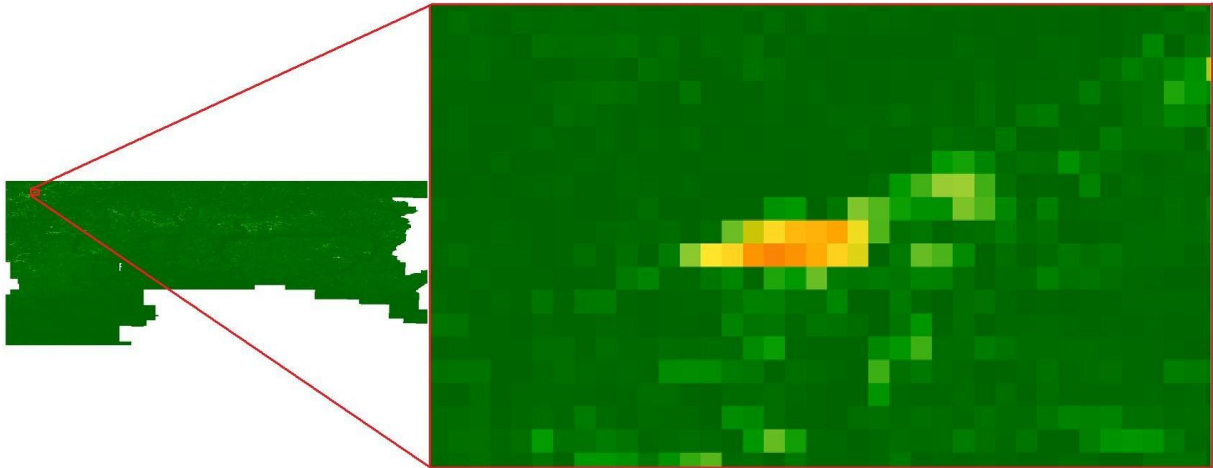


Figure 91 Zoom of the area presenting outliers in Diff_GMTED_HELIDEM_7.5sec_cubic

8.4 Identification of correlation between the heights of HELIDEM and their differences with GMTED

Again two new parameters are calculated:

- Correlation coefficient between the HELI-DEM elevation (h) and the differences GMTED/HELI-DEM (Δh): The goal of using this coefficient is to verify if the differences between GMTED and HELI-DEM models depend on the terrain height.

The obtained matrix is:

$$\begin{vmatrix} 1 & -0.16 \\ -0.16 & 1 \end{vmatrix}$$

The value -0.16 does not indicate a significant correlation, meaning that the differences between the two models do not depend on the height, which is shown also on the figure:

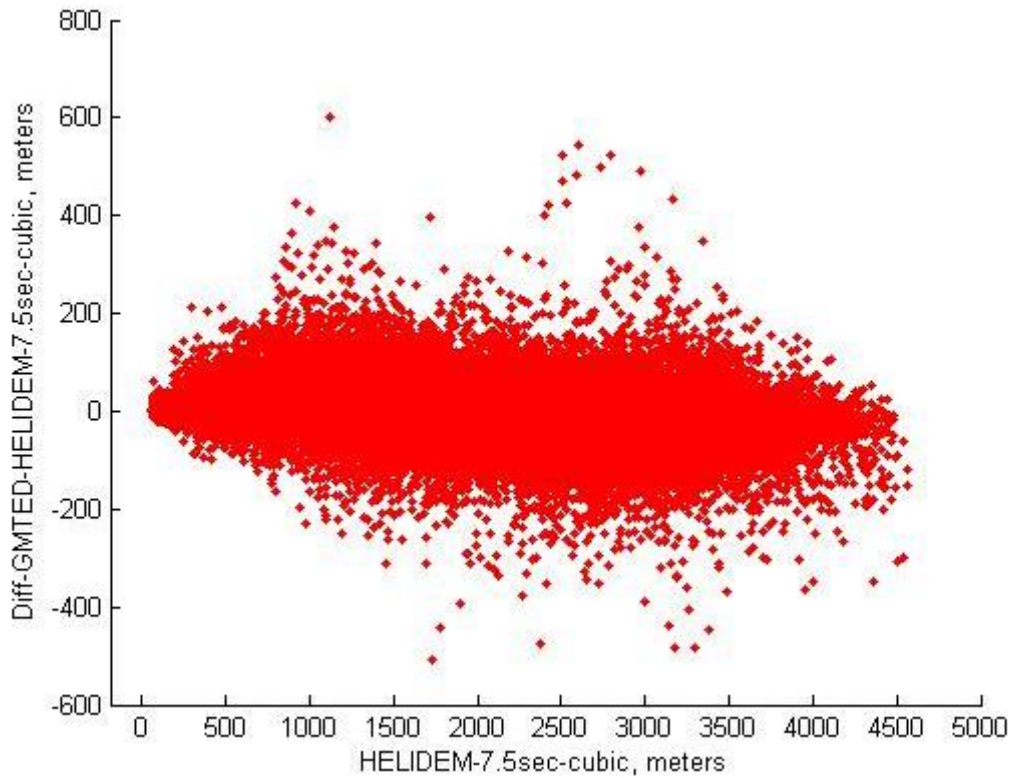


Figure 92 HELIDEM_7.5sec_cubic vs. Diff_GMTED_HELIDEM_7.5sec_cubic

Further analysis is done by computing the correlation index again but using the absolute values of the differences.

Getting:

$$\begin{vmatrix} 1 & 0.23 \\ 0.23 & 1 \end{vmatrix}$$

The new obtained value is 0.23 and as expected it is higher than the previous one. It still indicates that the two values are not related. The produced scatter plot is visualized on the next figure.

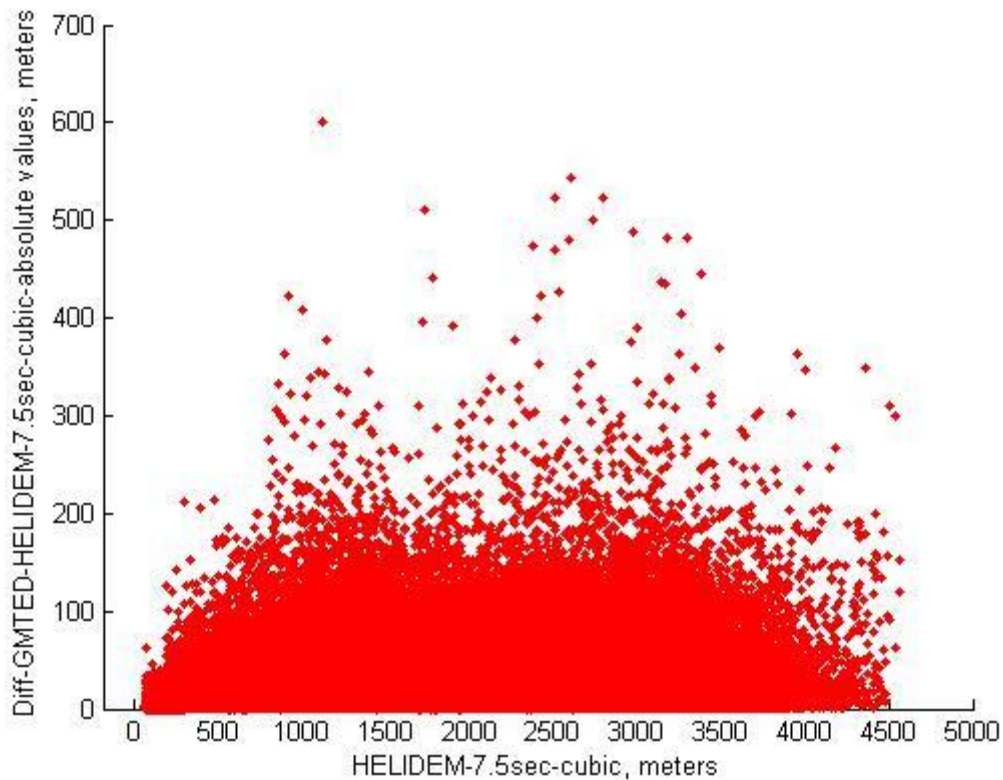


Figure 93 HELIDEM_7.5sec_cubic vs. Diff_GMTED_HELIDEM_7.5sec_cubic_absolute values

8.5 Identification of correlation between the slopes of HELIDEM and the differences between GMTED and HELIDEM

The correlation coefficient can be used to present as well a non linear dependence on the slope.

- Correlation coefficient between the HELI-DEM slope (degrees) and the differences GMTED/HELI-DEM (Δh): The goal of using this coefficient is to verify if the differences between GMTED and HELI-DEM models depend on the terrain slope.

As in the previous two chapters, at first two new raster maps representing the slopes of GMTED and HELIDEM_7.5sec are produced and then are computed their differences. They are shown on the figures on the next pages.

Figure 94 GMTED_slope

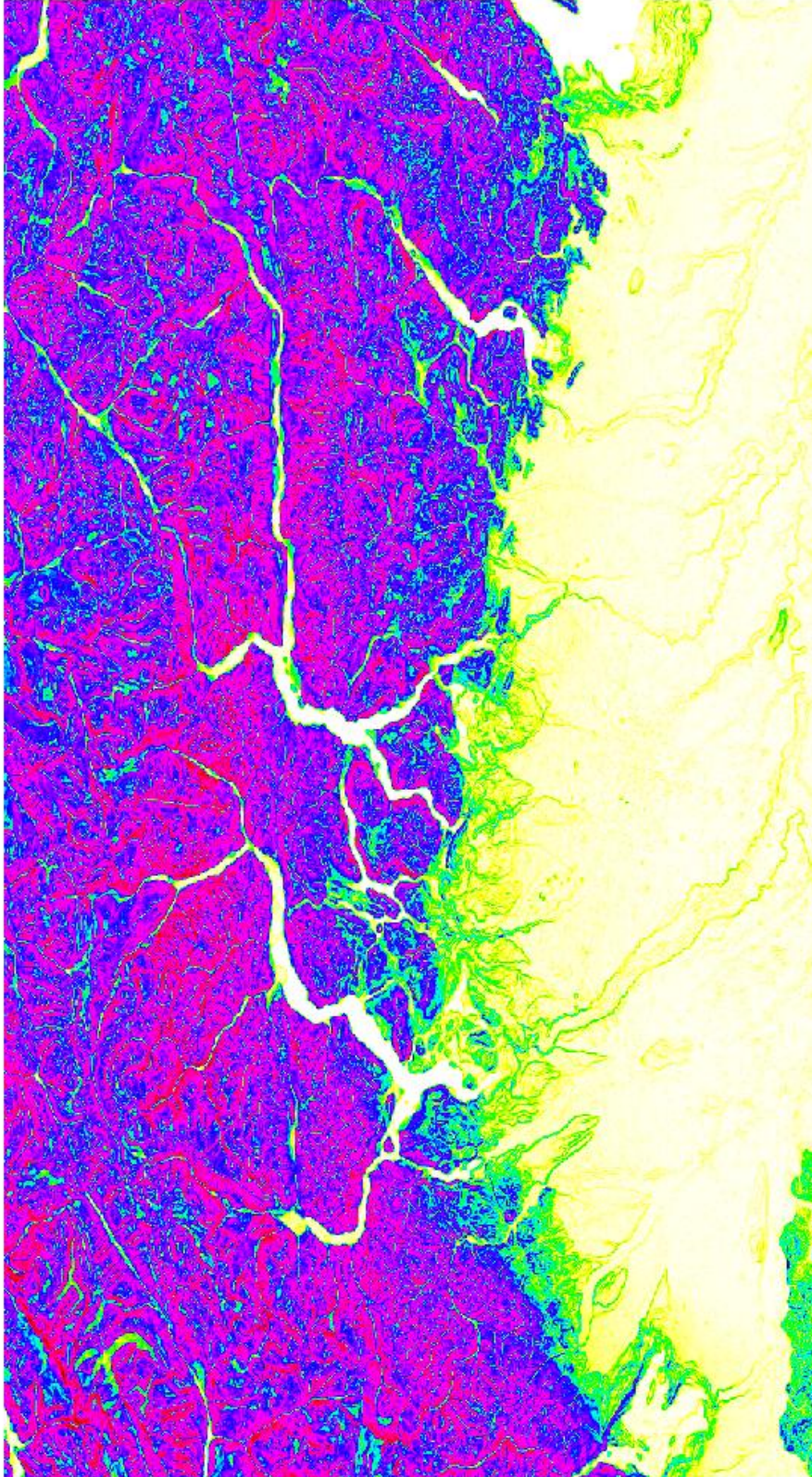
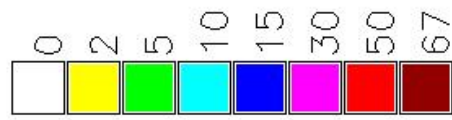


Figure 95 HELIDEM_7.5sec_cubic_slope

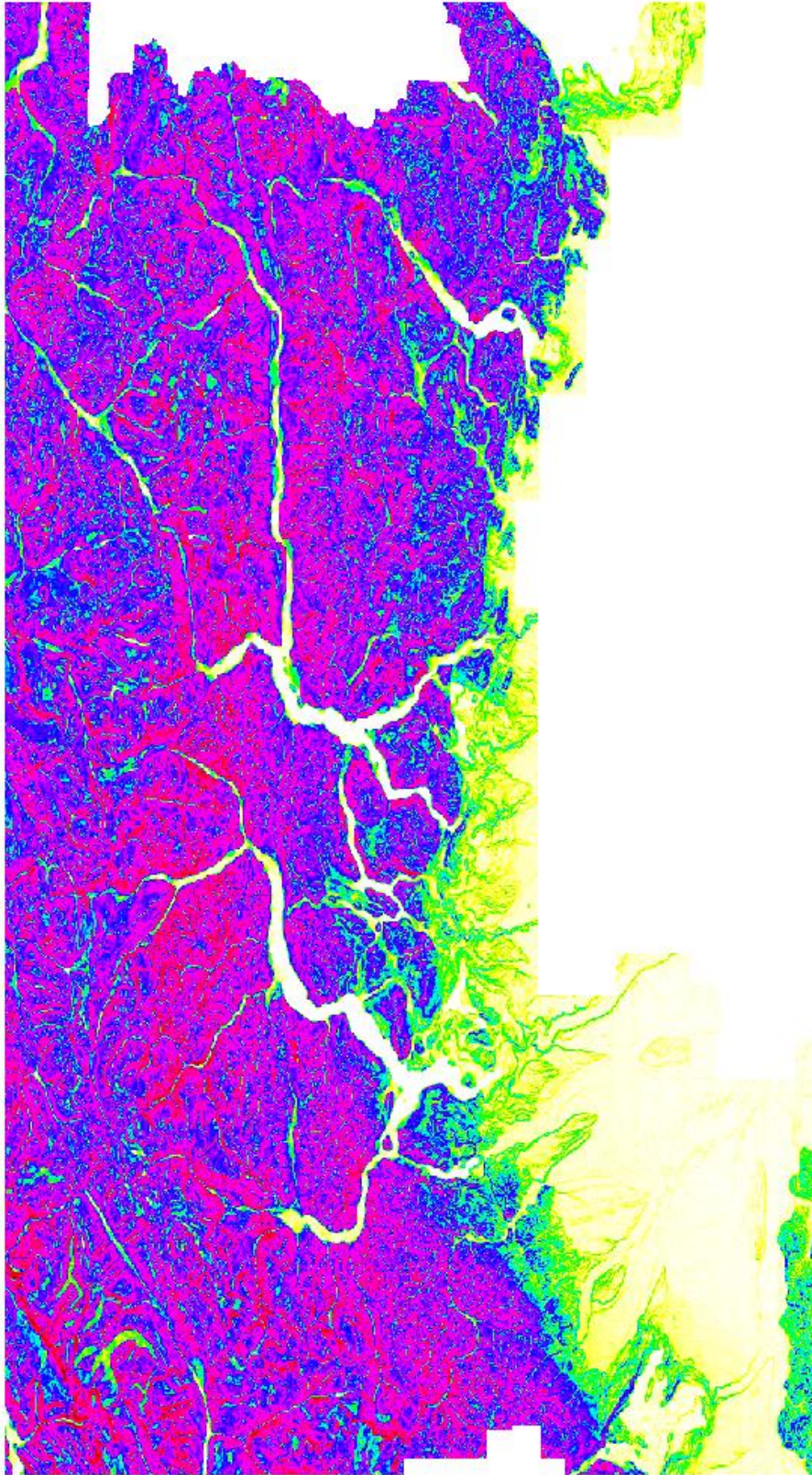
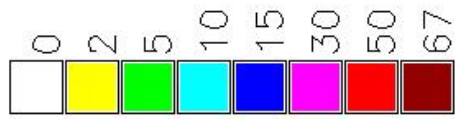
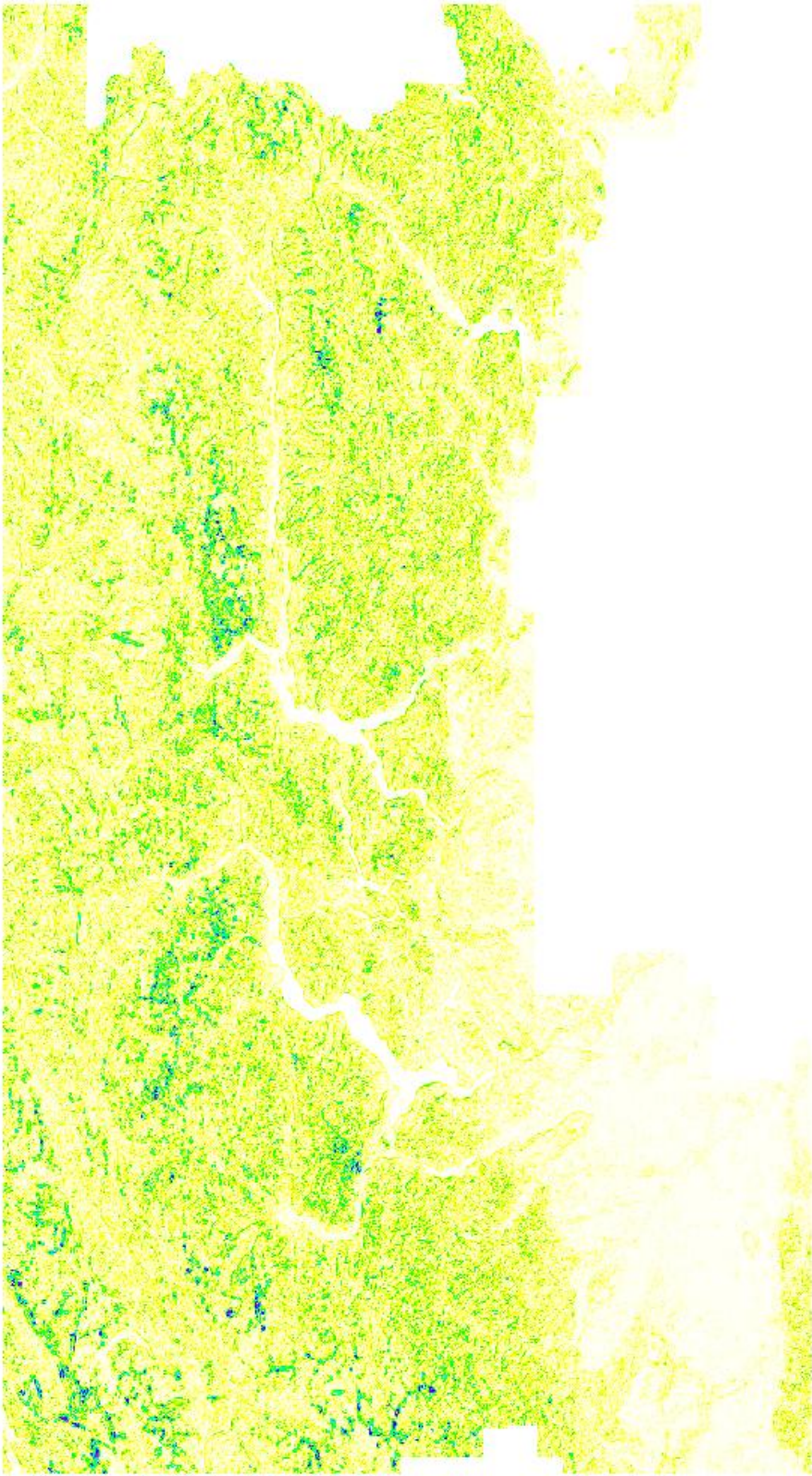
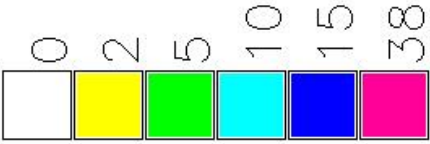


Figure 96 Diff_GMTED_slope_HELIDEM_7.5sec_slope_cubic_Absolute Values



Some basic statistics are extracted as well:

	GMTED_slope	HELIDEM_7,5sec_cubic_slope	Diff_GMTED_slope_HELIDEM_7.5sec_cubic_slope_abs.val
total non-null cells	1'064'740	809'407	808'994
minimum, deg	0	0	0
maximum, deg	67,65	67,72	38,05
mean, deg	14,39	18,34	1,19
standard deviation, deg	13,16	12,90	1,55

Table 18 Statistics of GMTED_slope, HELIDEM_7.5sec_cubic_slope and their difference in absolute values

Finally the correlation index is computed, getting:

$$\begin{vmatrix} 1 & 0.08 \\ 0.08 & 1 \end{vmatrix}$$

The results obtained by the covariance matrix present a correlation coefficient equal to 0.08 which indicates a not significant relationship between these two parameters. It is visualized also on the figure:

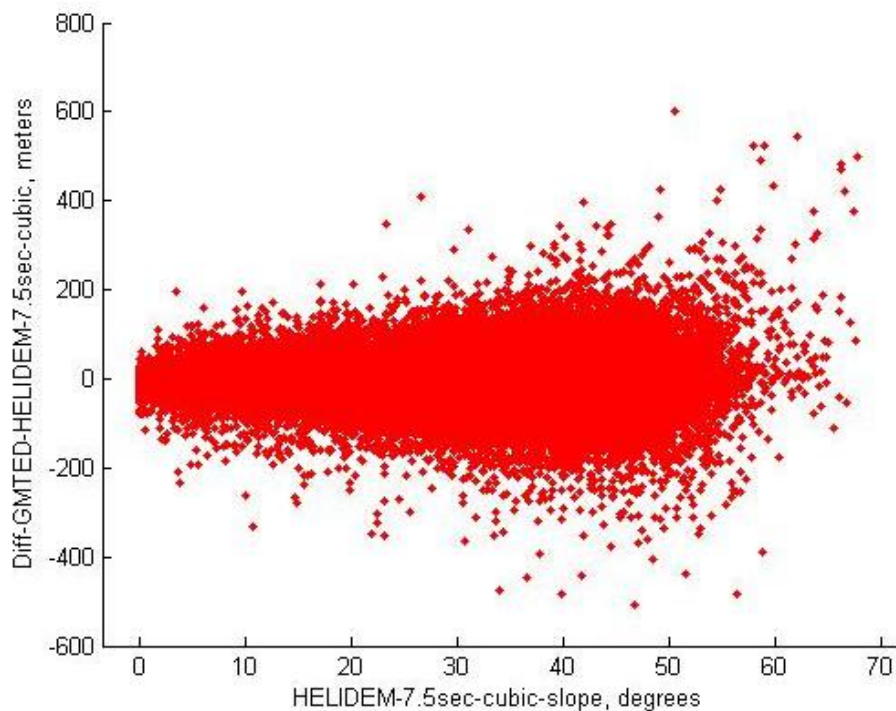


Figure 97 HELIDEM_7.5sec_cubic_slope vs. Diff_GMTED_HELIDEM_7.5sec_cubic

One step more consists in converting all the negative differences into positive and recalculation of the correlation, obtaining:

$$\begin{vmatrix} 1 & 0.35 \\ 0.35 & 1 \end{vmatrix}$$

The new value is 0.35. It is clear that this new correlation increases significantly but still the study parameters are not strictly correlated. There is an increase of the dispersion of the differences with the increase of the slope, as shown also on the scatter plot:

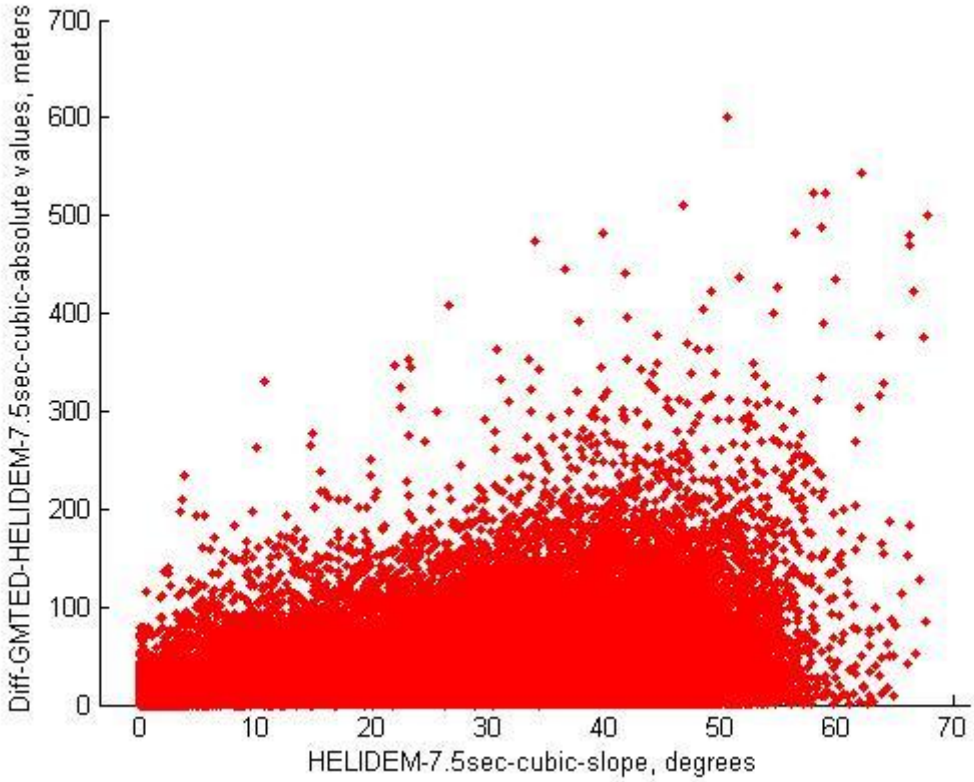


Figure 98 HELIDEM_7.5sec_cubic_slope vs. Diff_GMTED_HELIDEM_7.5sec_cubic_absolute values

As a final point, the analysis of the differences between the GMTED and the HELI-DEM DEMs shows presence of outliers which are concentrated in one area or mainly present as isolated points. Going more detailed through histograms and correlation indices could be said that the height (h) of the local model and the difference of heights between the local and the global models (Δh) are not related. It is present an increase of the dispersion of the differences between GMTED and HELI-DEM (Δh) with the increase of the slope of HELI-DEM.

CONCLUSION

The Global Digital Elevation Models cover the entire Earth surface, nevertheless in some areas they are the only source of elevation data, while in others models with higher resolution and accuracy could be found.

The scope of this thesis was the comparison between the most well-known global DEMs namely Advanced Spaceborne Thermal Emission and Reflection Radiometer (ASTER), Shuttle Radar Topography Mission (SRTM) and Global Multi-resolution Terrain Elevation Data 2010 (GMTED2010), and the local transalpine Helvetia-Italy Digital Elevation Model (HELI-DEM) and further problem identification.

For this work the following data have been collected, described and used:

Model	Resolution	Accuracy	Year of production
ASTER – global DEM	1 arc-second (≈ 30 m)	7-14 vertical 7-14 horizontal	1999
SRTM – global DEM	3 arc-second (≈ 90 m)	16 vertical 20 horizontal	2000
GMTED – global DEM	7.5 arc-second (≈ 250 m)	26-30 vertical	2010
HELI-DEM – local DEM	0.72 arc-second (≈ 20 m)	15 vertical 22 horizontal	2013

Table 19 Digital Elevation Models used in the present study, their resolutions, accuracies and year of production

For the comparisons GRASS (Geographic Resources Analysis Support System) GIS software has been used as it is free Geographic Information System (GIS) software allowing geospatial data management and analysis, spatial modeling, image processing, visualization and computed maps production.

The first operations that have been realized were the download and the import of the available elevation data. Then, using a bicubic interpolation function, the local HELI-DEM has been projected in three different resolutions of the global models respectively 1, 3 and 7.5 arc-second in order to make possible a further comparison.

Regarding to the statistics of the comparison between ASTER and HELI-DEM was obtained that the mean value is 4 m and the standard deviation is 25 m.

The next comparison has been done between SRTM and HELI-DEM. The mean value is 1.5 m and the standard deviation is 22 m.

The comparison between GMTED and HELI-DEM has generated the following statistics: mean around 1.5 m and standard deviation equal to 19 m.

Regarding to the previous statistic results, the mean values are close to zero which means that the global DEMs do not have biases with respect to the local DEM, even though some outliers exist. The standard deviations show that the differences are satisfactory since their values are lower than the values of the resolutions of the global models.

The classification of the outliers done further shows that the differences between HELI-DEM and GMTED give the best results, while the ones regarding ASTER contain the biggest amount of outliers from all the three cases. Considering the differences with ASTER, there are three main areas in which there are constellations of outliers which are present also in the global model as constant values for a certain small areas of points; while in SRTM and GMTED these areas are less, respectively two and one. Moreover, the one called “area 1” regarding the ASTER differences is partially covering with the area of GMTED differences. There is not present overlapping between the other areas or present outliers intersect only as isolated points.

To complete this general analysis, the correlations between heights of the local model and differences between local and global models have been calculated, obtaining that no significant correlation has been found in any of the comparisons. There is just partially a linear relation in case of differences between ASTER and HELI-DEM due to the constant values present in the global model.

Other correlations between slopes of the local model and differences between local and global models have been calculated. In the three cases the indices showed that there is not a strict correlation but increase of the dispersion with the increase of the slope.

It could be concluded that the differences between the local and the global models depend on the topography roughness of the terrain.

List of figures

Figure 1 DSM vs. DTM	7
Figure 2 Patterns of sampled data points	8
Figure 3 Example of a topographic map	10
Figure 4 GPS segments	11
Figure 5 A stereo model is formed by projecting image points from a stereo pair	13
Figure 6 Imaging geometry of SAR	15
Figure 7 Principle of LiDAR.....	16
Figure 8 Different DEM representation methods: GRID and TIN	18
Figure 9 ASTER subsystems and their applications	24
Figure 10 ASTER global DEM	26
Figure 11 SRTM configuration: the main antenna sends the signal, both main and outboard antenna receive the backscattered signal.	27
Figure 12 SRTM global DEM.....	29
Figure 13 Example of implementing maximum aggregation method; applicable as well for minimum, mean and median methods.	31
Figure 14 Example of implementing a Blockstd function applied for the creation of Standard deviation map.....	32
Figure 15 GMTED2010 global DSM	33
Figure 16 Area of interest of HELI-DEM project: Lombardy and Piedmont Italian Regions and Ticino and Grisons Swiss Cantons.....	35
Figure 17 Coverage of the local DTMs collected for the HELI-DEM project...	36
Figure 18 Overlapping areas of the DTMs collected for the HELI-DEM project	37
Figure 19 GNSS permanent stations inside the HELI-DEM project area (area in grey).....	39
Figure 20 Area covered by the regional Lombardy DTM (on the left) and the Lombardy part of the PST-A DTM (on the right)	42
Figure 21 IGM95 points that fall inside the area of the Lombardy LR DTM (left) and inside the area of the PST-A DTM (right)	43
Figure 22 Unified HELI-DEM DTM (HD-1) obtained through merging of Lombardy, Piedmont and Swiss low/medium resolution models	47
Figure 23 Portion of PST-A LiDAR DTM overlapped with HD-1.....	48
Figure 24 On the left: coverage of PST-A DTM and its differences with HD-1. At the right: Differences values in meters, zoom.....	50

Figure 25 GRASS Structure in general	55
Figure 26 GRASS Structure in the current work	55
Figure 27. Website - ASTER and SRTM, defining boundaries	58
Figure 28. Website - ASTER and SRTM, region of interest	58
Figure 29 Download format - ASTER	59
Figure 30 Download format - SRTM	59
Figure 31 Website - ASTER output.....	59
Figure 32 Website - SRTM output	59
Figure 33 Output window for ASTER	60
Figure 34 Output window for SRTM	60
Figure 35 Defining rectangular border for GMTED by coordinates	61
Figure 36 Choosing GMTED2010 for downloading	62
Figure 37 Selecting resolution 7.5 arc-second	62
Figure 38 Creating a new location into the GRASS platform	64
Figure 39 Giving a directory and a name of the new location.....	64
Figure 40 Choosing a method for creating a new location	64
Figure 41 Choosing ASTER projection file	65
Figure 42 Set default region extents.....	66
Figure 43 Created new location and the corresponding mapset	67
Figure 44 Choosing method for creating HELIDEM location	68
Figure 45 Selecting georeferenced file.....	68
Figure 46 GRASS Locations available	69
Figure 47 Selecting ASTER ascii file for import.....	70
Figure 48 Importing ASTER	71
Figure 49 Selecting GMTED mean value file for import	72
Figure 50 Add multiple raster or vector map layers.....	72
Figure 51 Displayed raster maps	73
Figure 52 ASTER	74
Figure 53 SRTM.....	75
Figure 54 GMTED	76
Figure 55 Changing current location.....	77
Figure 56 Importing HELIDEM	78
Figure 57 HELIDEM display	78
Figure 58 HELIDEM.....	79
Figure 59 Reprojection of HELIDEM	82
Figure 60 HELIDEM_1sec_cubic.....	85
Figure 61 HELIDEM_3sec_cubic.....	86

Figure 62 HELIDEM_7.5sec_cubic.....	87
Figure 63 Diff_ASTER_HELIDEM_1sec_cubic	89
Figure 64 Diff_ASTER_HELIDEM_1sec_cubic – Comparison empirical with normal distribution	91
Figure 65 Zoom of area 1 presenting outliers in Diff_ASTER_HELIDEM_1sec_cubic.....	92
Figure 66 Zoom of area 1 in ASTER	92
Figure 67 Zoom of area 2 presenting outliers in Diff_ASTER_HELIDEM_1sec_cubic.....	93
Figure 68 Zoom of area 2 in ASTER	93
Figure 69 Zoom of area 3 presenting outliers in Diff_ASTER_HELIDEM_1sec_cubic.....	94
Figure 70 Zoom of area 3 in ASTER	94
Figure 71 HELIDEM_1sec_cubic vs. Diff_ASTER_HELIDEM_1sec_cubic...	95
Figure 72 HELIDEM_1sec_cubic vs. Diff_ASTER_HELIDEM_1sec_cubic_absolute values	96
Figure 73 ASTER_slope.....	98
Figure 74 HELIDEM_1sec_cubic_slope	99
Figure 75 Diff_ASTER_slope_HELIDEM_1sec_cubic_slope_Absolute Values	100
Figure 76 HELIDEM_1sec_cubic_slope vs. Diff_ASTER_HELIDEM_1sec_cubic.....	102
Figure 77 HELIDEM_1sec_cubic_slope vs. Diff_ASTER_HELIDEM_1sec_cubic_absolute values	103
Figure 78 Diff_SRTM_HELIDEM_3sec_cubic	105
Figure 79 Diff_SRTM_HELIDEM_3sec_cubic – Comparison empirical with normal distribution	106
Figure 80 Zoom of area 1 presenting outliers in Diff_SRTM_HELIDEM_3sec_cubic.....	108
Figure 81 Zoom of area 2 presenting outliers in Diff_SRTM_HELIDEM_3sec_cubic.....	108
Figure 82 HELIDEM_3sec_cubic vs. Diff_SRTM_HELIDEM_3sec_cubic...	109
Figure 83 HELIDEM_3sec_cubic vs. Diff_SRTM_HELIDEM_3sec_cubic_absolute values	110
Figure 84 SRTM_slope	111
Figure 85 HELIDEM_3sec_cubic_slope	112

Figure 86 Diff_SRTM_slope_HELIDEM_3sec_cubic_slope_Absolute Values	113
Figure 87 HELIDEM_3sec_cubic_slope vs. Diff_SRTM_HELIDEM_3sec_cubic	115
Figure 88 HELIDEM_3sec_cubic_slope vs. Diff_SRTM_HELIDEM_3sec_cubic_absolute values	116
Figure 89 Diff_GMTED_HELIDEM_7.5sec_cubic.....	118
Figure 90 Diff_GMTED_HELIDEM_7.5sec_cubic – Comparison empirical with normal distribution	119
Figure 91 Zoom of the area presenting outliers in Diff_GMTED_HELIDEM_7.5sec_cubic	121
Figure 92 HELIDEM_7.5sec_cubic vs. Diff_GMTED_HELIDEM_7.5sec_cubic	122
Figure 93 HELIDEM_7.5sec_cubic vs. Diff_GMTED_HELIDEM_7.5sec_cubic_absolute values.....	123
Figure 94 GMTED_slope.....	124
Figure 95 HELIDEM_7.5sec_cubic_slope	125
Figure 96 Diff_GMTED_slope_HELIDEM_7.5sec_slope_cubic_Absolute Values	126
Figure 97 HELIDEM_7.5sec_cubic_slope vs. Diff_GMTED_HELIDEM_7.5sec_cubic	127
Figure 98 HELIDEM_7.5sec_cubic_slope vs. Diff_GMTED_HELIDEM_7.5sec_cubic_absolute values.....	128

List of tables

Table 1 Comparison of various DEM acquisition methods	17
Table 2 Vertical accuracies of the GMTED2010 products.....	30
Table 3 Statistics of the differences between the two DTMs (Lombardy regional and PST-A LiDAR) and the IGM95 points.....	44
Table 4 Statistics of the differences between PST-A LiDAR DTM and HD-1 DTM / HD-2	49
Table 5 Statistics of the modulus of the differences between HD-1, PST-A and HD-2 DTMs and RTK.....	50
Table 6 Statistics global and local DEMs.....	80
Table 7 HELIDEM input raster map	83
Table 8 HELIDEM Output raster maps.....	83
Table 9 Statistics of HELIDEM data in different resolutions	84
Table 10 Statistics of Diff_ASTER_HELIDEM_1sec_cubic	90
Table 11 Classification of outliers in Diff_ASTER_HELIDEM_1sec_cubic	91
Table 12 Statistics of ASTER_slope, HELIDEM_1sec_cubic_slope and their difference in absolute values	101
Table 13 Diff_SRTM_HELIDEM_3sec_cubic	106
Table 14 Classification of outliers in Diff_SRTM_HELIDEM_3sec_cubic	107
Table 15 Statistics of SRTM_slope, HELIDEM_3sec_cubic_slope and their difference in absolute values	114
Table 16 Diff_GMTED_HELIDEM_7.5sec_cubic	119
Table 17 Classification of outliers in Diff_GMTED_HELIDEM_7.5sec_cubic	120
Table 18 Statistics of GMTED_slope, HELIDEM_7.5sec_cubic_slope and their difference in absolute values	127
Table 19 Digital Elevation Models used in the present study, their resolutions, accuracies and year of production	129

Bibliography

- Abrams, M., & Hook, S. (2002). ASTER User Handbook Version 2. *Jet Propulsion, 2003*(23/09/2003), 135. Retrieved from Abrams2002NASA.pdf
- Biagi, L. (2012). Lectures “Satellite navigation and monitoring”
- Biagi, L., Caldera, S., Carcano, L., Lucchese, a., Negretti, M., Sansò, F., ... Visconti, M. G. (2014). The HELI-DEM model estimation. *ISPRS - International Archives of the Photogrammetry, Remote Sensing and Spatial Information Sciences, XL-4*(May), 15–20. doi:10.5194/isprsarchives-XL-4-15-2014
- Carcano, L. (2013). Merging Local Dtms : Heli-Dem Project , Problems and Solutions. *PhD Thesis*, 226. Retrieved from https://www.politesi.polimi.it/bitstream/10589/89463/1/2014_03_PhD_Carcano.pdf
- Danielson, J. J., & Gesch, D. B. (2011). Global Multi-resolution Terrain Elevation Data 2010. *Terrain, 2010*, iV, 26.
- Farr, T. G., & Others, 17. (2007). The Shuttle Radar Topography Mission. *Reviews of Geophysics, 45*(2), RG2004. doi:doi: 10.1029/2005RG000183
- Freeman, A. (1992). SAR calibration: an overview. *IEEE Transactions on Geoscience and Remote Sensing, 30*(6). doi:10.1109/36.193786
- Gao, J. (1995). Comparison of sampling schemes in constructing DTMs from topographic maps. *ITC Journal, 1995-1*, 18–22. Retrieved from <http://www.scopus.com/inward/record.url?eid=2-s2.0-0029519475&partnerID=40&md5=bfc1302e5b022f60344c68c75b4a151d>
- Graham, L. C. (1974). SYNTHETIC INTERFEROMETER RADAR FOR TOPOGRAPHIC MAPPING. *Proceedings of the IEEE*. doi:10.1109/PROC.1974.9516
- Karel, W., Pfeifer, N., & Briese, C. (2006). DTM QUALITY ASSESSMENT. *ISPRS Technical Commission II Symposium, Vienna, (July)*, 12–14.
- Lemmens, M. (2007). Airborne Lidar Sensors. *GIM International, 21*(2), 24–27.

- Li, Z., Zhu, Q., & Gold, C. (2005). *Digital Terrain Modeling: Principles and Methodology*. ... *Neuroradiology: Endovascular Therapy of the Central* Retrieved from <http://scholar.google.com/scholar?hl=en&btnG=Search&q=intitle:Principles+and+Methodology#9>
- Maune, D. (2001). Digital Elevation Model Technologies and Applications. The DEM Users Manual. *American Society for Photogrammetry and Remote Sensing, Bethesda*, 540 pp.
- Pfeifer, N., & Briese, C. (2007). Laser scanning—Principles and applications. In *3rd International Exhibition & Scientific Congress on Geodesy, Mapping, Geology, Geophysics, Cadaster GEO-SIBERIA* (pp. 1–20). Retrieved from <http://www.ipf.tuwien.ac.at/np/Publications/geosibirPfeifer.pdf>
- R. Barzaghi, A. Borghi, D. Carrion, and G. Sona. (1987). Refining the estimate of the Italian quasi-geoid. Springer Verlag.
- Snyder, J. P. (2011). Emergence of Map Projections, from Flattening the Earth: Two Thousand Years of Map Projections. In *The Map Reader: Theories of Mapping Practice and Cartographic Representation* (pp. 164–169). doi:10.1002/9780470979587.ch23
- Tachikawa, T., Hato, M., Kaku, M., & Iwasaki, A. (2011). Characteristics of ASTER GDEM version 2. *International Geoscience and Remote Sensing Symposium (IGARSS)*, 3657–3660. doi:10.1109/IGARSS.2011.6050017
- Tachikawa, T., Kaku, M., Iwasaki, A., & Gesch, D. (2011). ASTER Global Digital Elevation Model Version 2—Summary of Validation Results. ... *Summary GDEM2 Validation* Retrieved from <http://scholar.google.com/scholar?hl=en&btnG=Search&q=intitle:ASTER+Global+Digital+Elevation+Model+Version+2+?+Summary+of+Validation+Results#7>
- Thome, K. (n.d.). Terra | The EOS Flagship. Retrieved from <http://terra.nasa.gov/>
- Wehr, A., & Lohr, U. (1999). Airborne laser scanning—an introduction and overview. *ISPRS Journal of Photogrammetry and Remote Sensing*. doi:10.1016/S0924-2716(99)00011-8

Web sources

About the Open Source Geospatial Foundation | OSGeo.org. (n.d.). Retrieved from <http://www.osgeo.org/content/foundation/about.html>

Advanced Spaceborne Thermal Emission and Reflection Radiometer (ASTER) | The Long Term Archive. (n.d.). Retrieved from https://lta.cr.usgs.gov/satellite_aster

AGNES. (n.d.). Retrieved from <http://www.swisstopo.admin.ch/internet/swisstopo/en/home/topics/survey/ermnet/agnes.html>

ASTER Global Digital Elevation Map. (n.d.). Retrieved from <http://asterweb.jpl.nasa.gov/gdem.asp>

ASTGTM | LP DAAC :: NASA Land Data Products and Services. (n.d.). Retrieved from https://lpdaac.usgs.gov/products/aster_products_table/astgtm

EarthExplorer. (n.d.). Retrieved from <http://earthexplorer.usgs.gov/>

Global datasets - GRASS-Wiki. (n.d.). Retrieved from http://grasswiki.osgeo.org/wiki/Global_datasets

Global Data Explorer (Powered by GeoBrain). (n.d.). Retrieved from <http://gdex.cr.usgs.gov/gdex/>

Global Multi-resolution Terrain Elevation Data 2010 (GMTED2010) | The Long Term Archive. (n.d.). Retrieved from <https://lta.cr.usgs.gov/GMTED2010>

Gps Lombardia. (n.d.). Retrieved from <http://www.gpslombardia.it/>

GRASS GIS - Detailed Software Download. (n.d.). Retrieved from <http://grass.osgeo.org/download/software/>

GRASS GIS - General overview. (n.d.). Retrieved from <http://grass.osgeo.org/documentation/general-overview/>

GRASS GIS manual: g.region. (n.d.). Retrieved from <http://grass.osgeo.org/grass64/manuals/g.region.html>

Projections in GRASS GIS. (n.d.). Retrieved from <http://grass.osgeo.org/grass64/manuals/projectionintro.html>

Rete GNSS Regione Piemonte. (n.d.). Retrieved from <http://gnss.regione.piemonte.it/frmIndex.aspx>

Shuttle Radar Topography Mission. (n.d.-a). Retrieved from <http://srtm.usgs.gov/mission.php>

Shuttle Radar Topography Mission. (n.d.-b). Retrieved from <http://www2.jpl.nasa.gov/srtm/>

Shuttle Radar Topography Mission (SRTM) Void Filled | The Long Term Archive. (n.d.). Retrieved from <https://lta.cr.usgs.gov/SRTMVF>

SRTM 90m Digital Elevation Database v4.1 | CGIAR-CSI. (n.d.). Retrieved from <http://www.cgiar-csi.org/data/srtm-90m-digital-elevation-database-v4-1>

SRTMGL1 | LP DAAC :: NASA Land Data Products and Services. (n.d.). Retrieved from https://lpdaac.usgs.gov/products/measures_products_table/srtmg11

The Open Definition - Open Definition - Defining Open in Open Data, Open Content and Open Knowledge. (n.d.). Retrieved from <http://opendefinition.org/>

Vertici e Capisaldi IGM. (n.d.). Retrieved from <http://www.igmi.org/geodetica/>

Acknowledgments

I wish to express my sincere thanks to Prof. Ludovico Biagi for providing me with all the necessary facilities for the research as well for the valuable guidance and encouragement extended to me.

I would like to thank also to Laura Carcano for sharing her dissertation with me.

I also place on record, my sense of gratitude to my colleagues, who have helped me and showed me their support through all the time of my studies.